Non-destructive evaluation of photovoltaic materials and solar cells using Photoluminescence

Thesis submitted to

Cochin University of Science and Technology

in partial fulfilment of the requirements

for the award of the degree of

Doctor of Philosophy

Poornima N.

Applied Optics Division
Department of Physics
Cochin University of Science and Technology
Cochin – 682 022, Kerala, India

November 2013

Non-destructive evaluation of photovoltaic materials and solar cells using Photoluminescence

Ph.D Thesis in the field of Applied Optics

Author

Poornima N.
Applied Optics Division
Department of Physics
Cochin University of Science and Technology
Cochin – 682 022, Kerala, India
email: 22.poornima@gmail.com

Supervising Guide

Dr. C. Sudha Kartha
Professor, Department of Physics
Cochin University of Science and Technology
Cochin – 682 022, India
email: csk@cusat.ac.in

November 2013

Applied Optics Division, Department of Physics, Cochin University of Science and Technology, Cochin – 682 022, Kerala, India.

Department of Physics
Cochin University of Science and Technology
Cochin – 682 022

Dr. C. Sudha Kartha
Professor

Certificate

Certified that the thesis entitled **"Non-destructive evaluation of photovoltaic materials and solar cells using Photoluminescence"** submitted by **Ms. Poornima N.** is an authentic record of research work carried out by her under my supervision at the Department of Physics in partial fulfilment of the requirements for the award of degree of Doctor of Philosophy of Cochin University of Science and Technology and the work embodied in this thesis has not been included in any other thesis submitted previously for the award of any other degree.

Cochin – 22
Date: 04/11/2013

Prof. C. Sudha Kartha
Supervising Guide

Phone: +91 4842577404. **Fax:**. +91 484 2577595. **Email:** csk@cusat.ac.in

Declaration

I hereby declare that the thesis entitled *"***Non-destructive evaluation of photovoltaic materials and solar cells using Photoluminescence***"* submitted for the award of degree of Doctor of Philosophy of Cochin University of Science and Technology is based on the original work done by me under the guidance of **Dr. C. Sudha Kartha**, Professor, Department of Physics, Cochin University of Science and Technology, Cochin - 682 022 and this work has not been included in any other thesis submitted previously for the award of any other degree.

Cochin – 22
Date: 04/11/2013

Poornima N.

Dedicated to

My Family ...

Acknowledgement

Over these six long years of research in CUSAT, I have experienced and learned many things which have moulded me as a person and changed the way I look things at. At this point I am deeply indebted to all those who helped me realize this dream of mine.

My supervising guide Prof. C. Sudha Kartha is the first and foremost person whom I would like to thank. Her critical evaluation, questions and comments always have instilled in me a spirit for betterment. Her suggestions on how to make effective presentations were quite useful. Speaking at a personal level, she was always ready to lend ears to my problems, support and correct me when I was wrong. In fact, I have not been able to utilize the opportunity that I had to interact with her, to the fullest extent. But from the bottom of my heart, I am extremely thankful to her for letting me pursue this work and for providing me a pressure-free working environment.

My sincere gratitude goes to Prof. K.P. Vijayakumar whose relentless passion for, and consistent assessment of, this work has helped me drift through effortlessly. His vision and ideas have helped me expand my thought horizons.

I would like to express my sincere gratitude to Prof. B. Pradeep, Head of the Department and former Heads, Prof. M.R. Anantharaman, Prof. Godfrey Louis & Prof. Ramesh Babu T. for the help extended throughout. I humbly thank all my teachers in this department for their support. I remember with gratitude the patience and commitment that Prof. M.K.Jayaraj has shown in clearing my doubts. I am grateful to all the non-teaching staff for their timely help. I would also like to thank Prof. Y. Kashiwaba and T. Abe for their help with XPS measurements.

I am extremely fortunate to enjoy the friendship of Mr. Rajeshmon V.G. who has redefined all concepts of friendship. He was always there whenever I needed him– be it studies or repairing my experimental set up or for any personal help. During all tough times and happy moments he always stood unshaken beside me. I could share my concerns and crazy ideas with him. Accepting his advices has always made my life better.

I owe a lot to Dr. Rajesh Menon who has helped me a lot in doing experiments in a refined way. Discussions with him and his suggestions were always beneficial. He has always been there like an elder brother offering mental support at times of distress. Dr. Tina Sebastian is another person I consider close to my heart. In the initial stages of Ph.D, she was the person who propelled me to work. Her smiling face is the best thing I can remember about.

One person I cannot leave without mentioning is Deepu. Words fail me when I think of describing his affection and concern for me. His frank suggestions and corrections related to my thesis, have made my job much easier. My labmates– Rajesh C.S., Sreeroop, Santhosh, Anas, Geethu, Gincy, Gisa, Sreejith, Vipin, Titu, Anshad, Aswathi, Nitya, Jalaja, Jubimol, Saneesh, Aneesh George, Subramanyan and Jafar, of course have made every day of mine cheerful. The days we went for treats, conferences and daily evening tea are moments that I shall cherish forever.

I am also grateful to my seniors Dr. R.Jayakrishnan, Dr. R.Sreekumar, Dr. Kishore V.C., Dr. Deepa K.G., Dr. Meril Mathew, Dr. T.V.Vimalkumar, Dr. Sajeesh T.H., Dr. Angel Susan Cherian, Dr. Anita Warrier and Dr. Pramitha V., for their help.

Some people make your life better and accept you as you are. I would like to wholeheartedly acknowledge Dr. Senoy Thomas and Dr. Vijutha Sunny for being so and for treating me as their sweet little sister. I would also

like to acknowledge Subin, who is a person I can rely on any time. I have shared a good relation with my seniors~ Arun, Bhavya, Nijo, Priyesh, Sanal & Sreeja. I thank them for the good days. I have always tried to maintain a good rapport with members of other research labs. I never had to hear any negative answers when I sought help from them.

Hostel friends are always unforgettable. I cannot forget the support extended to me by my roommate Dr. Anisha. She was a good listener and I could relieve my stress talking to her.

My family is my greatest strength. When everybody discouraged me, my parents and my brother stood beside me and were a constant source of encouragement. I am also fortunate to have an understanding and loving husband. I do not have words to express my love and gratitude for him. It is just because of the support extended by him and his parents, that I am submitting this thesis.

Poornima N.

Preface

Photoluminescence (PL) spectroscopy is an optical technique that has emerged successful in the field of semiconductor material and device characterization. This technique is quite a powerful one which gives idea about the defect levels in a material, the band gap of the material, composition as well as material quality. Over the recent years it has received an elevation as a mainstream characterization technique.

This thesis is an attempt to characterize each individual layer used in a thin film solar cell with special focus on the electrical properties. This will be highly beneficial from the lab as well as industrial point of view because electrical measurements generally are contact mode measurements which tend to damage the surface. As far as a thin film solar cell is concerned, the constituent layers are the transparent conducting oxide (TCO), absorber layer, buffer layer and top electrode contact. Each layer has a specific role to play and the performance of a solar cell is decided and limited by the quality of each individual layer. Various aspects of PL spectroscopy have been employed for studying compound semiconductor thin films [deposited using chemical spray pyrolysis (CSP)] proposed for solar cell application. This thesis has been structured in to seven chapters.

Chapter 1 highlights the various material characterization techniques and gives an introduction to PL technique. A detailed account of how PL can be used to characterize semiconductor thin films is given. Different types of transitions in semiconductor and the signatures of each transition type have been given discussed in detail. A detailed review on how PL has been used by various research groups for semiconductor material and device characterization has also been incorporated in this chapter.

Chapter 2 briefly discusses the experimental set up for PL measurements. Details regarding supporting characterization techniques as XRD, XPS, Raman and SEM-EDAX measurements are also provided. A concise description of

chemical spray pyrolysis (CSP) technique using which films for the current study are deposited has also been provided.

Chapter 3 deals with PL studies on Zinc Oxide (ZnO) thin films which are prospective TCO candidates. A novel and less time consuming method for estimation of order of resistivity of ZnO thin films just from PL analysis is proposed. Films deposited by varying deposition conditions, i.e., solvent variation, pH variation, spray rate variation etc were studied and the method to evaluate resistivity using PL was found to hold for all these cases. An empirical relation connecting resistivity and ratio of integrated intensities of the two emissions- I_{DLE}/I_{NBE} could be proposed; where DLE is deep level emission and NBE is the near band edge emission from ZnO thin films. It was observed that order of resistivity was always one order less than the order of I_{DLE}/I_{NBE} . It could also be identified from PL that a propanol to water ratio of 1:1, pH of 4 for the spray solution and a spray rate of 7 ml/min are the optimum parameters for obtaining films with resistivity 2.4 X 10^{-2} Ω.cm. From PL we could also identify that in-situ doping was effective than ex-situ doping in bringing down resistivity and the optimum percentage of 'Al' doping for which ZnO thin films with resistivity 1.5 X 10^{-3} Ω.cm are obtained could be identified as 2.5 %.

Basic defect level analysis carried out on Copper Zinc Tin Sulphide (CZTS) thin films is presented in **Chapter 4**. The chapter begins with PL studies on stoichiometric CZTS thin films. An emission at 0.797 eV could be recorded from these films. Using temperature dependent PL measurements and excitation power dependent PL, the emission at 0.797 eV was identified to be a donor to acceptor (DAP) transition. From Arrhenious plot, the activation energy associated with the acceptor defect could be calculated as 0.12 eV and the defect was assigned to Cu_{Zn}. With the help of X-ray photoelectron spectroscopy (XPS) measurements, the donor defect at 0.533 eV from the conduction band edge associated with the transition at 0.797 eV could be identified as O_{Sn}. In Cu-rich samples an emission at 0.805 eV could be identified which has also been identified as a DAP transition. The defects involved with this transition could be identified as Cu_i donors and acceptors due to ionized states of Cu_{Sn}. The

preparation conditions for obtaining a quality sample relatively devoid of defects could be indirectly identified from PL. A band diagram could be proposed for stoichiometric as well as Cu-rich CZTS thin films based on our observations indicating the position of defect levels.

In **Chapter 5**, PL studies on Zinc Sulphide (ZnS) thin films meant for window/buffer layer application has been presented. A broad red emission (at 1.88 eV) could be recorded for all the films. From PL measurements and supporting data from X-ray diffraction studies and J-V measurements deposition conditions could be optimized- zinc chloride as the precursor for zinc, 460 ^{o}C as the substrate temperature and Zn:S ratio as 1:4. Temperature dependent and excitation power dependent PL measurements indicate that the transition is DAP type. Two activation energies- at 38 meV and 166 meV could be calculated. The activation energy of 166 meV could be attributed to delocalization energy of electrons in elemental sulphur species. From studied on vacuum annealed samples and supportive data from XPS measurements we could confirm that surface states due to oxygen are responsible for the level at 38 meV. In Cu doped ZnS thin films a green luminescence could be recorded at ~ 2.28 eV in addition to the emission at 1.88 eV. Variation of resistivity of Cu doped ZnS thin films with different percentages of doping could be related to the variation in PL spectra.

The possibility of using PL to extract the open-circuit voltage of In_2S_3/MEH-PPV heterojunction has been studied and is presented in **Chapter 6**. The theory that is generally used for silicon based solar cells was used to predict the open circuit voltage obtainable from this bilayer heterojunction with reasonable degree of accuracy. It could be observed that open circuit voltage values obtained from PL deviated from the voltage values obtained from J-V measurements by a maximum of 5.8 %. We could also demonstrate that PL measurements do not damage the device under study by monitoring the device using PL and J-V measurements for a period of 30 days. Apart from the normal ageing of the device, the devices were intact. In **Chapter 7**, summary of the entire work and scope for future work has been suggested.

Contents

Publications

JOURNAL PAPERS

[1]. Reliable and damage-free estimation of resistivity of ZnO thin films for photovoltaic applications using photoluminescence technique, **N.Poornima**, T.V.Vimalkumar, V.G.Rajeshmon, C.Sudha Kartha, K.P.Vijayakumar, International Journal of Photoenergy, Volume 2013, Article ID 105796, 9 pages. http://dx.doi.org/10.1155/2013/105796.

[2]. Composition and Conductivity-type Analysis of Spray Pyrolysed ZnS Thin Films using Photoluminescence, **N. Poornima**, Anjaly Jose, C. Sudha Kartha and K.P. Vijayakumar, Energy Procedia, 15, 2012, 347-353.

[3]. Modification of the optoelectronic properties of sprayed In_2S_3 thin films by indium diffusion for application as buffer layer in CZTS based solar cell, V.G.Rajeshmon, **N.Poornima**, C.Sudha Kartha, K.P.Vijayakumar, Journal of Alloys and Compounds, 553, 2013, 239-244.

[4]. Effect of precursor medium on structural, electrical and optical properties of sprayed polycrystalline ZnO thin films, T.V. Vimalkumar, **N.Poornima**, C.Sudha Kartha, K.P.Vijayakumar, Material Science and Engineering B, 175 (1), 2010, 29–35.

[5]. Enhancement of electrical conductivity in sprayed ZnO thin film through zero-energy process, T.V. Vimalkumar, **N.Poornima**, C.Sudha Kartha, K.P.Vijayakumar, T.Abe, Y.Kashiwaba, Physica B, 405, 2010, 4957–4960.

[6]. Unveiling the defect levels in SnS thin films for photovoltaic applications using photoluminescence technique, T. H. Sajeesh, **N. Poornima**, C. Sudha Kartha, and K. P. Vijayakumar, Physica Status Solidi A 207 (8), 2010, 1934-1939

[7]. On tuning the orientation of grains of spray pyrolysed ZnO thin films, T.V. Vimalkumar, **N. Poornima**, C. Sudha Kartha, K.P. Vijayakumar, Applied Surface Science, 256 (20), 2010, 6025-6028.

[8]. On single doping and co-doping of spray pyrolysed ZnO films: Structural, electrical and optical characterization, T.V. Vimalkumar, **N. Poornima**, K.B. Jinesh, C. Sudha Kartha, K.P. Vijayakumar, Applied Surface Science, 257, 2011, 8334–8340.

CONFERENCE PROCEEDINGS

[1]. Defect analysis of CZTS thin films using Photoluminescence technique, **N.Poornima**, V.G.Rajeshmon, C.Sudha Kartha and K.P.Vijayakumar, AIP Conf. Proc. 1512, (2013) 464.

[2]. Predicting The Performance Parameters of In_2S_3/MEHPPV Heterojunction Using Photoluminescence Technique, **N. Poornima**, M. R. Rajesh Menon, C. Sudha Kartha and K. P. Vijayakumar, AIP Conf. Proc. 1349, (2011) 457.

[3]. Preparation and Characterization of Spray Pyrolysed ZnS Thin Films and the Effect of Chlorine Doping, Anjaly Jose, V. G. Rajeshmon, **N. Poornima**, C. Sudha Kartha and K. P. Vijayakumar, AIP Conf. Proc. 1349, (2011)707.

[4]. Photoluminescence studies on off-stoichiometric defects in sprayed CZTS thin films, **N. Poornima**, V. G. Rajeshmon, C. Sudha Kartha and K.P.Vijayakumar. (Accepted for publication in AIP Conf. Proc.)

PAPERS PRESENTED IN CONFERENCES

[1]. Characterization of spray pyrolysed ZnO thin films to be used as back contact in solar cell using Photoluminescence, **N. Poornima**, T.V. Vimalkumar, C.Sudha Kartha, K.P.Vijayakumar, Proceedings of the National Conference on Materials for Energy Storage and Conversion (NCEMSC-2010) January 23-24, 2010.

[2]. Spatial PL mapping of deep level emission from spray pyrolysed Zinc oxide thin films, **N.Poornima**, T.V.Vimalkumar, C.Sudha Kartha, K.P.Vijayakumar, Proceedings of the conference Horizons in Thin Film Technology (HTFT 2011), January 20-21, 2011.

[3]. Temperature dependent dark conductivity measurements on ZnO:In thin films deposited using Chemical spray pyrolysis, **N.Poornima**, T.V.Vimalkumar, V.K.Dhanisha, C.Sudha Kartha, K.P.Vijayakumar, Proceeding of National Conference on Current Trends in Material Science (CTMS 2011), August 4-6, 2011.

LIST OF ABBREVIATIONS

PL	Photoluminescence
TCO	Transparent conducting oxide
CSP	Chemical spray pyrolysis
CB	Conduction band
VB	Valence band
XRD	X-ray diffraction technique
XPS	X-ray photoelectron spectroscopy
SEM	Scanning electron microscopy
EDAX	Energy dispersive X-ray analysis
FWHM	Full width at half maxima
PMT	Photomultiplier tube
SIT	Silicon intensified target
PDA	Photodiode array
CCD	Charge coupled device
RTA	Rapid thermal annealing
NBE	Near band edge emission
DLE	Deep level emission
I_{DLE}/I_{NBE}	Ratio of integrated intensities of deep level-emission to near band edge emission
CZTS	Copper zinc tin sulphide
DAP	Donor to acceptor pair
BT	Band to tail
BI	Band to impurity
BB	Band to band
O_{Zn}	Oxygen in zinc antisite
Cu_{Zn}	Copper in zinc antisite
V_O	Vacancy of oxygen
Zn_i	Zinc interstitial
O_{Sn}	Oxygen in tin antisite
V_{Cu}	Vacancy of copper
Cu_i	Copper interstitial
Cu_{Sn}	Copper in tin antisite
V_{OC}	Open circuit voltage

.....ꕥ.....

Chapter 1

INTRODUCTION TO PHOTOLUMINESCENCE

1.1 Introduction

The invention of laser in the 1960s was the undeniable reason why optical spectroscopy gained trust as a useful tool for characterization of materials [1]. Studies on materials which seemed impossible with incoherent light sources suddenly seemed to be all the more plausible with lasers. Once ultrafast lasers were discovered, development in the field of fast detection electronics also hastened. Thus, if it were not for the laser, optical spectroscopy would not have emerged as a leading technique for characterization of semiconductor materials as well as devices. Photoluminescence (PL) spectroscopy is one such powerful optical technique that has emerged successful with a proven track record in the area of semiconductor material and device characterization.

1.2 Different Material characterization techniques

Speaking of characterization techniques for material analysis, they should be in possession of some qualities which have been listed below. They ought to:

1) Possess spatial and depth resolution
2) Be non-destructive

3) Be sensitive
4) Be less time consuming
5) Be economical

It would be too unrealistic to expect all these to be satisfied simultaneously by any characterization technique. Even though we prefer that measurements shouldn't damage the sample surface, contact mode measurements generally tamper the sample surface. Electrical characterization for example requires contacts. So ultimately we will have to compromise with certain qualities based on the sort of information required from the sample.

Generally characterization techniques for semiconductors [2-3] can be broadly classified as:

1) **Physical/Chemical-** Scanning electron microscopy, Transmission electron microscopy, Auger electron spectroscopy, Electron beam induced current measurements, Secondary ion mass spectroscopy, Rutherford backscattering, Energy dispersive X-Ray analysis, X-Ray Phototelectron spectroscopy, X-Ray diffraction, X-Ray fluorescence, Neutron diffraction, Atomic force microscopy, Scanning tunneling microscopy etc are some techniques which offer a better understanding of the **surface, composition, crystal structure**, **grain size** etc.

2) **Optical-** Optical microscopy, Absorption spectroscopy, Photoluminescence, Photothermal beam deflection technique, Ellipsometry, Raman spectroscopy, Optical modulation spectroscopy, Optical beam induced current measurements etc are powerful tools using which **microcharacterization of defects in semiconductor as well as electronic devices can be done and bandgap, different recombination mechanisms, structure, optical constants** etc, can be found out.

3) **Electrical**- Two-probe measurements, Four-probe measurements, Hall Effect measurements, Capacitance-voltage measurements, Thermoelectric probe measurements, Haynes-Shockley experiment, temperature dependent dark conductivity measurements, Thermally stimulated current measurements, Photoconductivity measurements etc are important electrical characterization techniques which yield information regarding **resistivity, carrier concentration, mobility, conductivity type, contact resistance, barrier height, lifetime, position of deep level impurities** etc.

If we analyze all these techniques, information obtained from physical/chemical and electrical techniques is too specific, i.e. by employing physical methods as X-ray diffraction technique we cannot obtain information about defects in the material or its resistivity**.** Some electrical measurements may be able to offer both these information but their downside is the requirement of contacts. Photoluminescence (PL) spectroscopy in contrast to these is an optical technique, which offers electrical characterization and is a selective probe of discrete electronic states [4]. How is it different and why is it so versatile? The focus of this doctoral thesis work is to employ different aspects of PL spectroscopy for characterization of semiconductors and solar cells.

1.3 What is PL spectroscopy?

Radiative emission is in one way the inverse of absorption and the radiation rate is governed by Fermi's Golden rule which states that density of final states and density of carriers in the higher energy state are the parameters governing radiation rate. A semiconductor emitting photons thus should not be in equilibrium and needs energy injected from an excitation source; but what type of excitation source? Different excitation sources are practically possible. Excitation by electric current (eg. injection through Schottky barrier) results in

electroluminescence whereas electron beam excitation, as in Scanning Electron Microscope (SEM), triggers cathodoluminescence. Mechanical excitation yields triboluminescence, thermal excitation mechanisms result in thermoluminescence and light from a chemical reaction is chemiluminescence. So to sum up light emission processes are termed luminescence. Obviously in photoluminescence (PL), electrons in the material are excited to the conduction band by means of an optical excitation and on de-excitation to ground state, electrons release the excess energy as radiation. The emitted radiation is monitored and from the peak energy, peak height and peak width, a wealth of information can be obtained [5-7]. A schematic of some of the possible de-excitation pathways is given in Figure 1.1.

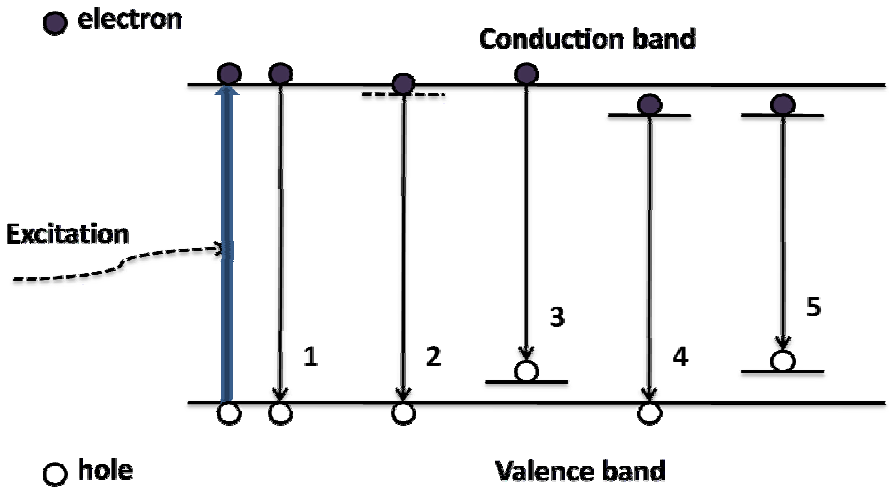

Figure 1.1: Different radiative transitions possible in a semiconductor.

Transition 1 is nothing but band-to-band recombination where a free electron in the conduction band (CB) recombines with a free hole in the valence band (VB). Such transitions have energies equal to or higher than the bandgap energy. Transitions with energy higher than bandgap energy are due to recombination of 'hot carriers' which are carriers that have not relaxed to the bottom (top) of CB (VB). Intrinsic quasiparticle states such as free excitons can also be formed in a

semiconductor and free excitonic recombination has been depicted in transition 2. Why is the term 'free' so important? Excitons can also be associated with impurity levels and such recombination yields energy in the sub bandgap regime. Transitions 3 and 4 come under the category of free to bound transitions where a free carrier is involved in recombination with a carrier bound at an impurity; the two transitions are CB-to-acceptor and donor-to-VB. Transition 5 involves recombination of electrons bound to donor and holes bound to acceptor. The schematic clearly explains that we can get information regarding:

a) Bandgap
b) Various recombination mechanisms
c) Position of various defect levels within the gap.

Other information that can be obtained from PL analysis[3]includes:

a) Carrier lifetimes
b) Quality of surfaces and interfaces
c) Disorder present in the material
d) Characteristics of quantum wells
e) Analysis of dopant levels in various semiconductors

1.4 How PL spectroscopy can be used to characterize semiconductors?

We have mentioned various applications of PL, but how we derive this information depends on what all factors affect the PL response from a material. The first and foremost parameter is the nature of optical excitation whose energy determines the states that are being probed and also the penetration depth. Intensity of optical excitation decides the density of excited carriers and thereby the intensity of the PL signal. Transient phenomena can be studied using pulsed excitation. PL is sensitive to the electronic states present in the surfaces and interface and it originates near the surface. Excitation power dependent PL measurements can help in understanding the energy distribution and density of interface states. Presence of

surface adsorbates affects the PL signal intensity. Depth of the trap can be estimated by activation of the traps by temperature dependent PL analysis. PL is surface sensitive and any modification in the surface can be monitored real-time from the PL spectrum. Unlike other surface characterization techniques which are sensitive to the pressure inside the chamber, PL is not sensitive to pressure within the sample chamber. PL strongly depends on temperature and spectral resolution is maximum at temperatures close to liquid helium temperature. For many purposes room temperature PL measurements shall suffice. Sample surface is seldom affected by PL measurement. Unlike other optical methods which are stringent about beam alignment, surface flatness etc, PL is more liberal. Indirect bandgap materials generally have low PL efficiency. Non-radiative events dominate the excited state carrier relaxation process in such materials. PL measurements thus give an idea of radiative and non-radiative events in the material. Difficulty in estimating the density of surface/interface as well as impurity states is another shortcoming of PL. Reviewing basic semiconductor physics relevant to recombination processes would be a better way to understand how PL can be used for semiconductor characterization. Band structure, free carrier properties, quasi- and many- particle states, impurities and recombination processes etc are relevant in this context and we shall see them one by one.

(1) Band structure

Bandgap is the energy difference between conduction band edge and valence band edge. Band gaps are realized by optical absorption processes. Beyond a particular frequency ω, continuous absorption results and the energy corresponding to ω is the band gap E_g. If absorption of a photon results in the formation of an electron-hole pair, it is a direct process. This happens in *direct gap semiconductor* where the minimum of the conduction band and maximum of the valence band are at the same point in k-space [Figure 1.2 (a)]. In some cases the minimum energy gap

involves electrons and holes separated in k-space. Thus in addition to a photon, the absorption process is mediated by a phonon which accounts for the momentum that a photon cannot provide. Absorption processes mediated by phonons along with photons occur in *indirect gap semiconductor* [Figure 1.2 (b)]. Depending on the magnitude of the bandgap, semiconductors may also be classified as *narrow gap* semiconductors (eg. PbS, InSb), intermediate gap semiconductors (eg. GaAs, CZTS) and *wide gap* semiconductors (eg.SiC, AlN, ZnS). Bandgap decides the energy range and intensity of the emission whose temporal response is governed mainly by the band structure.

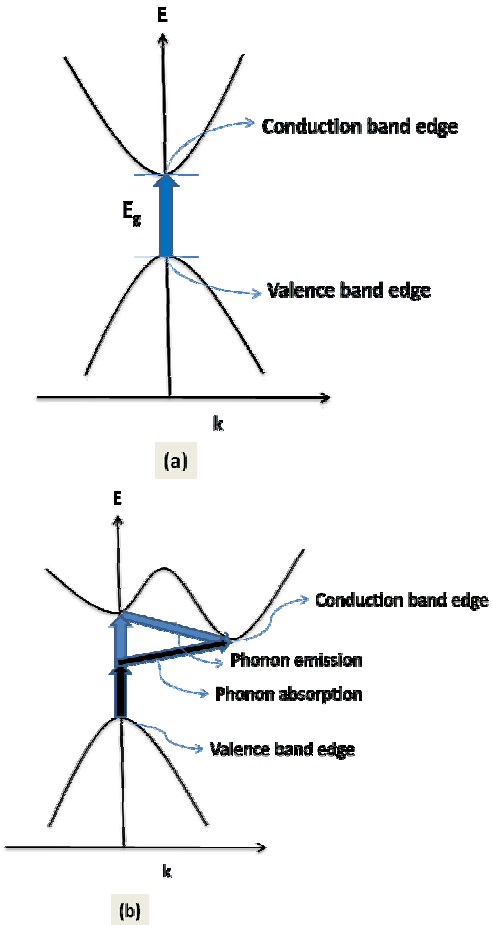

Figure 1.2: Schematic of (a) Direct band gap (b) Indirect band gap semiconductor.

(2) Free carrier properties

There are mainly two types of free carriers in a semiconductor- electrons and holes. Free carriers are mainly characterized based on their origin [i.e. whether they are free or defect related], density, mass and scattering time. Density of free carriers is decided mainly by whether the semiconductor is intrinsic or extrinsic. Doping can create extremely high carrier concentration ($\sim 10^{20}$ cm^{-3}) and dopant levels are created within the forbidden gap. Mass of these free electrons or holes within the material is different from the mass of electrons owing to interaction with positive ion cores in the material. Effective mass is thus decided by the band structures which in turn affect the PL spectra. Various scattering mechanisms can occur for free carriers such as phonon scattering, free carrier scattering, impurity scattering etc which alter properties like mobility, lifetime etc which are relevant factors in time resolved PL measurements.

(3) Quasi- and many-particle states

At low temperatures numerous many-particle states are likely to be formed like excitons, biexcitons, excitonic molecules, electron-hole plasmas etc. Coulomb attraction-bound electron-hole pairs are called excitons and it was Frenkel who postulated the exciton in 1931 followed by Wannier's development in 1937. Frenkel and Wannier excitons are tightly and loosely bound electron-hole pairs respectively and the latter type of exciton seems appropriate to describe excitons in semiconductors because the large dielectric constant in semiconductors reduces the Coulombic interaction between electron and hole. Biexcitons and excitonic molecules result from van der Waal pairing of two or more excitons. Sometimes at low temperature when the concentration of excitons is extremely large there is a phase transition from ensemble of neutral particles to an ensemble of charged particles. All these quasi-particles are likely to exist and yield radiative emission on recombination. Excitons can be ionized

into free charge carriers but as such their energy is reduced than the fundamental gap energy by their binding energy factor. All such recombinations have specific signatures and properties of their own and can be identified from the PL spectra.

(4) Impurities

They can either be intrinsic or extrinsic. Intrinsic impurities imply the physical defects such as vacancies, interstitials, defect pairs etc. Extrinsic impurities are formed when atomic elements distinct from the elements belonging to the pure lattice are incorporated. It depends on the valency of the specific impurity incorporated as to whether they shall act as donors or acceptors. Many-particle states involving impurities- like donor bound exciton, acceptor bound exciton, donor acceptor pairs etc can also be formed in semiconductors. Features specific to each case can be observed in the PL spectra.

If we attempt a review on how various aspects of PL spectroscopy have been clubbed together and employed for semiconductor characterization then it wouldn't be too much of a surprise that we come across reports mainly on GaAs and 'Si', portraying many of the aforementioned processes. In this review we shall discuss, the most common type of PL spectroscopy- continuous wave (cw) PL, time resolved PL, spatially resolved PL, quasi-steady state and Suns PL. We shall also see as we proceed as to how variation of parameters as excitation energy, intensity, surface and interface states, applied bias etc affect the PL response from a semiconductor.

1.5 Features of various transitions and their observation in PL spectrum: Theory cum Review

(1) Band to band recombination

Occurs at energies greater than or equal to the band gap energy and is dependent on the non-equilibrium concentration of holes and electrons. In terms of equilibrium concentration of electrons (n_o) and holes (p_o) and intrinsic carrier concentration (n_i), recombination rate can be expressed as

$$R \alpha \frac{np}{n_i^2}$$

where $n = n_o + \Delta n$ and $p = p_o + \Delta p$. Explicitly expressing R (neglecting $\Delta n \Delta p$), we get

$$R \alpha \frac{n_o p_o + \Delta n p_o + \Delta p n_o}{n_o p_o}$$

Examining non equilibrium contribution to recombination rate,

$$\frac{\Delta R}{R} = \frac{\Delta n}{n_o} + \frac{\Delta p}{p_o}$$

It is clear that recombination rate is governed by population of minority carriers. From the temperature dependence of carrier concentration, recombination rate is proportional to $T^{-3/2}$. Equilibrium energetics of free electrons and holes decide the band to band recombination spectrum.

Generally Fermi-Dirac distribution best describes the equilibrium energetics; it approximates to Boltzmann distribution at high temperature. In a report [8], the authors have provided the temperature dependent PL spectra of GaAs/AlGaAs double heterostructures where the high energy side of the PL spectra exhibit Boltzmann tail whereas low energy side of the spectrum is complicated and is governed by residual impurity states. The peak energy of this band-to band recombination indicates the bandgap.

(2) Free exciton recombination

Dexter and Knox [9], Elliot [10], Dimmock [11], Reynolds and Collins [12], have detailed the theory of excitons in their books. Energy of free-excitons comprises mainly of two parts- the Coulombic interaction energy that binds the two particles and the translational kinetic energy. Owing to the binding energy

the energy levels of excitons[hydrogen-like levels) occur below the conduction band minimum and the presence of excitons is realized either by absorption or radiative recombination which ultimately is the annihilation of excitons. Till 1967 free-excitons could not be observed in GaAs owing to poor sample quality [13]. Observation of free-exciton luminescence in undoped MBE prepared GaAs layer has been reported [14-17]. The authors report that intensity of excited states fall as n^{-3}, so only excited states up to $n = 2$ could be observed. Presence of defects, impurities, strain, interfaces etc mask the intrinsic properties of free-excitons and generally these features dominate the PL spectra. A close examination of the PL spectra recorded for MOCVD and MBE grown heterostructures and MOCVD grown homostructures [18] indicate that relative strength and line-shape of the peak varies from sample to sample. Another feature is the rapid thermal quenching of free exciton emission. Poor quality of surfaces and interfaces has always been a concern with GaAs especially among members of the photovoltaic community as this reduces efficiency to a large extent. The very same problem affects free-exciton recombination which can be quite very well understood from reports where the authors have presented the results on a double heterostructure before and after removal of the passivation layer by etching [19-22].

(3) Defect luminescence

PL is extremely suitable for detecting impurity concentrations as low as 10^{12} cm^{-3} and also to determine specific impurities by identifying spectral signatures.

(a) Bound excitonic emission

Binding energy of free excitons may be increased by a point defect. Excitons may be bound to neutral donors or acceptors- denoted by (D^o, X) and (A^o, X) respectively. Excitons bound to ionized donors D^+ comprise of a donor ion (+), an electron (e) and a hole (h) and are denoted by (D^+, X).

Ionized acceptor bound excitons are represented as (A^-, X). As the chemical nature of each impurity is different, signatures in the PL spectrum will also differ. Bound excitons generally contribute a sharp line to the PL spectra in undoped and moderately doped samples. Early but comprehensive reports on impurity related emission in GaAs were published in the 1970s [23-25]. Several bound exciton complexes are possible in a material like GaAs and there are reports regarding the activation energies of possible donors and acceptors in the material [26-28]. More than one impurity species may be present in the same sample and features related to both can be obtained in the PL spectra [29-31]. Intensity of PL emission lines depend on exciton concentration in that particular state, their energy distribution and of course, the transition probability for radiative recombination. Complicated effects may occur due to interaction of defects and concentration quenching which makes interpretation difficult as spectra may become muddled. Slight variation in temperature/ excitation power can also induce changes in relative intensities of lines in the PL spectra. There are other factors such as growth technique and growth parameters which decide the details of such emissions [23-33]. Passivation with hydrogen is a technique generally employed for reduction of impurities in semiconductors. Full-width at half maxima (FWHM) of the dominant impurity related peak (D^0, X) has been taken as a relative measure of sample purity [34]; with removal of impurities, FWHM decreases.

It is easy to distinguish between free and bound excitonic luminescence in crystals. Excitons travelling in crystals interact with phonons, and are scattered by defects, impurities and compositional fluctuations in crystals. As a result, luminescence bands are broadened. Whereas when exciton is associated with a donor or acceptor, it becomes immobile and therefore its

radiation line width is much smaller compared to free exciton emission. Excitons are modelled as hydrogen atoms and have levels just beneath the CB edge. Ground level (n=1) of bound exciton lies beneath the ground level of free exciton; it lies lower by an energy value equal to the binding energy of the exciton with the impurity. As a result, bound exciton lines appear at lower energies than free exciton lines. Bound excitons are characterized by 'giant oscillator strengths'- implying that their lifetime is too short and they recombine quickly.

One important application of PL lies is in determining shallow impurity concentration. Most common technique for determining the same is temperature dependent Hall measurements which require good ohmic contacts. The most important feature of PL is that all donors and acceptors are made neutral by excitation with above bandgap light. Thus simultaneously all donors and acceptors are identified which is in sharp contrast to electrical measurements which has sensitivity to only the uncompensated fraction of majority carriers. Impurity concentration is measured by a precise determination of ratio of intensities of bound exciton to free exciton lines [35-36].

(b) Free to bound (FB) transitions

Generally at low temperatures, excitonic states are populated, but it so happens that even under these conditions, some carriers exist as free carriers. They may give rise to band to band recombination. It may also happen that electron (hole) may recombine with an acceptor (donor) level. These transitions are denoted generally as (e, A^0) and (D^0, h). Theoretical fitting of the line-shape of the emission, say (e, A^0), helps in determining the activation energy of the acceptor [37].

(c) Donor-to-acceptor pair (DAP) transition

Donors and acceptors interact via Coulomb interaction to form pairs behaving like stationary molecules in semiconductor. DAP complexes consist of four point charges- D^+A^-eh. Recombination energy of a DAP pair is given by

$$h\vartheta = E_g - (E_A + E_D) + \frac{e^2}{\varepsilon R}$$

where ε is the dielectric constant, E_g the bandgap, E_A and E_D are the acceptor and donor binding energies, R is the separation between acceptor and donor. Hopfield et al [38] identified unambiguously such pairs in 1963 and since then a lot of work has been going on examining the properties of these pairs. Lucovsky et al suggested for the first time, a DAP transition at 1.49 eV in Zn-doped GaAs layers [39].

For any transition belonging to DAP class, there are certain characteristic features:

- Line shifts to higher energies with increase in excitation intensity
- Narrowing of the emission band occurs with increase in excitation intensity
- Band shifts towards higher energies with increase in donor concentration
- Intensity of the emission falls with increase in temperature
- Peak position of the emission shifts towards lower energies with increase in temperature

(d) Transitions involving deep levels

Deep levels exhibit properties quite different from that of shallow donors and acceptors. Generally such levels are not characterized by separation from valence band and conduction band but by their dispersion in momentum space [40]. Isoelectronic impurities [41] transition metal ions [42] and rare earth ions [43] are some of the simplest examples that can be quoted for deep levels.

1.6 Review on PL studies in semiconductors

In addition to its application in characterizing and quantifying basic optical, structural and electronic properties of semiconductors, PL has also been used for determining alloy composition, emission mechanisms specific to different structures, impurity incorporation at specific positions of the layers etc.

The effect of incorporation of defects, growth parameters and alloy composition on the PL spectrum of $Al_xGa_{1-x}As$ layers grown by MOVPE was studied by Kuech et al [44]. No emission was observed in samples with higher 'Al' content. Indirect gap samples exhibited lower emission intensity. Differences in background impurity concentration, carrier lifetime and penetration depth of pump laser were reflected in the variation of PL intensity with 'Al' concentration and the authors conclude that PL intensity depends primarily on oxygen incorporation.

In 1984 Yuan et al [45] observed a new emission specific to GaAs/AlGaAs heterostructures. The emission energy lies between PL peaks observed for near-edge bound exciton and free to bound transitions. The authors comment that the emission occurs due to recombination of electrons in the potential notch next to the heterointerface caused by band-bending and free holes in the valence band. That the emission is related to heterostructure is proved by the disappearance of the emission in samples subjected to chemical-etch treatment where a part of the structure has been removed.

PL has been used to characterize quantum wells and superlattices – determination of well-width is quite easily possible with PL emission measurements. In fact fluctuations in well widths can also be determined precisely from PL measurements [46]. PL line width of quantum well excitonic recombination is dependent on the 'island' size of interfacial roughness and lateral extent of

exciton [47]. Wolfard et al [32, 48] tried to determine the band offset of GaAs/$Al_xGa_{1-x}As$ structures with the help of PL measurements. Specific aspects of dynamics of semiconductors can be elucidated by combining PL measurements with some perturbation like magnetic field, electric field, pressure, uniaxial stress etc. It is quite interesting to observe that band structure and electronic levels associated with impurities are sensitive to changes in pressure-induced changes in interatomic distance. A fundamental thermodynamic perturbation is hydrostatic pressure. PL spectrum of bulk GaAs varies drastically with pressure [49]. At high pressures bandgap of bulk GaAs is indirect; transitions in PL spectra are dominated by indirect free excitons, indirect donor-bound excitons etc. At low pressures, direct free excitonic, direct donor-bound excitonic transitions dominate.

PL measurements in the presence of magnetic field offer information about the electronic structure of free carriers, excitons and impurities. Under magnetic field, allowed optical transitions are helpful in the calculation of reduced effective mass of the electron-hole system [50]. Measurements of the net polarization of luminescence of a sample under applied magnetic field can be used to determine spin relaxation time. Miller et al [51] have measured the magnetic field dependence of polarization of excitonic luminescence from GaAs quantum wells.

Application of external electric field can shift/split energy levels in a semiconductor and those due to impurities; it can also be used to accelerate charge carriers. Bias tilts the conduction and valence bands retaining Fermi level constant throughout. Band tilting accelerates carriers; high fields cause ionization of carriers from impurities and very high fields even cause across the gap ionization. Electron-hole pairs are produced subsequently by collisions and radiative recombination is extremely likely to occur. Bludau and Wagner observed impact ionization of excitons in bulk GaAs crystals [52]. With increase in field, shallow luminescence lines are quenched.

A technique that is more of a combination of luminescence and absorption is photoluminescence excitation spectroscopy (PLE) where a specific emission is monitored by scanning over different excitation wavelengths. It is useful in identifying defects in semiconductors and also the excited states of impurity complexes. Beckett et al [53] have used PLE measurements in a magnetic field to identify the excited states of certain donor impurities. PLE can also be used to study deep levels; Wolfard et al [54] used PLE to study isoelectronic N centres in GaAs.

Time-resolved PL measurements are useful in determining carrier lifetimes and different recombination mechanisms. Excitation is pulsed and is generally much shorter than the recombination time and a carrier density is immediately generated on excitation. Effect of Zn doping in AlGaInP/GaInP double heterostructures was analyzed by Domen et al [55] Lifetimes were estimated for different doping concentrations. Surface-state and depletion layer contributions can be differentiated using time-resolved PL. Decrease in integrated PL intensity is a sign of increase in non-radiative centres. GaInP has been characterized after wet-chemical etching using continuous wave (CW) and time-resolved PL [56] Increase in integrated PL intensity in CW PL is an indication of increased carrier lifetime and decrease in non-radiative recombination rate.

Spatially resolved luminescence studies or spatial mapping of PL of a semiconductor structure may directly provide information about structural properties, distribution of impurity content, homogeneity of luminescence from the sample. PL spectrum has been recorded as a function of position to determine dislocations or stress in laterally overgrown InP on InP-coated Si substrates [57].

The immense potential of different aspects of PL spectroscopy has been dealt with by Gfroerer et al in his theory cum review article in 2000 [4]. Krustok et al have used PL for the analysis of defects in $CuInSe_2$ thin films. Low temperature

PL measurements have been done to calculate the position of various defect levels within the band gap. Compositional variations and its effect on the PL spectrum have been studied. Broadening of spectral lines due to phonon emission has also been observed [58]. Deep levels in p type CdTe:Cl have been probed by Krustok et al. A defect model has been proposed for the system [59].

As per a report on PL bands in $CuGaTe_2$ crystals by Krustok et al in 1998, the observed emissions were greater than the fundamental gap value of 1.3 eV and the emissions were ascribed to transitions from either a higher lying conduction band minimum to an acceptor or from a donor level to a lower lying valence band minimum [60]. PL has been used to investigate the role of spatial potential fluctuations in compound semiconductors. From the temperature dependent and excitation power dependent measurements it has been concluded that potential fluctuations can cause deep localized states within the band gap [61]. A systematic study and comparison of the various defects in $CuGaSe_2$ and $CuInS_2$ crystals was done for the first time by Krustok in 1999 [62].

Fine structures in PL spectrum arising due to transitions between deep donor-acceptor complexes in $CuInS_2$ have been correlated to possible lattice distortion in crystals [63]. Mac Donald et al in his report in 2008 proposed that monitoring the band to band PL in silicon wafers is one of the best means to get an idea of the lifetime. So taking PL images prior to and after dissociation of FeB pairs in boron doped silicon helps in identifying the interstitial concentration of iron [64]. Optical studies of as-deposited ZnO thin films have been correlated to the structural and electrical properties and optical study has been regarded as a novel tool for quality evaluation of the sample [65]. An interesting work was reported in 2009 on silicon rich oxide films where a strong correlation was observed between surface morphology and PL, which depends strongly on the nature of the surface. A red emission was observed which was related to surface morphology [66].

Another work is on correlation of surface morphology of InGaN/GaN quantum wells with photoluminescence measurements which has been done by comparing the AFM and PL measurements [67]. Radiative recombination via traps in Si wafers could be identified by hyper-spectral imaging using PL because it offers high resolution in the near infrared. Hyper-spectral imaging offers highly resolved data in spectral and spatial dimensions and photoluminescent properties of multicrystalline silicon wafers have been used in this work [68]. An interesting work in 2011 by Kistner et al identified that silicon nitride thin films are inappropriate matrices for studying luminescence from silicon nanocrystals embedded in them because silicon nitride is by itself a good emitter [69]. A detailed study of low temperature PL measurements on ZnS nanobelts and nanowires provides crucial information on the nature of electronic states and the recombination mechanisms in these nanostructures [70].

An interesting application that we now have is the use of PL technique to monitor the different stages of silicon solar cell production. Much work that was published in 2005 [71, 72] and 2006 [73, 74] dealt with developing the theory as to how quasi-steady-state PL technique (QSS PL) can be used for silicon solar cell characterization. Light emission from silicon either in the form of PL or electroluminescence (EL) has been used since long back for studying wafers. In fact EL spectra and photographic images of EL emission from silicon p-n junction were reported in 1956 by Chynoweth and McKay [75]. Work progressed and with the introduction of cooled charge coupled camera systems [76] a lot of tools have become commercially available and we have longer wavelength imaging systems [77] too.

Spectrally resolved PL has been used at especially cryogenic temperatures to investigate dopant and defect properties in silicon and to determine the absorption coefficient for band-to band transitions [78, 79]. Scanning room temperature PL

measurements (RTPL) has been employed for assessing spatial variations of material quality and to correlate such changes with dislocation densities and also to determine diffusion length maps [80, 81]. RTPL has also been used to monitor the effects of various processes like gettering, hydrogenation etc on the initial material quality and subsequently the device performance [82-84].

In a report by Abbott et al [85] they have used three recently established PL techniques to address issues related to solar cell fabrication. The three techniques employed by them are- a) QSS PL lifetime measurements, for characterizing minority carrier recombination as a function of injection level b) suns-PL, for describing the solar cell terminal characteristics in terms of recombination and c) PL imaging for spatial resolution of junction shunting effects and recombination.

1.7 Conclusions

On the whole, the scope of PL technique is assuming newer dimensions and currently it happens to be one of the most sought-after characterization techniques by the optoelectronics industry. By monitoring the PL intensity, PL peak energy and polarization lot of information can be acquired from the sample, as we saw in the review. In the beginning if it was just cw-PL measurements now we have time-resolved PL measurements, magneto-luminescence, bias-dependent PL, suns-PL, PL imaging etc which have made the job quite easier. Now, studying surfaces and interfaces is not a problem. Heterostructures are also easy to study using PL- alloy composition, interface roughness etc can be found using PL. The advantage of PL is of course that it is a non-invasive optical technique that offers electrical characterization as it is a direct probe of all electronic states. Thus the resistivity of the samples under study shouldn't pose a problem. In future, we believe newer and newer aspects of PL spectroscopy shall be explored.

References

[1]. **G.D. Gilliland.** 1997, Materials Science and Engineering, Vol. R18, p. 99.

[2]. **Edited by, Gary E. McGuire.***Characterization of Semiconductor Materials- Principles and Materials.* s.l. : Noyes Publications, 1989. Vol. 1. 0-8155-1200-7(v.1).

[3]. **Dieter K. Schroder.***Semiconductor Material and Device Characterization.* s.l. : John Wiley & Sons Inc., 2006. 978-0-471-73906-7.

[4]. **T. H. Gfroerer.***Photoluminescence in Analysis of Surfaces and Interfaces.* Chichester : John Wiley & Sons Ltd, 2000. p. 9209.

[5]. **Edited by, D.R.Vij.***Luminescence of Solids.* s.l. : Plenum Press, 1998. 0-306-45643-5.

[6]. **R. C. Ropp.***Studies in Inorganic Chemistry 21- Luminescence and the Solid State.* s.l. : Elsevier B.V., 2004. 0-444-51661-1..

[7]. **J. Dekker, Adrianus.***Solid State Physics.* s.l. : Prentice-Hall Inc., 1958.

[8]. **D. J. Wolford, G. D. Gilliland, T. F. Kuech, L. M. Smith, J. Martinsen, J. A. Bradley, C. F. Tsang, R. Venkatasubramanian, S. K. Ghandhi, H. P. Hjalmarson.** 1991, Journal of Vacuum Science and Technology, Vol. B9, p. 2369.

[9]. **D. L. Dexter, R. S. Knox.***Excitons.* New York : Wiley-Interscience, 1965.

[10]. **R. J. Elliot.** Theory of Excitons 1. *Polarons and Excitons.* New York : Plenum, 1963.

[11]. **J. O. Dimmock.***Semiconductors and Semimetals* . New York : Academic Press, 1967, p. 270.

[12]. **D. C. Reynolds, T. C. Collins.***Excitons-Their Properties and Uses.* New York : Academic Press, 1981.

[13]. **M. A. Gllleo, D. E. Hill, F. V. Williams.** 1967, Bulletin of American Physical Society, Vol. 12, p. 656.

[14]. **M. Heiblum, E. E. Mendez, L. Osterling.** 1983, Journal of Applied Physics, Vol. 54, p. 6982.

[15]. **M. T. Ramsbey, I. Szafranek, G. Stillman, J. P. Wolfe.** 1994, Physical Review B, Vol. 49, p. 16427.

[16]. **G. S. Elman, E. S. Koteles, S. A. Zemon, Y. J. Clu.** 1987, Journal of Vacuum Science and Technology, Vol. B7, p. 57.

[17]. **E. S. Koteles, B. S. Elman, S. A. Zemon.** 1987, Solid State Communication, Vol. 62, p. 703.

[18]. **D. J. Wolford, G. D. Gilliland, T. F. Kuecb, J. Martinsen, J. A. Bradley, C. F. Tsang, R. Venkatasubramanian, S. K. Ghandhi, H. P. Hjalmarson, L. Klein.** 1992, Inst. Phys. Conf Set, Vol. 120, p. 401.

[19]. **J. M. Calleja, A. R Goni, S. Weiner, B. S. Dennis, A. Pmezuk, L.N. Pfeiffer, K. W. West.***Optical Phenomena m Semiconductor Structures of Reduced Dimensions.* London : Kluwer, 1992. p. 267.

[20]. **D. Gershom, J. S. Weiner, E.A. Fitzgerald, L. N. Pfeiffer, N. Chand.***Optical Phenomena in Semiconductor Structl~res of Reduced Dimensions* . London : Kluwer, 1992. p. 337.

[21]. **E. S. Koteles, J. Y. Chi.** 1986, Superlattices and Microstructures, Vol. 2, p. 421.

[22]. **I. Brener, M. Olszaker, E. Cohen, E. Ehrenfreund, A. Ron, L. N. Pfeiffer.** 1992, Physical Review B, Vol. 46, p. 7927.

[23]. **U. Helm, P. Hiesinger.** 1974, Physica Status Solidi B, Vol. 66 , p. 461.

[24]. **A. M. White, P. J. Dean, B. Day.** 1974, Journal of Physics C: Solid State Physics, Vol. 7, p. 1400.

[25]. **A. M. White, P. J. Dean, L. L. Taylor, R. C. Clarke, D. J. Ashen, J. B. MuUin.** 1972, Journal of Physics C: Solid State Physics, Vol. 5, p. 1727.

[26]. **D. J. Ashen, P. L. Dean, D. T. J. Hurle, J. B. Mulhn, A. M. White, P. D. Greene.** 1975, Journal of Physics and Chemistry of Solids, Vol. 36, p. 1041.

[27]. **V. A. Karasyuk, D. G. S. Beckett, M. K. Nissen, A. Vtllemaire, T. W. Steiner, M. L.W. Thewalt.** 1994, Physical Review B, Vol. 49, p. 16381.

[28]. **S. K. Brierley, H. T. Hendriks, W. E. I-loke, P. J. Lemomas, D.G. Weir.** 1993, Applied Physics Letters, Vol. 63, p. 812.

[29]. **B. J. Skromme, C. J. Sandroff, E. Yablonovitch, T. Gmitter.** 1987, Applied Physics Letters, Vol. 51 , p. 2022.

[30]. **D. J. Ashen, P. L. Dean, D. T. J. Hurle, J. B. Mulhn, A. M. White, P. D. Greene.** 1975, Journal of Physics and Chemistry of Solids, Vol. 36, p. 1041.

[31]. **T. D. Harris, M. S. Skolnick, J. M. Parsey, Jr. R. Baht.** 1988, Appied Physics Letters, Vol. 52, p. 389.

[32]. **D. J. Wolford, J. A. Bradley.** 1985, Solid State Communication, Vol. 53, p. 1069.

[33]. **J. C. Garcia, A. C. Beye, J. P. Contour, G. Neu, J. Massies, A. Barski.** 1988, Applied Physics Letters, Vol. 52, p. 1596.

[34]. **B. J. Skromme, S. S. Bose, B. Lee, T. S. Low, T. R. Lepkowski, R. Y. DeJule, G. E. Stallman, J. C. M.Hwang.** 1985, Journal of Applied Physics, Vol. 58, p. 4688.

[35]. **Tajima, M.** 1982, Japanese Journal of Applied Physics, Vols. 21 (Suppl. 21-1), p. 113.

[36]. **P. Mc Colley, E. C. Lightowlers.** 1987, Semiconductor Science and Technology, Vol. 2, p. 157.

[37]. **E.W. Williams, H. B. Bebb.** 1968, Journal of Physics and Chemistry of Solids, Vol. 30, p. 289.

[38]. **J. J. Hopfield, D. G. Thomas, M. Gershenzon.** 1963, Physical Review Letters, Vol. 10, p. 162.

[39]. **G. Lucovsky, A. J. Varga, R. F. Schwartz.** 1965, Solid State Communication, Vol. 3, p. 9.

[40]. **Jaros, M.** 1980, Adv. Phys, Vol. 29, p. 409.

[41]. **D.G. Thomas, J. J. Hopfield.** 1966, Physical Review, Vol. 150 , p. 680.

[42]. **Ch. Uihlein, L. Eaves.** 1982, Physical Review B, Vol. 26, p. 4473.

[43]. **G. S. Pomrenke, H. Ennen, W. Haydle.** 1986, Journal of Applied Physics, Vol. 59, p. 601.

[44]. **T. F. Kuech, D. J. Wolford, E. Veuhoff, V. Deline, P. M. Mooney, R. Potemski, J. Bradley.** 1987, Journal of Applied Physics , Vol. 62, p. 632.

[45]. **Y. R. Yuan, K. Mohammed, M. A. A. Pudensi, J. L. Merz,.** 1984, Applied Physics Letters, Vol. 45, p. 739.

[46]. **H. Kawai, K. Kaneko, N. Watanabe.** 1984, Journal of Applied Physics, Vol. 56, p. 463.

[47]. **M. Tanaka, H. Sakaki.** 1987, Journal of Crystal Growth, Vol. 81, p. 153.

[48]. **D. J. Wolford, T. F. Kuech, L. A. Bradley, M. A. Gell, D. Ninno, M. Jaros,.** 1986, Journal of Vacuum Science and Technology, Vol. B4, p. 1043.

[49]. **Wolford, D. J.** s.l. : World Publishing, 1987. 18th Int Conf on the Physics of Semiconductors. p. 1115.

[50]. **D. C. Reynolds, D. C. Look, B. Jogm, C. E. Stutz, R. Jones, K. K. Bajaj,.** 1994, Physical Review B, Vol. 50 , p. 11710.

[51]. **R. C. Miller, D. A. Kleinman, W. A. Nordland, Jr. A.C. Gossard.** 1980, Physical Review B , Vol. 22, p. 863.

[52]. **W. Bludau, E. Wagner.** 1976, Physical Review B, Vol. 13, p. 5410.

[53]. **D. J. S. Beckett, M. K. Nissen, M. L.W.Thewalt.** 1991, Canadian Journal of Physics, Vol. 69, p. 427.

[54]. **D. J. Wolford, J. A. Bradley, K. Fry, J. Thompson.** s.l. : Springer-Verlag, 1985. Proc. of the 17th Int. Conf on the Physics ofSemlconductors . p. 627.

[55]. **K. Domen, M. Kondo, T. Tanahashi.** 1992, Institute of Physics Conference Series, Vol. 129, p. 447.

[56]. **S. S. Kocha, M. W. Peterson, A. J. Nelson, Y. Rosenwaks, D. J. Arent, J. A. Turner.** 1995, Journal of Physical Chemistry, Vol. 99, p. 744.

[57]. **S. Naritsuka, T. Nishinaga.** 1997, Journal of Crystal Growth , Vol. 174, p. 622.

[58]. **J. Krustok, J. Madasson, K. Hjelt, H. Collan.** 1995, Solid State Communications, Vol. 94, p. 889.

[59]. **J. Krustok, V. Valdna, K. Hjelt, H. Collan.** 1996, Journal of Applied Physics, Vol. 80, p. 1757.

[60]. **J. Krustok, H. Collan, K. Hjelt, M. Yakushev, A. E. Hill, R. D. Tomlinson, H. Mandar, H. Neumann.** 1998, Journal of Applied Physics, Vol. 83, p. 7867.

[61]. **J. Krustok, H. Collan, M. Yakushev, K. Hjelt.** 1999, Physica Scripta, Vol. T79, p. 179.

[62]. **J. Krustok, J. H. Schon, H. Collan, M. Yakushev, J. Madasson, E. Bucher.** 1999, Journal of Applied Physics, Vol. 86, p. 364.

[63]. **J. Krustok, J. Raudoja, H. Collan.** 2001, Thin Solid Films, Vol. 387, p. 195.

[64]. **D. Macdonald, J. Tan, T. Trupke.** 2008, Journal of Applied Physics, Vol. 103, p. 073710.

[65]. **E. Przezdziecka, L. Wachnicki, W. Paszkowicz, E. Lusakowska, T. Krajewski, G. Luka, E. Guziewicz, M. Godlewski.** 2009, Semiconductor Science and Technology, Vol. 24, p. 105014.

[66]. **J. A. Luna-Lopez, A. Morales-Sanchez, M. Aceves-Mijares, Z. Yu, C. Dominguez.** 2009, Journal of Vacuum Science and Technology A, Vol. 27(1), p. 57.

[67]. **J. Danhof, C. Vierheilig, U. T. Schwarz, T. Meyer, M. Peter, B. Hahn, M. Maier, J. Wagner.** 2009, Physica Status Solidi C, Vol. 6(S2), p. S747.

[68]. **E. Olsen, A. S. Flo.** 2011, Applied Physics Letters, Vol. 99, p. 011903.

[69]. **J. Kistner, X. Chen, Y. Weng, H. P. Strunk, M. B. Schubert, J. H. Werner.** 2011, Journal of Applied Physics, Vol. 110, p. 023520.

[70]. **P. Li, S. Deng, L. Zhang, G. Liu, J. Yu.** 2012, Chemical Physics Letters, Vol. 531, p. 75.

[71]. **T. Trupke, R. A. Bardos.** s.l. : IEEE, 2005. Proceedings of the 31st IEEE PVSC. p. 903.

[72]. **T. Trupke, R. A. Bardos, M. D. Abbott, J. E. Cotter.** 2005, Applied Physics Letters, Vol. 87, p. 093503 .

[73]. **R. A. Bardos, T. Trupke, M. C. Schubert, T. Roth.** 2006, Applied Physics Letters, Vol. 88, p. 053504.

[74]. **T. Trupke, R. A. Bardos, M. C. Schubert, W. Warta.** 2006, Applied Physics Letters, Vol. 89, p. 044107.

[75]. **A. G. Chynoweth, K. G. McKay.** 1956, Physical Review , Vol. 102, p. 369.

[76]. **V. J. Bruce, ,.** s.l. : IEEE, 1993. Proceedings of the 31st Reliability Physics Symposium. p. 178.

[77]. *http://www.usa.hamamatsu.com/en/products/system-division/semiconductor-industry/failure-analysis/phemos-2000.php*. [Online] 2000.

[78]. **A. Perez-Rodriguez, A. Cornet, J. R. Morante, J. Jimenez, P. L. F. Hemment, K. P. Homewood.** 1991, Journal of Applied Physics , Vol. 70, p. 1678.

[79]. **E. Daub, P. Würfel.** 1995, Physical Review Letters, Vol. 74, p. 1020.

[80]. **Y. Koshka, S. Ostapenko, J. Cao, J. P. Kalejs.** s.l. : IEEE, 1997 . Proceedings of the 26th IEEE PVSC. p. 115.

[81]. **E. Daub, P. Klopp, S. Kugler, P. Würfel.** s.l. : H. S. Stephens and Associates, 1994 . Proceeding of the 12th EPVSC. p. 1772.

[82]. **I. Tarasov, S. Ostapenko, V. Feifer, S. McHugo, S. V. Koveshnikov, J. Weber, C. Haessler, E.-U. Reisner.** 1999, Physica B , Vol. 549 , p. 273.

[83]. **S. Ostapenko, I. Tarasov, J. P. Kalejs, C. Haessler, E. U. Reisner.** 2000, Semiconductor Science and Technology, Vol. 15, p. 840.

[84]. **I. Tarasov, S. Ostapenko, K. Nakayashiki, A. Rohatgi.** 2004, Applied Physics Letters , Vol. 85, p. 4346.

[85]. **M. D. Abbott, J. E. Cotter, F. W. Chen, T. Trupke, R. A. Bardos, K. C. Fisher.** 2006, Journal of Applied Physics, Vol. 100, p. 114514.

.....ൠ.....

Chapter 2

EXPERIMENTAL TECHNIQUE

2.1 Introduction

Photoluminescence (PL) spectroscopy is an important optical spectroscopic technique for semiconductor material characterization. As we have discussed in chapter 1, from the PL response of materials, information regarding recombination mechanisms [1, 2], presence of defects & impurities [3, 4], effects of surface passivation [5] and post-deposition treatments [6], quantum efficiencies etc can be obtained. Not just for PL spectroscopy, be it any optical spectroscopic technique, there should be three essential components - a light source, light dispersing elements and a light detector. There has been a switch over from broad light sources to lasers because they are monochromatic, focussed and intense sources [7]. Currently lasers are the most preferred sources for PL measurements. Conventional PL techniques make use of scanning stage monochromator equipped with Photomultiplier tube (PMT) or single element detector but the problem with this technique is that even for taking a single spectrum considerable time is required [8, 9]. An imaging spectrometer mounted with an array detector is a good option for rapid and simultaneous measurements. Multichannel detectors were provided initially with silicon intensified target (SIT) vidicon detectors [10], photodiode array detectors (PDA) [11] and more recently with charge coupled device (CCD) arrays. Modern PL

systems are equipped with flexible fibre optic inputs, flat field internal optical components and sensitive CCDs which have greatly enhanced the versatility of this technique.

2.2 Details regarding the PL experimental set up used in this work

Figure 2.1 is a schematic of the experimental set up used for PL measurements included in this thesis.

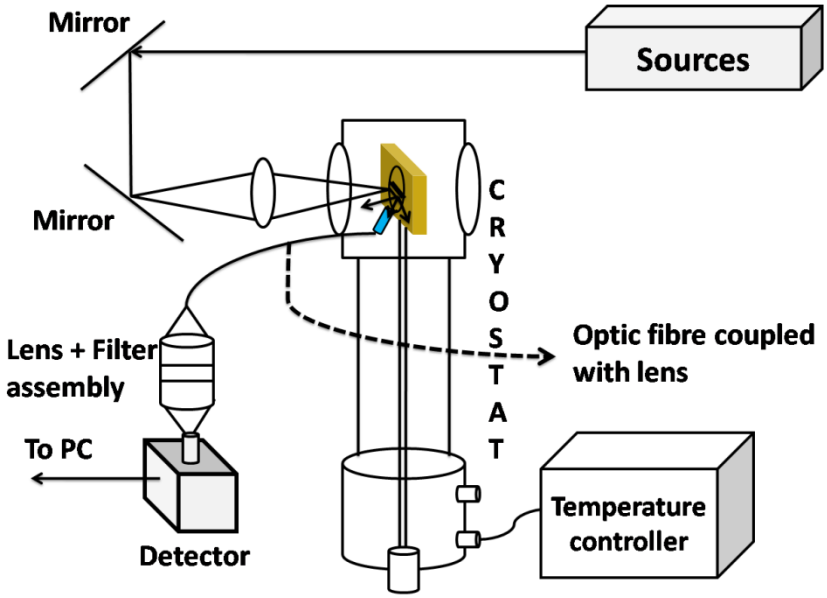

Figure 2.1: Experimental set up used for PL measurements.

We can use this experimental set up for PL measurements in the temperature range from 10-300 K. Reducing temperature brings down thermal noise and temperature dependence of PL emission from materials can be studied. Depending on the bandgap of the material under study, laser with the corresponding excitation wavelength can be chosen. With the help of two detectors we can monitor emission ranging from 350 -1730 nm.

2.3 Specifications of different components of the PL measurement set up

2.3.1. Excitation sources

Depending on the bandgap of the material under study, different lasers were selected.

2.3.1.1 He-Cd laser

He-Cd laser (Kimmon Koha Ltd.) was used for studying wide bandgap samples like zinc oxide (ZnO) and zinc sulphide (ZnS) whose bandgaps are 3.3 and 3.5 eV respectively. This laser can be used to study materials with bandgaps up to 3.82 eV. Some basic features of the laser are:

- Has two output wavelengths- 325 nm and 442 nm. The output powers of 325 and 442 nm wavelengths are respectively 20 mW and 80 mW.
- Unfocussed beam diameter is 1±5 % mm with a divergence of 0.3±5 % mrad.

2.3.1.2 He-Ne laser

He-Ne laser (Melles Griot) was used for studying copper zinc tin sulphide (CZTS) samples with a bandgap of 1.5 eV. Some basic features of the laser are:

- Output wavelength of 632.8 nm having maximum power of 15 mW was used.
- Unfocussed beam diameter is 0.62±5 % mm with a divergence of 0.5±5 % mrad.

2.3.2 Detection system

Any simple detection system would comprise of lens and sensor. Using two detectors we were able to cover emissions spanning the entire UV-Vis-IR regions. The detectors used were spectrophotometers which measures light

intensity as a function of wavelength. This is done generally by dispersing light into its constituent wavelengths and monitoring the intensities using, generally a CCD, and then plotting the results as a graph of intensity vs. wavelength.

We have made use of spectrophotometers by 'Ocean Optics', in which the optics is quite simple. Light enters through a slit and is incident on a concave mirror which reflects the light to a dispersion grating. The grating is reflecting type and light after dispersion is reflected to another concave mirror which focuses the light on to the detector which is nothing but a charge coupled device (CCD).Each pixel on the CCD is designed to measure intensity of specific wavelengths of light. When more photons are incident, the electrical signal generated is also intense; in short the intensity of light of specific wavelength determines the strength of the electrical signal.

2.3.2.1 Ocean Optics USB 2000 spectrophotometer

It has a slit width of 25 μm and a grating with 600 lines/mm. The detector is 2048 pixel (SONY ILX511) charge coupled device (CCD) detector with an average sensitivity of 0.7 in the 350-1000 nm wavelength range. Peak efficiency is obtained in the 400-700 nm range as it contains a grating that is blazed at 500 nm. Integration time can be varied from 3 ms to 65 s. The f/# number of this spectrometer is f/4 with a focal length of 40 mm. Optical resolution in the 350-900 nm range is 1.67 nm.

2.3.2.2 Ocean Optics NIR 512 spectrophotometer

It has a slit width of 50 μm and a grating with 1200 lines/mm. The detector attached is a thermoelectrically cooled 512 element, InGaAs array detector (Hamamatsu G9204-512). The average sensitivity of the array is 0.7 in the wavelength range 900-1700 nm. The f/# number of this spectrometer is f/4 with

a focal length of 40 mm. The integration time can be varied from 1 ms to 5 s. Optical resolution is 2.34 nm in the 900-1700 nm wavelength range.

2.3.3 Optical fibers

Signal collection was done using a reflection fibre probe containing 5 illumination fibres and 1 read fibre, each having a core diameter of 400 μm. The fibre has a flexible metal sheathing with sub-miniature version A (SMA) termination so that it can be connected to the spectrophotometer. Bifurcated fibre cable was used when two spectrophotometers have to be operated simultaneously so that the entire wavelength range 350-1700 nm can be scanned. An in-line filter holder with SMA termination is connected to the spectrophotometer to avoid detection of excitation wavelength while recording the PL spectrum.

2.3.4 Software package

The custom-made software OOIBase32, used for controlling the spectrophotometers and recording data has many interesting features. There was an option to take several measurements and average the readings obtained. A boxcar averaging program is provided which can be used to improve signal-to-noise ratio. The software also has a provision to provide electronic shutter using which signal collection timing can be controlled.

2.3.5 Closed cycle liquid 'He' cryostat

The closed cycle 'He' optical cryostat (Model No: CCS-100/202) from Janis Research Inc. was used for lowering sample temperatures up to 15 K. The cryostat has a 'two stage cold head' and sample was mounted on a sample mount made of copper, fixed on the cold finger of diameter 3.81 cm. A 25 Ω heater is provided for raising the sample temperature. A 'Si' diode is provided as a sensor for monitoring the temperature variations. A temperature controller by

Lakeshore (Model 321) was used to vary the sample temperature with an accuracy of ± 1K.

2.3.6 Additional features for accurate signal collection

The sample is mounted on the cold finger of cryostat which is enclosed by a shroud with four optical windows. The sample chamber is evacuated to low pressure (~10^{-5} Torr) so that low temperatures of ~15 K can be obtained easily. Non-radiative events are suppressed at such temperatures and thus PL measurements at low temperature are better resolved and more intense. For effective collection of emission, one of the optical windows is removed and a steel mounting is provided which is open at one end. The other end of the steel mounting is a cylindrical tube extending to the interior of the sample chamber terminating at a distance of <1 cm from the sample holder and this end is closed with ordinary glass. A Teflon insertion is given through the steel mounting and it has a small hole through which the optical fibre can be inserted and emission can be collected from as close as < 1 cm from the sample. So without breaking vacuum inside the sample chamber, adjustments can be done with the position of the optical fibre to enable efficient collection.

For spatial mapping PL measurements, i.e., PL measurement from different points of the same sample, the sample was mounted on to a translation stage equipped for movements in the XY direction. This translation stage was controlled using a stepper motor control and translation step size of 1mm was given so as to overcome limitation imposed by excitation beam spot-size. PL spectrum can be recorded from many points of the same sample. The emission intensity obtained at each point is noted and plotted as a color map. The X- and Y-axes of the plot shows the different points from which PL spectra are recorded. Colors in the map indicate the values of PL intensity at these points. Colors in the map range from blue to red where blue and red represent the

minimum and maximum values of PL intensity. Such a representation would be helpful in analyzing how spatial variation can cause differences in PL spectra.

2.3.7 Analysis of PL spectrum recorded using this experimental set up

As we had discussed in Chapter 1, PL spectra can arise due to different transitions. Analysis of PL spectrum is as important as recording the spectrum. There are many factors on which PL spectrum depends- the important factors being temperature and excitation power. We can understand the nature of transition and also find the position of various defects within the bandgap by calculating activation energies. This is done by monitoring the variation of PL emission with temperature as well as excitation power.

2.3.7.1 Temperature dependence of PL emission

Theoretically, PL intensity bears dependence with temperature as

$$\frac{I(T)}{I(0)} = \frac{1}{\left[1 + Ce^{-\frac{\Delta E}{kT}}\right]} \quad \text{----------(1)}$$

where *I(T)* is the PL intensity at any temperature *T*,*C* is a constant treated as a measure of capture cross-section and ΔE is the activation energy.

To calculate activation energy, PL spectrum was recorded for different sample temperatures ranging from 15 to 300 K. A graph was plotted with integrated PL intensity values on Y-axis and 1000/T on X-axis. This plot is called the Arrhenious plot [see Figure 2.2].

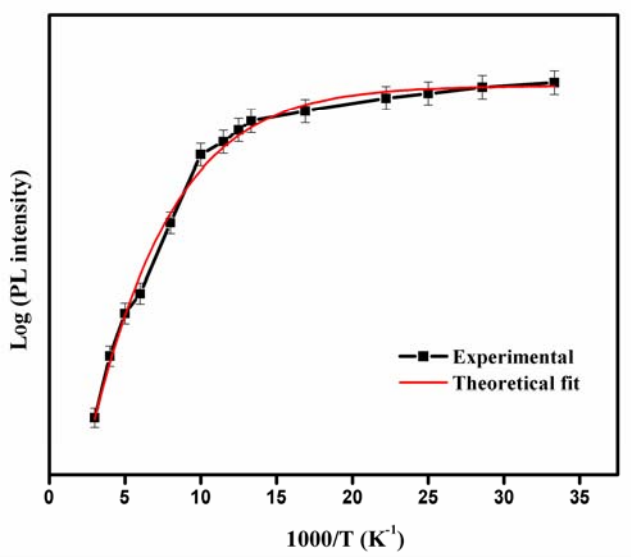

Figure 2.2: Arrhenious plot.

Theoretical fitting to this experimental curve, is done using software 'Origin'. The red line in Figure 2.2 shows the theoretical fit to the experimental curve [black line]. From the fitting parameters yielded by the software, activation energy can be obtained.

2.3.7.2 Excitation power dependence of PL emission

PL intensity I, is related to excitation power P, as

$$I \alpha P^{\gamma} \text{ ---------- (2)}$$

where 'γ' is an exponent which decides the transition type. 'γ'< 1 or ~1, implies that the transition is defect assisted and 'γ'value between 1 and 2 is typical for excitonic transitions [12]. Taking log on both sides of equation (2), we obtain the equation for a straight line whose slope is 'γ'.

To understand the transition type of a particular emission obtained, PL spectrum is recorded for different excitation powers (excitation power varied

using neutral density filters). A graph is plotted between log (PL intensity) on Y-axis and log (excitation power) on X-axis [Figure 2.3]. Slope of the graph gives value of 'γ'. Depending on the value that 'γ' takes, we can identify the transition type.

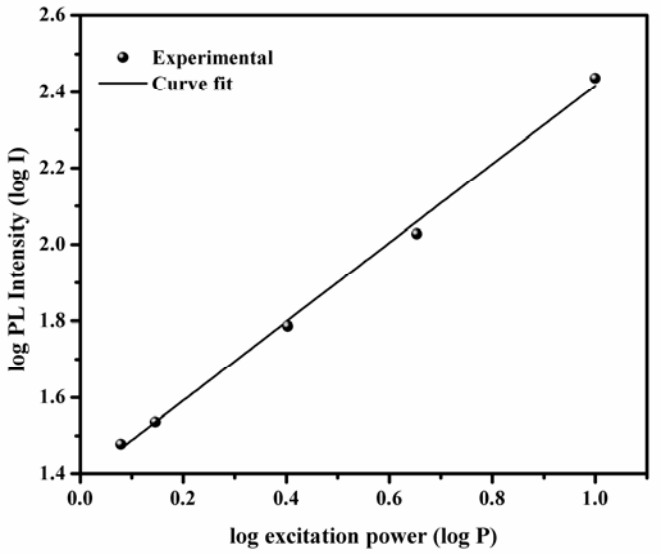

Figure 2.3: Log-log plot of PL intensity with excitation power.

'γ' value less than or nearly equal to 1 suggests the transition is defect assisted; thus it can either be donor-to-acceptor pair (DAP) or free-to-bound transition. The important feature of DAP transition is the blue shift in PL peak energy with increase in excitation power and red shift in PL peak energy with increasing temperature. Thus if we obtain a 'γ' value less than or nearly equal to 1, then by monitoring the variation of PL peak energy with excitation power and temperature the transition type can be understood.

2.3.8 Details about other techniques mentioned in the current study

In the current study we have chosen zinc oxide (ZnO), copper zinc tin sulphide (CZTS) and zinc sulphide (ZnS) thin films prepared using chemical

spray pyrolysis (CSP) technique. Automated CSP technique has been used for film deposition and films prepared by varying different spray parameters like spray rate, precursor, substrate temperature etc were selected for study.

We have collected supporting evidences from other characterization techniques, for some specific samples. X-ray diffraction (XRD) studies have been done using Rigaku (D. Max. C) X-ray diffractometer (employing Cu-Kα line (λ = 1.5405 Å) and Ni filter) operated at 30 kV and 20 mA. Raman studies were done using Jobin Yvon Horiba LABRAM-HR visible (400-1100 nm) with spectral resolution of 1 cm^{-1}. X-Ray Photoelectron spectroscopy (XPS) measurements were done using ULVAC-VHI unit (Model- ESCA 5600 CIM) employing argon ion sputtering. J-V measurements were done using Keithley 236 Source Measure Unit.

2.4 Aim of the present work

As part of our work, we have selected certain materials like zinc oxide (ZnO), copper zinc tin sulphide (CZTS) and zinc sulphide (ZnS) which are preferred candidates for transparent conducting oxide (TCO), absorber and buffer layers in thin film solar cells. We have also selected In_2S_3/MEH-PPV bilayer heterojunction for study. The major aim of this doctoral thesis work is not only to use PL as a characterization technique suitable for analysis of each individual layer of a solar cell but also to find the obtainable open-circuit voltage from a solar cell.

References

[1]. **V. Vinciguerra, G. Franzo, F. Priolo, F. Iacona, C. Spinella.** 2000, Journal of Applied Physics, Vol. 87, p. 8165.

[2]. **K. Watanabe, H. Tamaoka, M. Fuji, S. Hayashi.** 2002, Journal of Applied Physics, Vol. 92, p. 4001.

[3]. **N. A. Sobolev, O. B. Gusev, E. I. Shek, V. Vdovin, T. G. Yugova, A. M. Emel'yanov.** 1998, Applied Physics Letters, Vol. 72, p. 3326.

[4]. **E. Degoli, S. Ossicini, D. Barbato, M. Luppi, E. Pettenati.** 2000, Materials Science and Engineering B, Vols. 69–70, p. 444.

[5]. **B. G. Fernandez, M. Lopez, C. Garcia, A. Perez-Rodriguez, R. Moerante, C. Bonafos, M. Carrada, A. Claverie.** 2002, Journal of Applied Physics, Vol. 91, p. 798.

[6]. **Y. C. Fang, W. Q. Li, L. J. Qi, L. Y. Li, Y. Y. Zhao, Z. J. Zhang, M. Lu.** 2004, Nanotechnology, Vol. 15, p. 494.

[7]. **O. H. Y. Zalloum, M. Flynn, T. Roschuk, J. Wojcik, E. Irving, P. Mascher.** 2006, Review of Scientific Instruments, Vol. 77, p. 023907 .

[8]. **M. Fuji, M. Yoshida, S. Hayashi, K. Yamamoto.** 1998, Journal of Applied Physics, Vol. 84, p. 4525.

[9]. **F. Iacona, G. Franzo, C. Spinella.** 2000, Journal of Applied Physics, Vol. 87, p. 1295.

[10]. **J. W. Olesik, J. P. Walters.** 1984, Applied Spectroscopy, Vol. 38, p. 578.

[11]. **T. Vo-Dinh, D. Eastwood.** *Laser Techniques in Luminescence Spectroscopy.* s.l. : ASTM International , 1990. p. 175.

[12]. **K. Hones, E. Zscherpel, J. Scragg, S. Siebentritt.** 2009, Physica B, Vol. 404, p. 4949.

.....ஜ۞ஜ.....

Chapter 3

INDIRECT ESTIMATION OF ELECTRICAL PROPERTIES OF ZnO THIN FILMS USING PHOTOLUMINESCENCE TECHNIQUE

3.1 Introduction

ZnO is a II-VI compound with excellent optoelectronic properties namely wide band gap, high exciton binding energy, strong luminescence etc which makes this material an inevitable component in the optoelectronics industry [1-5]. Researchers are also keen to explore this material even though work has been going on for more than three decades. This is because, the potential of this material unexplored is still by and large greater than what has been explored.

Our interest in this material is limited to developing it as transparent conducting oxide (TCO) for photovoltaic (PV) applications. Commercially available TCO is indium tin oxide (ITO) which unfortunately is still precious. Developing an alternative to ITO with performance at par and reasonable cost is the major pursuit. We have used CSP for deposition of films; so the concern of cost-effectiveness is addressed to a certain extent. For use as TCO, resistivity should be brought down to the order of 10^{-4} Ω.cm which practically seems impossible to attain in pristine ZnO films. So some treatments or doping might be necessary to bring down the resistivity so that ZnO fits in to the slot of TCO. Generally two probe, four probe, Hall measurements etc employed to measure resistivity of the sample, require contacts and can tamper the sample surface. A

non-contact mode technique is thus highly preferred. Photoluminescence (PL) is an optical technique which can offer electrical characterization and it is also a selective and sensitive probe of discrete electronic states. ZnO is a material exhibiting strong luminescence. Excitation in PL is by optical means and since contacts are absolutely unnecessary, information can be obtained from both highly resistive as well as conducting samples. The major aim of this work was to analyze the suitability of PL to evaluate the variation in resistivity of ZnO thin films. A detailed review of various works so far reported on PL studies in ZnO is discussed in the following section.

3.2 Review on PL studies in ZnO

Krunks et al. [6] have reported the deposition of ZnO thin films by spray pyrolysis and the effect of 'In', 'Ce' and 'Eu' doping on the structural, optical and electrical properties of ZnO. Films exhibit excitonic emission and this is taken as a signature of crystalline quality of the films. Nanocrystalline ZnO thin films were prepared by Zhang et al. [7] through oxidation of ZnS thin films. Strong UV emission and barely observable visible emission was recorded from the samples. Quality of the films was adjudged by the presence of free exciton and bound exciton emission peaks at low temperatures. The effect of face to face annealing on the luminescence properties of ZnO thin films was reported by Wang et al. [8] where they have observed that it is an excellent technique for enhancement of Near Band Edge Emission (NBE) and control of non radiative recombination centres.

The effect of doping of radioactive '^{111}In' on the structural and optical properties of nanocrystalline ZnO has been dealt with, by Agne et al. [9]. The onset of crystal growth was marked by incorporation of '^{111}In' and this was reflected in PL spectrum as the presence of bound excitonic emission peak. Excitation dependent PL analysis has been carried out by Zhang et al. [10]. They

have observed UV, blue as well as bluish green emission peaks for various excitations, from films prepared on sapphire, glass, silicon and quartz substrates. ZnO thin films were grown on InP substrates and the effect of thermal annealing on various properties has been studied by Shim et al. [11]. Degradation of crystallinity of thin films was the reason for reduced intensity as well as shift in the peak position of UV emission. Kim et al. [12] prepared p-type ZnO thin films by phosphorus doping. A strong PL peak at 3.35 eV could be recorded and the emission could be assigned to neutral acceptor bound exciton.

Viswanathamurthi et al. [13] studied zinc oxide nanofibres and have observed two emissions- one in ultraviolet and the other in green. Djurisic et al.. [14] reported green luminescence from ZnO tetrapod and multipod structures as occurring from surface defects. In order to confirm that surface defects are responsible for the emission, the structures were coated with a surfactant which significantly reduced the emission intensity. Shan et al. [15] reported on 'Mg' doped ZnO thin films that, increase in dopant concentration has a significant impact on band gap as well as PL spectra. Defect related PL could be reduced by 'Mg' doping. With progress in time, defect related PL from films subsided to a large extent due to incorporation of oxygen, as sub band gap emission was associated with oxygen vacancies. The authors have quantified this in terms of ratio of intensity of NBE peak to defect related peak.

Ratheesh et al. [16] have come up with interesting observations on properties of indium doped ZnO thin films. Emissions at 408, 590 and 688 nm have been observed as a result of indium doping and have been attributed to radiative recombination at interface traps in the grain boundaries, localized indium impurities and oxygen interstitials respectively. Undoped ZnO nanorods and ZnO:In nanorods were analyzed by Chen et al. [17]. Strong UV emission and feeble visible emission was observed in ZnO nanorods. Due to indium incorporation

quenching of UV emission was observed and possibility of improved photocurrent is opened up. Fan et al. [18] synthesized ZnO thin films on 'Si' substrates using PLD technique. Defect related emission in the PL spectra was assigned as a transition from conduction band to O_{Zn} defect. It was observed that both high and low substrate temperatures suppress the defect related emission.

Enhanced UV emission was observed in 'Ag' doped ZnO films and this is due to creation of more excitons with relative ease. 'Ag' doping has little impact on visible emission. ZnO-Ag_2O has thus been quoted as a promising semiconductor material for UV light emission [19]. A study on the properties of 'In' doped dodecagonal ZnO disks was reported by Liu et al. [20]. Room temperature PL spectra of the samples indicate an enhancement as well as broadening of UV emission peak as a result of doping. Borseth et al. [21] have used PL to study vacancy of oxygen and vacancy of zinc in single crystalline ZnO samples annealed in different conditions. It has been observed that the choice of annealing ambient alters the position of defect related emission.

Carrier recombination processes have been evaluated in ZnO nanocrystals and quantum dots using PL by Fonoberov et al. [22]. Experimental data suggests that UV emission in ZnO quantum dots is due to recombination of acceptor bound excitons. In larger size ZnO nanocrystals, dominant recombination at low temperatures involves acceptor bound excitons and at higher temperatures donor bound excitonic recombination dominates. Photoluminescence properties of ZnO thin films grown on 'Si' substrates using RF magnetron sputtering, with and without ITO buffer have been reported by Teng et al. [23]. PL characteristics depend on oxygen partial pressure as well as type of substrate. Enhanced PL intensity has been observed from ZnO films on ITO buffer layer by giving appropriate annealing treatment. Properties of ZnO/ITO/ZnO sandwich structures have been studied by Hong et al. [24]. Enhanced near band edge emission was

observed for ZnO films coated on ITO and ITO/ZnO buffer layer compared to that coated on bare fused silica substrates.

Przezdziecka et al. [25] performed PL and structural studies on 'N' or 'As' doped ZnO layers. Luminescence related to 'N' as well as 'As' acceptor could be distinguished from the features in PL spectrum. Jiao et al. [26] prepared nitrogen doped ZnO thin films for different nitrogen concentrations using plasma-assisted molecular beam epitaxy. From low temperature PL spectra, a strong red shift and broadening of DAP emission band as a function of nitrogen concentration was observed. Xiaong et al. [27] have observed a correlation between size, defects and PL in ZnO nanoparticles. Particles of larger size exhibited fewer surface impurities; oxygen vacancy centres are not affected by particle size variations. Near excitonic as well as defect related emission are enhanced in intensity with increase in particle size which indicates that these emissions are non-radiatively quenched by surface defects. ZnO thin films were coated on ITO substrates using RF magnetron sputtering by Teng et al. [28]. It has been observed that exciton related emission depends on oxygen partial pressure and visible emission is independent of oxygen partial pressure. Properties of ZnO thin films deposited on sapphire substrates were studied by Shan et al. [29]. Aging effect of the films was studied and it was observed that NBE was enhanced and Defect Level emission (DLE) was suppressed with progress in time. DLE emission was attributed to oxygen vacancies.

Low temperature PL studies on ZnO nanowires embedded in polymers were done by Richters et al. [30]. The authors have observed quenching of DLE and enhancement of NBE after embedding and have correlated NBE enhancement/DLE reduction to the balling ability of the polymer using molecular dynamics simulation. Guziewicz et al. [31] have deposited ZnO for transparent electronics and organic heterojunction applications using atomic layer deposition. In this

report the authors have commented of a correlation between optical and electrical properties. As per their observation, films with weak or no defect band exhibit excellent electrical properties. Studies on 'Er' doped ZnO has been discussed by Yamaoka et al. [32] where the authors have observed an emission at 1.54 μm originating from $^4I_{13/2}$ -$^4I_{15/2}$ transitions in 'Er^{3+}' ions in addition to the emission arising from host ZnO lattice. Yu et al. [33] have discussed the relation between PL and conductivity of ZnO thin films prepared using PLD. The authors have observed a correlation between PL, electrical conductivity and oxygen partial pressure. The authors have plotted the ratio of intensities of visible to near band edge emission (I_{DLE}/I_{NBE}) and conductivity and they have commented that when I_{DLE} is high, conductivity is also high.

Studies on developing p-type ZnO thin films by co-doping with 'B-N' were reported by Sui et al. [34]. Two new emission bands at 3.303 and 3.208 eV were observed and have been attributed to 'B-N' co-doping. The effect of doping 'Na' in ZnO thin films has been dealt with, by Lu et al. [35]. Due to the incorporation of 'Na' in ZnO thin films the emission has shifted to green which in undoped samples was predominant in the yellow-green region of electromagnetic spectrum. Annealing temperature and its effects on the properties of ZnO films covered by TiO_2 nanoparticles was reported by Xu et al. [36]. UV emission was enhanced and green emission suppressed for such films. Annealing at a relatively high temperature resulted in suppression of UV emission intensity. Violet and blue emissions have appeared and this has been related to atomic interdiffusion between TiO_2 nanoparticles and ZnO thin films.

Cho et al. [37] developed polycrystalline ZnO films capable of lasing action by oxidation of metallic Zn films. The PL spectra recorded was devoid of any defect related emission and had only the UV emission with a very small FWHM of 23 meV. Sentosa et al. [38] reported on the temperature dependent PL

studies of ZnO films grown on YSZ substrates. The authors have taken the small line-width of free exciton emission as a measure of crystallinity and optical quality of the samples. The effect of different spray parameters on the excitonic luminescence in ZnO nanorods was discussed by Karber et al. [39]. The authors have taken the ratio of intensities of NBE and defect related red emission (I_{NBE}/I_{RED}) as a measure of improvement in crystalline as well as optical quality of the samples.

In a work on ZnO nanowires, nanorods and nanoribbons by Dhara et al. [40], the ratio of intensity of NBE to DLE is considered as a measure of improved crystallinity and optical quality. Samples subjected to rapid thermal annealing (RTA) exhibit larger values for the ratio and RTA has been adjudged as an effective method to improve the properties of samples. Zhou et al. [41] deposited ZnO films on silica substrates embedded with 'Ag' nanoparticles prior to ZnO deposition. Bandgap emission can be enhanced or quenched depending on whether resonant coupling occurs between the excitons in ZnO & surface plasmons in Ag nanoparticles or electron transfer occurs from ZnO to 'Ag' nanoparticles. Controlling light emission by using semiconductor-metal coupling is of major use from the device point of view.

Kuo et al. [42] were successful in introducing sub bandgap absorption by embedding nanocrystalline Si quantum dots in ZnO thin films. An emission at 1.81 eV could be recorded as a testimonial for creation of sub bandgap levels. The influence of using GaN and MgO buffer layers on the properties of ZnO thin films was reported by Ting et al. [43]. In this work, the authors suggest that buffer layer is helpful in improving crystalline quality of the sample. Edge emission is quite intense and DLE is weak. The ratio of integrated intensity of DLE to EBE and reciprocal of FWHM from X-Ray rocking curve measurements has been compared and an increase in both the parameters have been correlated

to the enhancement in structural and optical properties. We observed a theoretical work by Noh et al. [44] where they have calculated the n-type doping limit in 'Al' doped ZnO. Doping limit occurs due to formation of V_{Zn}^{2-} compensating centres as they interact with Al_{Zn}^{1+} donors via Coulombic interaction and this interaction favours formation of V_{Zn}^{2-} centres which effectively compensate the n-dopants. Senthil Kumar et al. [45] reported extremely narrow line widths as low as 0.17 meV on undoped ZnO nanowires grown on highly mismatched sapphire substrates. The effect of Group III dopants on the PL spectrum has also been discussed vividly.

Substantially enhanced PL and Raman signals have been obtained from ZnO coated on 'Si' with 'Au' hybrid nanoparticles, by Saravanan et al. [46]. 14-fold enhancement in free-exciton emission intensity has been reported for ZnO-Au sample in comparison with ZnO-Si sample. Defect related emission has been suppressed in ZnO-Au nanoparticles. An interesting work on synthesis of ZnO nanoflowers by reactive vapour deposition was reported by Ai et al. [47]. The authors have observed an improvement in the optical quality when the nanoflowers were given a few nanometers thick coating of epitaxial ZnO. The increase in ratio of UV emission intensity to defect related emission intensity has been given as a proof for improvement in optical quality of the films.

Various aspects of PL spectroscopy have been dealt with in the aforementioned reports. Several authors have mentioned about taking the ratio of integrated intensities of the emissions- either I_{DLE}/I_{NBE} or I_{NBE}/I_{DLE}. Some authors have attributed an increase in I_{NBE}/I_{DLE} to lesser defects in the sample & improved sample quality whereas some others have tried to correlate the variation of I_{DLE}/I_{NBE} with variation in structural properties of the sample. Even though various authors have come up with values for the ratio I_{DLE}/I_{NBE} or I_{NBE}/I_{DLE}, a

quantitative relation has not been proposed between the ratios and electrical properties of ZnO thin films, especially the resistivity. We didn't come across reports where PL has been used to analyze the variation in resistivity of ZnO thin films. In the sections to follow we shall discuss our observations in ZnO thin films and how we progressively arrived at a conclusion that PL measurements are alone sufficient to know the variation in resistivity of ZnO thin films.

3.3 PL studies on ZnO thin films

3.3.1 PL measurement on ZnO samples prepared using different solvents and given post deposition treatment

ZnO thin films deposited on soda lime glass substrates maintained at 450 ^{o}C by spraying 100 ml of 0.3 M solution of zinc acetate dissolved in water, at a spray rate of 7ml/min, were chosen for analysis. Figure 3.1 shows the PL spectrum of samples Z-W, i.e., ZnO thin films prepared with water as solvent.

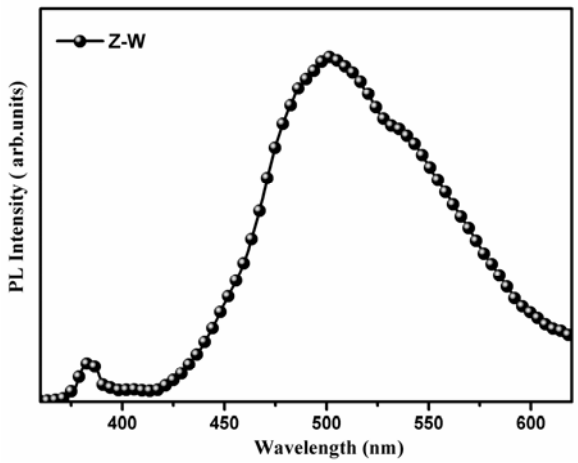

[1]Figure 3.1: PL spectrum of ZnO thin films deposited with water as solvent.

[1] There are two peaks in the emission spectrum- near band edge emission (NBE) at 380 nm, which is an indicator of quality & crystallinity of ZnO thin films and deep level emission (DLE) centered at 500 nm, which is related to the defects present in the sample. In sample Z-W, DLE is prominent which indicates a large concentration of defects and thus poor sample quality.

Films were a bit foggy in appearance [transmittance ~ 70% only]. I-V measurements indicate that films Z-W are highly resistive [~ 80 Ω.cm]. Thus films prepared with water as solvent were not found to be useful as TCO as the films showed poor transparency, conductivity and high defect concentration. There are reports that film transparency becomes better when alcohol is incorporated in the solvent [48, 49]. PL studies were also done on films prepared with propanol-water mixture and ethanol-water mixture as solvent. Films were named ZP and ZE respectively. The PL spectra of samples ZP and ZE is shown in Figure 3.2.

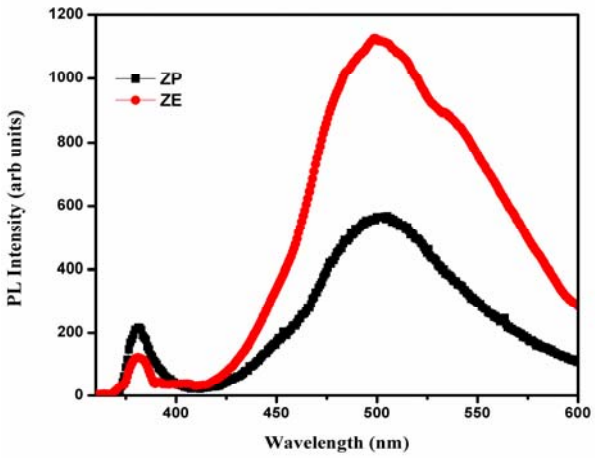

[2]Figure 3.2: PL spectra of films ZP and ZE.

As the priority was to develop TCO, resistivity had to be brought down further. We have already reported the effectiveness of a post deposition technique namely 'inversion cooling' in improving the properties of ZnO thin films. In inversion cooling, the sample surface is isolated from atmospheric contact immediately after deposition by inverting the sample on to a suitable

[2] DLE peak is more intense in ZE, indicating higher defect concentration compared to ZP. Silver electrodes of dimension 5 mm X 1 mm were given on the sample and I-V measurements were done using Keithley236 Source Measure unit. We observe that resistivity of ZP [40 Ω.cm] is lower than that of ZE [70 Ω.cm].

base material. The sample is then allowed to cool to room temperature. This process has been described in a report by Vimalkumar et al. [50]. Among the samples Z-W, ZE and ZP, resistivity of ZP was low and using 'inversion cooling', resistivity of ZP could be brought down from 40 Ω.cm to 2.4 X 10^{-2} Ω.cm. In order to find out whether there is any drastic change in PL spectrum on inversion, similar to the change observed in resistivity, PL measurement was done on samples ZP-R (ZP devoid of inversion) and ZP-I (ZP subjected to inversion cooling) [See Figure 3.3].

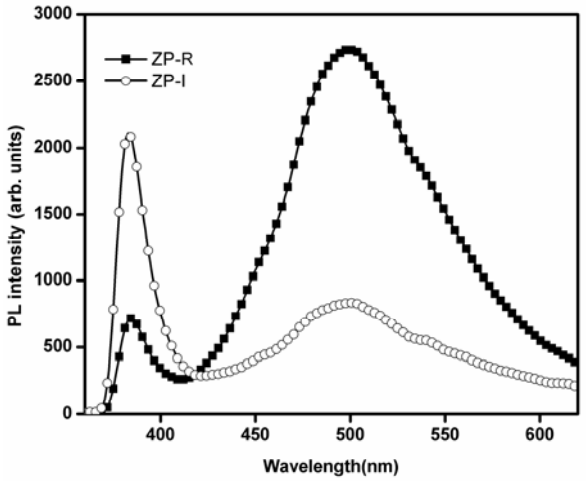

[3]Figure 3.3: PL spectrum of films ZP-R and ZP-I.

Thus it is clear that inversion has a tremendous impact on PL spectrum also. An explanation for reduction in resistivity has been given by Busch and Schade [51] in their book 'Lectures on Solid State Physics'. According to the authors, ZnO is a material where after film deposition, there is a tendency for 'Zn^{2+}' ions within the film to react with atmospheric oxygen and form resistive

[3] NBE is enhanced (indicating good sample quality) and DLE is quite suppressed (low defect concentration) in sample ZP-I compared to ZP-R. Resistivity of ZP-I (2.4 X 10^{-2} Ω.cm) is also orders less than that of ZP-R (40 Ω.cm). Transparency of ZP-I improves; in total, sample quality improves on inversion cooling [50].

ZnO layer on the surface. We thus believe that the main reason for reduction in resistivity of sample ZP-I is that we could cut off oxygen incorporation and restrict the formation of resistive ZnO. Such a proposal but needs proof and for that, X-ray Photoelectron Spectroscopy (XPS) studies was done. XPS depth profile studies give a clear idea of depth-wise composition of the sample. Interestingly XPS depth profile of ZP-I indicates a clear reduction in oxygen incorporation compared to ZP-R. Zn/O ratio is also high in ZP-I [50]. From PL spectra we have already seen that, intensity of DLE is curtailed in sample ZP-I; implying that the defect related emission may possibly be related to oxygen. Since emission energy is much less than the bandgap of ~3.3 eV, it has to arise from transitions other than band to band recombination. To understand the type of transition, excitation power dependent PL measurements were done [Figure 3.4]. PL intensity (*I*) is related to excitation power (*P*), as $I \alpha P^{\gamma}$. Value of exponent 'γ' obtained from the log-log plot of PL intensity vs excitation power is ~1, indicating that the transition is defect related. The most favorable explanation for DLE is that it is a transition from conduction band (CB) to some acceptor related to oxygen, probably oxygen antisite defect (O_{Zn}).

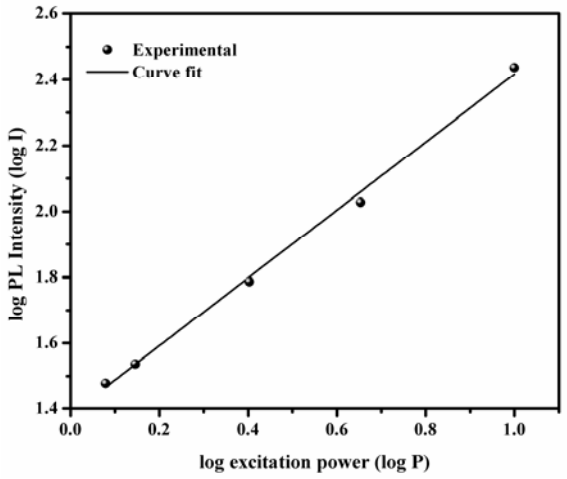

Figure 3.4: Excitation power dependent PL measurements on sample ZP-I.

In order to further confirm that the acceptor defect is due to oxygen, two more samples were analyzed- ZP-I samples vacuum annealed (ZP-Iv) and ZP-Iv subjected to air annealing (ZP-Iva). On vacuum annealing we expect a removal (even though not complete) of oxygen related defects which may reappear on air annealing. Any change for sure will reflect in the PL spectrum and resistivity values also. PL spectrum of samples ZP-Iv and ZP-Iva is shown in Figure 3.5.

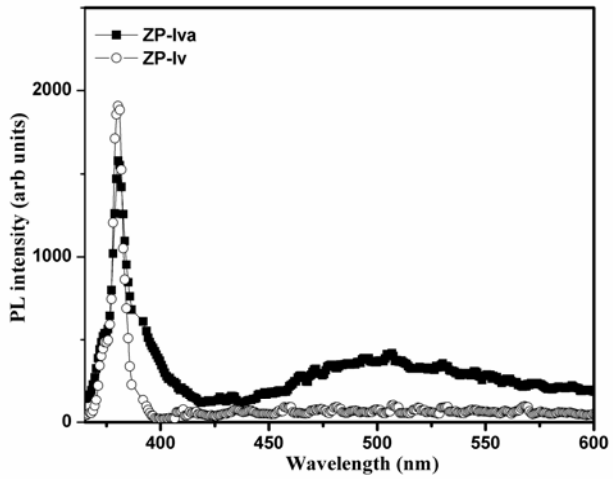

Figure 3.5: PL spectrum of ZnO thin films ZP-Iv and ZP-Iva.

NBE is sharper and DLE quenched in sample ZP-Iv indicating excellent sample quality. NBE is broadened and DLE gains intensity in ZP-Iva indicating oxygen incorporation on air annealing. There is not much consensus on the cause for green emission in ZnO. Many attribute it to vacancy of oxygen (V_O), zinc interstitial (Zn_i), oxygen in zinc antisite (O_{Zn}) etc of which O_{Zn} is appropriate to the energy of the emission in our observations [1, 52-54]. Assigning the acceptor defect to O_{Zn} antisite has been substantiated by irradiation studies on ZnO [55]. Resistivity of ZP-Iv and ZP-Iva are 2 $X10^{-3}$ Ω.cm and 4 X 10^{-1} Ω.cm respectively indicating that on air annealing oxygen incorporation is higher and as a result, resistivity increases.

From the observations on ZP-R, ZP-I, ZP-Iv, ZP-Iva etc we see that oxygen incorporation plays a vital role in deciding the nature of PL spectrum as well as resistivity. When oxygen incorporation is restricted:

- NBE is enhanced and DLE is suppressed
- Resistivity is lowered

Rather than speaking in terms of individual intensities, it is scientific to express in terms of ratio of integrated intensities of DLE to NBE, i.e., I_{DLE}/I_{NBE} [17, 39]. When I_{DLE}/I_{NBE} is small, resistivity is also small and vice versa. A plot of resistivity of samples ZP-R, ZP-I, ZP-Iv and ZP-Iva along with I_{DLE}/I_{NBE} values effectively communicates the idea [Figure 3.6].

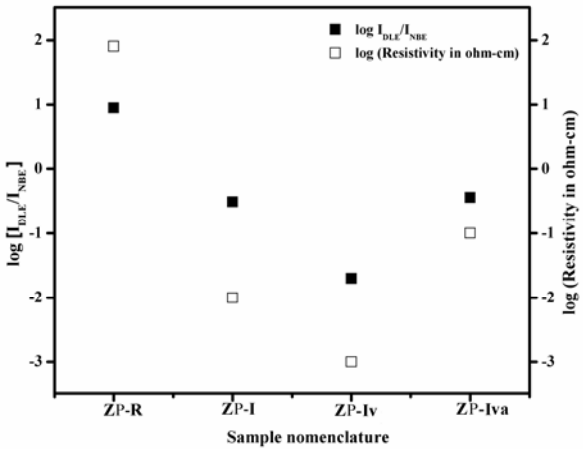

Figure 3.6: Log scale plot of resistivity and I_{DLE}/I_{NBE} for ZnO samples ZP-R, ZP-I, ZP-Iv and ZP-Iva.

All samples chosen for further studies are given the 'inversion-cooling' treatment so as to have the added benefit of inversion. Propanol to water ratio in the solvent was 1:1 for all samples selected for analysis so far. Proportion of alcohol in the solvent is an important parameter [56] that can bring about variation in optoelectronic properties. So, films prepared using different propanol to water ratios in the solvent (namely 0.25:1, 0.42:1, 1:1, 1.5:1 and 2.3:1), were chosen for study. PL spectrum was recorded [Figure 3.7] and resistivity was measured.

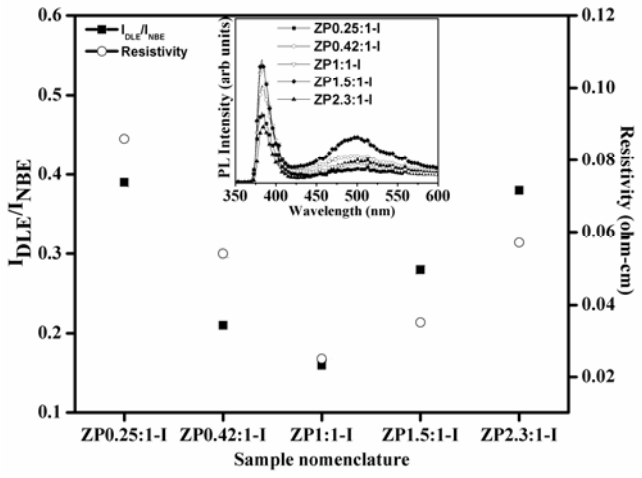

[4]Figure 3.7: I_{DLE}/I_{NBE} and resistivity values plotted for samples prepared using different propanol to water ratios in the solvent.

3.3.2 PL analysis to determine optimum pH

Another parameter that is extremely important in spray pyrolysis is pH of the spray solution. There are reports that pH determines the complexes formed at the beginning of reaction and also plays a role in enhancement of crystallinity, morphology etc of the films formed [57, 58]. In our case, pH control was attained by adding a few drops of acetic acid to the precursor solution. Adding acetic acid to the precursor solution lowers pH and also inhibits hydroxide formation. Films prepared for pH varied in the range 3 to 6 were chosen for study. Samples were named respectively as 3-I, 4-I etc. Acetic acid is not added at all in sample 6-I [pH of spray solution=6]. PL spectra of the samples were recorded. We have observed that films with excellent optical (transmittance- 80 %) and electrical properties (resistivity- 2.4 $X10^{-2}$ Ω.cm) were obtained when the spray solution was acidic [pH= 4] [59]. A plot of I_{DLE}/I_{NBE} and resistivity [Figure 3.8] would be

[4] It can be seen that I_{DLE}/I_{NBE} and resistivity values vary similarly as a function of propanol to water ratio in the solvent. These values are lowest for ZP1:1-I. Individual PL spectra are shown in the inset.

a better illustration of how we arrive at the conclusion regarding the optimum pH value. It has been well studied that pH determines the route of the reaction by controlling the intermediates formed as well as the rate of the reaction. Acidic pH favours Zn^{2+} ion formation which in turn facilitates ZnO formation [57].

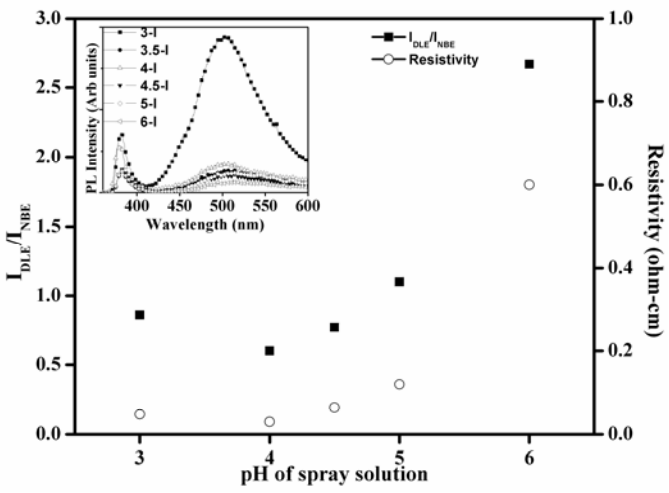

[5]**Figure 3.8: Variation of I_{DLE}/I_{NBE} and resistivity for samples prepared using spray solution of different pH.**

3.3.3 PL analysis to identify the optimum spray rate

In spray deposition the solution, in the form of fine droplets falls, on the pre-heated substrate and the desired compound forms on the substrate. The droplets that strike the substrate initiate formation of disk shaped structures which later coalesce and form a continuous film. Continuity and roughness of the film depends largely on the spray rate. In order to examine the impact of variation in spray rate on PL and resistivity, films prepared at spray rates from 3 to 12 ml/min (named ZP3-I, ZP5-I etc) were chosen for study. Figure 3.9 depicts the variation of I_{DLE}/I_{NBE} and resistivity for films prepared at different spray rates.

[5] Interestingly I_{DLE}/I_{NBE} and resistivity exhibit a similar variation and least values for both have been obtained when the pH of spray solution is maintained 4. i.e. the optimum pH to be maintained in the spray solution is 4.

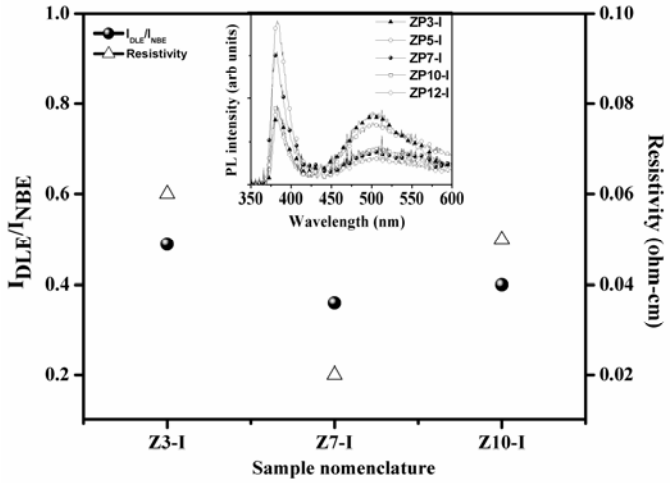

[6]Figure 3.9: Variation of I_{DLE}/I_{NBE} and resistivity for samples prepared at different spray rates.

3.3.4 PL studies on doped ZnO samples

Another method employed for reduction of resistivity is introduction of a suitable dopant. The process of doping was accomplished ex-situ and in-situ [60]. In ex-situ doping, a specific quantity of the dopant is vacuum evaporated and is thermally diffused in to the film. In in-situ doping the dopant is suitably incorporated in solution form along with the spray solution. In the present study, PL measurement is used to identify which method of doping is more adequate in bringing down the resistivity of ZnO. Doping with trivalent metal 'In' was done ex-situ and in-situ. PL and resistivity measurements were done and we have drawn a comparison between ex-situ and in-situ doping based on the two measurements. For ex-situ doping the quantities of 'In' taken was 2, 4, 6, 8 and 10 mg. Samples were named Z:2mgIn-I, Z:4mgIn-I, Z:6mgIn-I, Z:8mgIn-I and Z:10mgIn-I respectively. In the case of in-situ doping, percentage of indium nitrate added to the spray solution was varied from 0.5 to 2.5 % by volume.

[6] It can be observed that I_{DLE}/I_{NBE} and resistivity follow similar trend and both are minimum for Z7-I. Thus the optimum spray rate at which film deposition is to be done is 7 ml/min.

Samples were named Z:0.5In-I, Z:1In-I, Z:1.5In-I, Z:2In-I and Z:2.5In-I respectively. A plot of I_{DLE}/I_{NBE} and resistivity (for ex-situ and in-situ 'In' doped ZnO thin films) has been given in Figures 3.10 & 3.11.

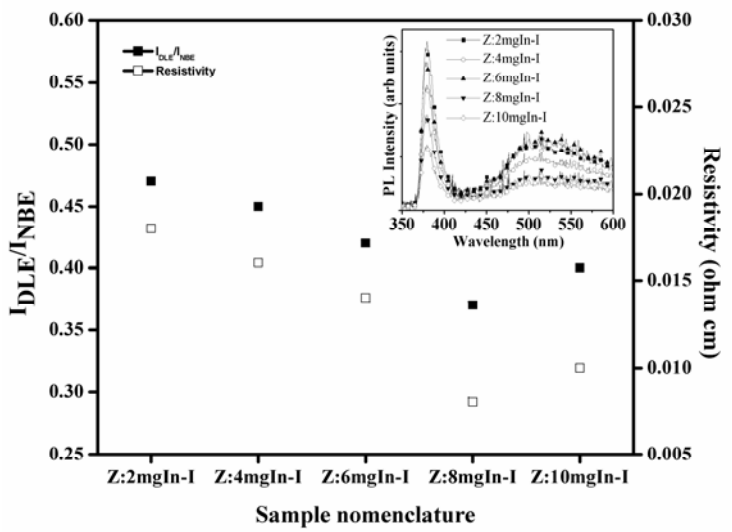

Figure 3.10: Variation of I_{DLE}/I_{NBE} and resistivity for ZnO films in which 'In' doping is done ex-situ.

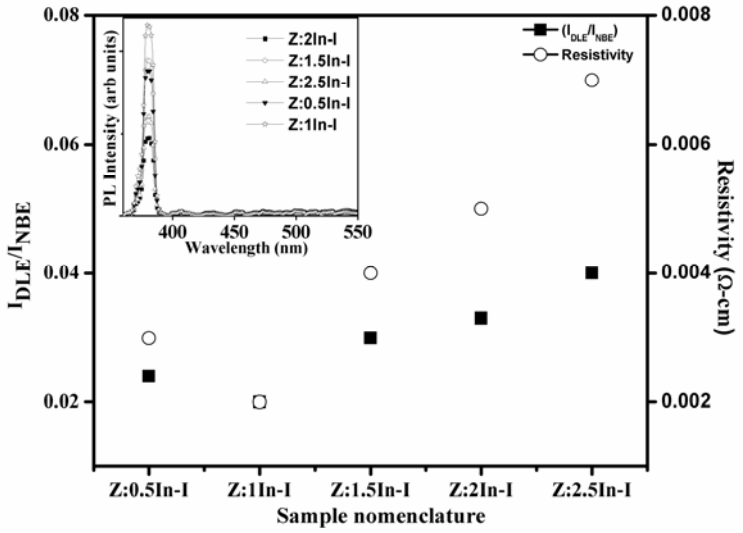

Figure 3.11: Variation of I_{DLE}/I_{NBE} and resistivity for ZnO films in which 'In' doping is done in-situ.

It can be inferred from the figures that I_{DLE}/I_{NBE} and resistivity are lower for in-situ doped ZnO thin films. Focusing on the intensity of DLE in graphs shown in the inset of Figures 3.10 & 3.11, we can see that the emission has nearly been 'wiped out' for in-situ 'In' doped ZnO samples when compared to ex-situ 'In' doped samples. From PL spectra, it can be clearly inferred that in-situ doping is much more effective than ex-situ doping in controlling O_{Zn} defect and hence resistivity (which is the least for Z:1In-I). In order to analyze the effect of another trivalent dopant on the properties of ZnO thin films, we studied 'Al' doped ZnO thin films. In-situ doped samples Z:0.5Al-I, Z:1.5Al-I, Z:2.5Al-I and Z:3.5Al-I (naming based on the percentages of 'Al' doped) were selected for analysis. Variation of I_{DLE}/I_{NBE} and resistivity traces similar trend [Figure 3.12] and sample Z:2.5Al-I is the least resistive.

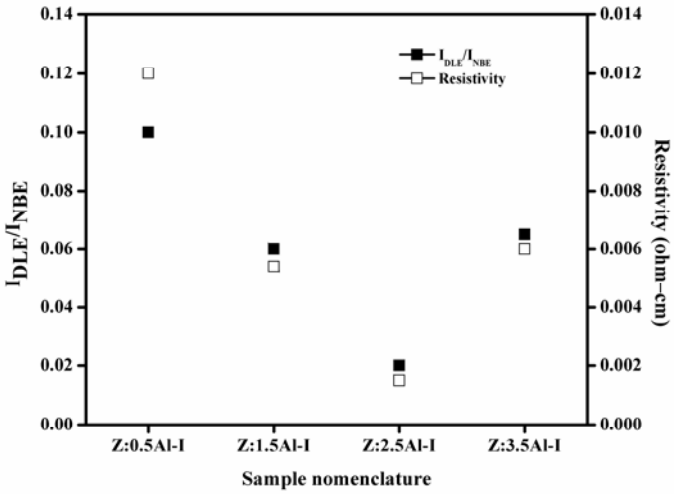

Figure 3.12: Variation of I_{DLE}/I_{NBE} and resistivity for ZnO films in which 'Al' doping is done in-situ.

The reduction in resistivity of 'In' and 'Al' doped ZnO is due to occupation of Zn^{2+} ion lattice sites by In^{3+}/Al^{3+} ions. As Zn^{2+} lattice sites are occupied by trivalent ions, formation of oxygen in zinc antisite defect [O_{Zn}] is also automatically controlled to a good extent as zinc sites are already occupied

by trivalent ions. This may be the reason for the absence of DLE in in-situ 'In' doped ZnO sample. With substitution of every trivalent ion, an electron is available for conduction and this causes a reduction in resistivity. It is observed that doping with 'Al' gives ZnO with least resistivity and this could be analyzed using the ratio of I_{DLE}/I_{NBE} from the PL spectrum of the sample.

Throughout our observations in the previous sections, we see that a strong connection has build up between I_{DLE}/I_{NBE} and resistivity. Even when several parameters were varied, these two quantities varied similarly. To find out the extent of correlation between the two, I_{DLE}/I_{NBE} and resistivity values obtained for all ZnO thin films studied has been plotted [Figure 3.13].

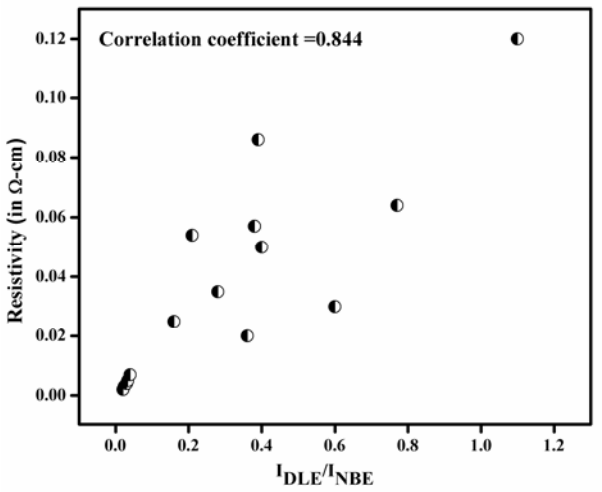

Figure 3.13: Variation of I_{DLE}/I_{NBE} and resistivity for all ZnO samples chosen for study.

The extent of correlation is usually expressed in terms of "correlation coefficient". Generally, if two parameters are perfectly correlated, correlation coefficient assumes the value 1. For perfectly uncorrelated data it is zero. Two parameters are positively correlated when they exhibit a similar trend in variation- i.e. when one parameter is high, the other is also high and vice versa. For perfect positive correlation, the plot would be linear with positive slope. We

observed that, resistivity and I_{DLE}/I_{NBE} exhibit positive correlation with a correlation coefficient of 0.844 which is a reasonably good value [61]. From our observations, we arrive at an empirical relation between the order of resistivity (Y) and order of I_{DLE}/I_{NBE} (X) as

$$Y = 10^{-1}X \quad \ldots\ldots (1)$$

This empirical relation holds true for all ZnO thin films we have studied. In order to reaffirm that using PL measurements and calculating I_{DLE}/I_{NBE} alone is sufficient to extract the order of resistivity of ZnO thin films, we performed a mapping of these parameters from different points of the sample and compared the values. In order to map I_{DLE}/I_{NBE} over the entire sample, we recorded PL spectra from different points and calculated I_{DLE}/I_{NBE} at each point. Resistivity measurements also were done from these points. Values of I_{DLE}/I_{NBE} and resistivity were plotted as a color map. The color palette chosen was from blue to red with blue representing the least value of parameter plotted and red indicating the maximum. We have presented the results of mapping I_{DLE}/I_{NBE} and resistivity on sample Z7-I (Figure 3.14 (a) & (b)).

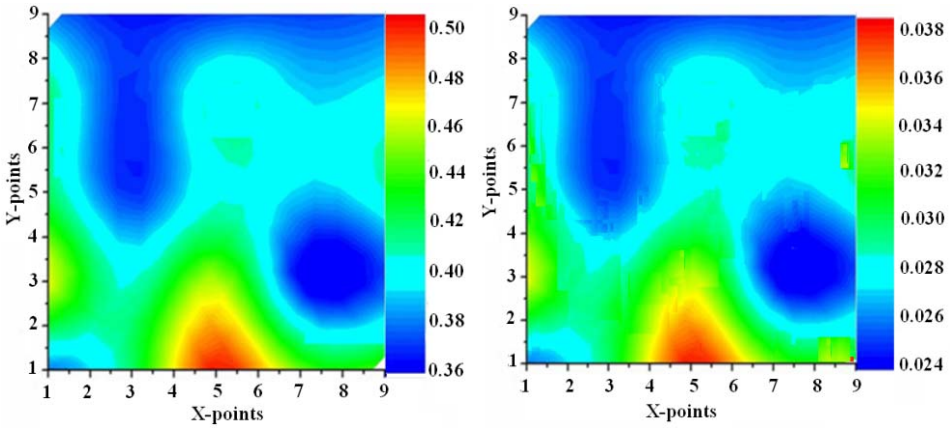

(a) **(b)**

Figure 3.14: Color map of (a) I_{DLE}/I_{NBE} (b) Resistivity (in Ω.cm) over sample Z7-I of dimension 2.5 cm X 2.5 cm.

Information obtained from the two images

- I_{DLE}/I_{NBE} can be taken as an indicator of resistivity. So by mapping I_{DLE}/I_{NBE} we can get an idea of how uniform (in terms of resistivity) the sample is.
- The values of I_{DLE}/I_{NBE} as well as resistivity are fairly uniform over a major area of the sample.

3.4 Conclusions

From the present study on ZnO thin films we observed a strong positive correlation between resistivity and I_{DLE}/I_{NBE} (ratio of integrated intensities of DLE to NBE) obtained from PL spectra. Based on our observations, we have proposed an empirical relation, $Y = 10^{-1}X$, connecting order of resistivity (Y) and order of I_{DLE}/I_{NBE} (X). We have studied ZnO samples prepared under different deposition conditions. Generally for TCO applications, resistivity has to be low. Using the connection between I_{DLE}/I_{NBE} and resistivity, we could identify low resistive samples simply by monitoring the values of I_{DLE}/I_{NBE} obtained from PL spectra. Using PL studies we could identify that in-situ doping is much more effective than ex-situ doping in bringing down the resistivity. From PL analysis we could also identify the optimum percentages of doping (1.5 % and 2. 5 % for 'In' and 'Al' respectively) for which resistivity was least.

References

[1]. **U. Özgür, Ya. I. Alivov, C. Liu, A. Teke, M. Reshchikov, S. Dogan, V. Avrutin, S. J. Cho, H. Morkoc.** 2005, Journal of Applied Physics, Vol. 98, p. 103.

[2]. **D. C. Look, C. Coskun, B. Claflin, G. C. Farlow.** 2003, Physica B, Vols. 340-342, p. 32.

[3]. **S. Mridha, D. Basak.** 2007, Journal of Applied Physics, Vol. 101, p. 08310.

[4]. **J. B. Baxter, E. R. Aydil.** 2005, Applied Physics Letters, Vol. 86, p. 05311.

[5]. **P. M. Misra, K. D. Amit, L. M. Kukreja.** 2010, Physica Status Solidi C, Vol. 7, p. 1718.

[6]. **K. Krunks, O. Bijakina, V. Mikli, T. Varema, E. Mellikov.** 1999, Physica Scripta, Vol. T79, p. 209.

[7]. **X.T. Zhang, Y. C. Liu, Z. Z. Zhi, J. Y. Zhang, Y. M. Lu, D. Z. Shen, W. Xu, G. Z. Zhong, X. W. Fan, X. G. Kong.** 2001, Journal of Physics D:Applied Physics, Vol. 34, p. 3430.

[8]. **Y. G. Wang, S. P. Lau, X. H. Zhang, H. H. Hng, H. W. Lee, S. F. Yu, B. K. Tay.** 2003, Journal of Crystal Growth, Vol. 259, p. 335.

[9]. **Th. Agne, Z. Guan, X. M. Li, H. Wolf, Th. Wickert, H. Natter, R. Hempelmann.** 2003, Applied Physics Letters, Vol. 83, p. 1204.

[10]. **D. H. Zhang, Q. P. Wang, Z. Y. Xue.** 2003, Applied Surface Science, Vol. 207, p. 20.

[11]. **E. S. Shim, H. S. Kang, S. S. Pang, J. S. Kang, I. Yun, S. Y. Lee.** 2003, Materials Science and Engineering B, Vol. 102, p. 366.

[12]. **K. K. Kim, H. S. Kim, D. K. Hwang, J. H. Lim, S. J. Park.** 2003, Applied Physics Letters, Vol. 83, p. 63.

[13]. **P. Viswanathamurthi, N. Bhattarai, H. Y. Kim, D. R. Lee.** 2004, Nanotechnology, Vol. 15, p. 320.

[14]. **A.B.Djurisic, Y.H.Leung, W.C.H.Choy, K.W.Cheah, W.K.Chan.** 2004, Applied Physics Letters, Vol. 84, p. 2635.

[15]. **F. K. Shan, B. I. Kim, G. X. Liu, Z. F. Liu, J. Y. Sohn.** 2004, Journal of Applied Physics, Vol. 95, p. 4772.

[16]. **P.M.Ratheesh Kumar, C.Sudha kartha, K.P.Vijayakumar.** 2005, Journal of Applied Physics, Vol. 98, p. 023509.

[17]. **Y.W.Chen, Y.C.Liu, S.X.Lu, C.S.Xu, C.L.Shao, C.Wang, J.Y.Zhang, Y.M.Lu, D.Z.Shen, X.W.Fan.** 2005, The Journal of Chemical Physics, Vol. 123, p. 134701.

[18]. **X.M. Fan, J.S. Lian, Z.X. Guo, H.J. Lu.** 2005, Applied Surface Science, Vol. 239, p. 176.

[19]. **L.Duan, B.Lin, W.Zhang, S.Zhong, Z.Fu.** 2006, Applied Physics Letters, Vol. 88, p. 232110.

[20]. **J.Liu, Y.Zhang, J.Qi, Y.Huang, X.Zhang, Q.Liao.** 2006, Materials Letters, Vol. 60, p. 2623.

[21]. **T.M.Borseth, B.G.Svensson, A.Y.Kuznetsov, P.Klason, Q.X.Zhao, M.Willander.** 2006, Applied Physics Letters, Vol. 89, p. 262112.

[22]. **V.A.Fonoberov, K.A.Alim, A.A.Balandin, F.Xiu, J.Liu,.** 2006, Physical Review B, Vol. 73, p. 165317.

[23]. **X.M.Teng, H.T.Fan, S. S. Pan, C. Ye, G. H. Li.** 2006, Journal of Physics D:Applied Physics, Vol. 39, p. 471.

[24]. **R. Hong, J. Shao, H. He, Z. Fan.** 2006, Journal of Applied Physics, Vol. 99, p. 093520.

[25]. **E.Przezdziecka, E.Kaminska, K.P.Korona, E.Dynowska, W.Dobrowolski, R.Jakiela, L.Klopotowski, J.Kossut.** 2007, Semiconductor Science and Technology, Vol. 22, p. 10.

[26]. **S. Jiao, Y.Lu, Z.Zhang, B. Li, B.Yao, J.Zhang, D.Zhao, D.Shen, X.Fan.** 2007, Journal of Applied Physics, Vol. 102, p. 113509.

[27]. **G.Xiaong, U.Pal, J.G.Serrano.** 2007, Journal of Applied Physics, Vol. 101, p. 024317.

[28]. **X.Teng, H.Fan, S.Pan, C.Ye, G.Li.** 2007, Materials Letters, Vol. 61, p. 201.

[29]. **F.K.Shan, G.X.Liu, W.J.Lee, B.C.Shin.** 2007, Journal of Applied Physics, Vol. 101, p. 053106.

[30]. **J.-P.Richters, T.Voss, L.Wischmeier, I.Ruckmann, L.Gutowski.** 2008, Journal of the Korean Physical Society, Vol. 53, p. 2844.

[31]. **E.Guziewicz, M.Godlewski, T.Krajewski, L.Wachnicki, A.Szczepanik, K.Kopalko, A.W.Glodowska, E.Przezdziecka, W.Paszkowicz, E.Lusakowska, P.Kruszewski, N.Huby, G.Tallarida, S.Ferrari.** 2009, Journal of Applied Physics, Vols. 122413 (1-5), p. 105.

[32]. **K.Yamaoka, Y.Terai, T.Yamaguchi, H.N.Ngo, T.Gregorkiewicz, Y.Fujiwara.** 2009, Journal of Physics:Conference Series, Vol. 165, p. 012027.

[33]. **C.F.Yu, C.W.Sung, S.H.Chen, S.J.Sun.** 2009, Applied Surface Science, Vol. 256, p. 792.

[34]. **Y.R. Sui, B.Yao, J.H.Yang, L.L.Gao, T.Yang, R.Deng, M.Ding, T.T.Zhao, X.M. Huang, H.L.Pan, D.Z.Shen.** 2010, Journal of Luminescence, Vol. 130, p. 1101.

[35]. **J.Lu, K.Huang, J.Zhu, X.Chen, X.Song, Z.Sun.** 2010, Physica B, Vol. 405, p. 3167.

[36]. **L.Xu, H.Shen, X.Li, R.Zhu.** 2010, Journal of Luminescence, Vol. 130, p. 2123.

[37]. **S.Cho, J.Ma, Y.Kim, Y.Sun, G.K.L.Wong, J.B.Ketterson.** 2010, Applied Physics Letters, Vol. 75, p. 2761.

[38]. **D.Sentosa, B.Liu, L.M.Wong, Y.V.Lim, T.I.Wong, Y.L.Foo, H.D.Sun, S.J.Wang.** 2011, Journal of Crystal Growth, Vol. 319, p. 8.

[39]. **E.Karber, T.Raadik, T.Dedova, J.Krustok, A.Mere, V.Mikli, M.Krunks.** 2011, Nanoscale Research Letters, Vol. 359, p. 1.

[40]. **S.Dhara, P.K.Giri.** 2011, Functional Materials Letters, Vol. 4, p. 25.

[41]. **X.D.Zhou, X.H.Xiao, J.X.Xu, G.X.Cai, F.Ren, C.Z.Jiang.** 2011, European Physics Letters, Vol. 93, p. 57009.

[42]. **K.Y.Kuo, S.W.Hsu, P.R.Huang, W.L.Chuang, C.C.Liu, P.T.Lee.** 2012, Optics Express, Vol. 20, p. 10470.

[43]. **S.Y.Ting, P.J.Chen,H.C.Wang, C.H.Liao, W.M.Chang, Y.P.Hsieh, C.C.Yang.** 2012, Journal of Nanomaterials, Vol. 2012, p. 1.

[44]. **J.Y.Noh, H.Kim, Y.S.Kim, C.H.Park.** 2013, Journal of Applied Physics, Vol. 113, p. 153703.

[45]. **E.Senthil Kumar, I. P. Anderson, Z. Deng, F. Mohammadbeigi, T. Wintschel.** 2013, Semiconductor Science and Technology , Vol. 28, p. 045014.

[46]. **K.Saravanan, B.K.Panigrahi, R.Krishnan, K.G.M.Nair.** 2013, Journal of Applied Physics, Vol. 113, p. 033512.

[47]. **Z. W. Ai, Y.Wu, H.Wu, T. Wang, C. Chen, Y. Xu, C. Liu.** 2013, Nanoscale Research Letters, Vol. 8:105, p. 1.

[48]. **A.Maldonado, M.D.L.Olvera, R.Asomoza, S.Tirado-Guerra.** 2007, Journal of Materials Science, Vol. 42, p. 2598.

[49]. **J.S.Cho, S.K.Hong, D.S.Jung, Y.C.Kang.** 2008, Journal of the Ceramic Society of Japan, Vol. 116, p. 334.

[50]. **T.V.Vimalkumar, N.Poornima, C.Sudha Kartha, K.P.Vijayakumar, T.Abe, Y.Kashiwaba.** 2010, Physica B, Vol. 405, p. 4957.

[51]. **Busch, Schade.***Lectures on Solid State Physics.* s.l. : Pergamon Press,1976.

[52]. **F.Leiter, H.Alves, A.Hofstaetter,D.M.Hofmann, B.K.Meyer.** 2001, Physica Status Solidi B-Basic Research, Vol. 226, pp. R4-R5.

[53]. **A.F.Kohan, G.Ceder,D.Morgan, C.G.Van de Walle.** 2000, Physics Review B, Vol. 61, p. 15019.

[54]. **K.H.Tam, C.K.Cheung, Y.H.Leung, A.B.Djurisic, C.C.Ling, C.D.Beling, S.Fung, W.M.Kwok, W.K.Chan, D.L.Philips, L.Ding, W.K.Ge.** 2006, Journal of Physical Chemistry B, Vol. 110, p. 20865.

[55]. **P.M.Ratheesh Kumar, K.P.Vijayakumar, C.Sudha Kartha.** 2007, Journal of Material Science , Vol. 42, p. 2598.

[56]. **T.V.Vimalkumar, N.Poornima, C.Sudha Kartha, K.P.Vijayakumar.** 2010, Materials Science and Engineering B, Vol. 175, p. 29.

[57]. **A.Maldonado, R.Asomoza, J.Canetas-Ortega, E.P.Zironi, R.Hernandez, R.Patino, O.Solorza-Feria.** 1999, Solar Energy Materials and Solar Cells, Vol. 57, p. 331.

[58]. **F.Caillaud, A.Smith, J.-F.Baumer,.** 1993, Journal of American Ceramic Society, Vol. 76, p. 998.

[59]. **T.V.Vimalkumar.***Highly conductive and transparent ZnO thin film using Chemical Spray Pyrolysis technique: Effect of doping and deposition parameters.* s.l. : Cochin University of Science and Technology, 2011. Ph.D Thesis.

[60]. **P. Nunes, E. Fortunato, P. Tonello, F. Braz Fernades, P. Vilarinho, E. Martins.** 2002, Vacuum, Vol. 64, p. 281.

[61]. **N.Poornima, T.V.Vimalkumar, V.G.Rajeshmon, C.Sudha Kartha, K.P.Vijayakumar.** 2013, International Journal of Photoenergy, Vol. 2013, p. 1.

[62]. **E.S.Kumar, I.P.Anderson, Z.Deng, F.Mohammadbeigi, T.Wintschel, D.Huang, S.P.Watkins.** 2013, Semiconductor Science and Technology, Vol. 28, p. 045014.

.....ꕥ.....

Chapter 4

PROBING DEFECTS IN COPPER ZINC TIN SULPHIDE THIN FILMS

4.1 Introduction

$CuIn_{1-x}Ga_xSe_2$ (CIGS) is presently positioned in the PV market as a healthy competitor to silicon but such compounds may not be able to satisfy the needs of the evergrowing demand for solar energy because competition for 'In' from other quarters is high and 'In' is relatively scarce [1]. Evolving quaternary compound semiconductors by sequential cross substitution of cations in I-III-VI_2 systems without bypassing the octet rule is highly preferred as it is a quite simple way to tailor optoelectronic properties for specific applications [2]. Such a breeding process may yield numerous materials but not every material can be promising for PV applications. Copper Zinc Tin Sulphide (CZTS) is one such material with optimal band gap (1.5 eV), absorption coefficient $>10^4$ cm^{-1} and over and above the constituent elements are abundant as of now, relatively non-toxic and adaptable to different growth techniques [3-5].

CZTS is stable only over a small thermodynamic range and secondary phases as well as intrinsic point defects accompany its formation [6-8]. The unfortunate fact about such materials is the lack of knowledge of the crystal structure and its effect on band structure and optoelectronic properties [9]. As of now the unbeaten efficiency of solar cell fabricated employing CZTS as absorber

is 8.4 % [10]. It has been observed that Cu-poor and Zn-rich compositions are favorable from device point of view; formation of secondary phases are but accelerated under these conditions [11]. To foster development of PV technology based on CZTS, priority is to be given to avoid secondary phases and develop the desired optoelectronic properties; but this is an uphill task when the electronic structure is quite obscure. First principle calculations suggest that ideas of electronic structure and defect formation physics proposed for CIGS may be extrapolated, even though not fully, to CZTS.

For $CuInSe_2$, it has been observed that p-type conductivity is due to vacancy of copper [V_{Cu}] defect and defect physics for this system has been well studied [12,13]. When it comes to CZTS, until recently [2, 14, 15] no theoretical and experimental works were carried out to explain the p-type conducting nature observed widely [16-18]. CZTS is a quaternary system where numerous intrinsic point defects can arise- vacancies, interstitials and antisite substitutions of Cu, Zn, Sn and S are likely. Detailed theoretical investigation as well as experimental works in this material has been carried out by some groups and not many reports have come exclusively on the defect analysis using PL. This material exhibits astonishingly favorable optoelectronic properties but devices fabricated employing CZTS still has not been able to reach the projected efficiency. An answer to this concern can only be obtained by analyzing the material properties more closely.

4.1.1 Properties of CZTS

Kesterite structure is the most stable phase of CZTS but stannite and partially disordered kesterite structures also do exist [9]. The crystal structure of CZTS is shown in Figure 4.1.

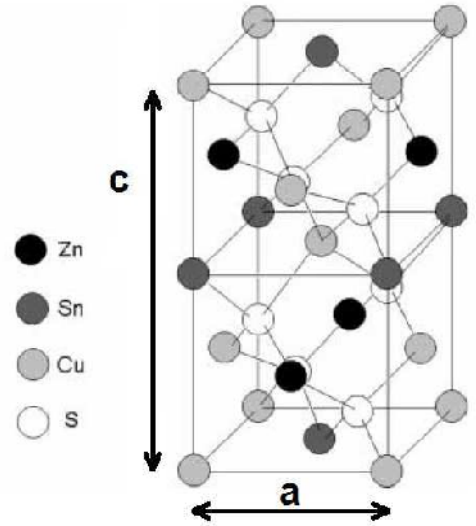

Figure 4.1: Crystal structure of CZTS.

The lattice constants for CZTS are a=0.54 nm and c=1.09 nm [19]. Bandgap values ranging from 1.36 to 1.6 eV have been reported which make this material highly suitable for use as absorber layer material in solar cells [20, 21]. In solar cells reported with 6.7 % efficiency, bandgap of CZTS layer employed was 1.45 eV. Such a wide variation in bandgap can be probably attributed to the deviation in composition from stoichiometry [22]. CZTS films exhibit p-type conductivity suggesting that there is an internal mechanism responsible for creation of acceptor states [23, 24]. Reports point out that, 'Cu' atoms occupying places of 'Zn' atoms (Cu on Zn antisite) accounts for the p-conductivity of CZTS. Small deviations from stoichiometry also lead to the formation of secondary phases [25, 26]. The chemical potential range of 'Cu', 'Zn' and 'Sn' favoring formation of CZTS is very narrow. A phase diagram [Figure 4.2] previously reported, suggests that even a slight deviation from stoichiometry can result in the formation of secondary phases [27].

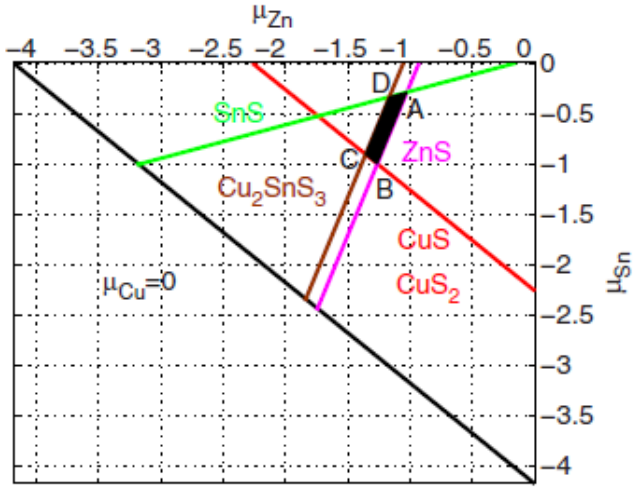

Figure 4.2: Phase diagram reported for CZTS [27]. The black shaded region indicates zone for CZTS formation.

Defect complexes are extremely likely to form in this quaternary system and the formation of defect complexes like $[V_{Cu} + Zn_{Cu}]$ is beneficial from photovoltaic application point of view. ZnS phase precipitation is but detrimental to device performance [2, 27]. Midgap antisite defects such as Cu_{Sn} have been identified to be parasitic and detrimental to device performance [1, 27]. As far as the electrical properties are concerned, charge carrier concentration in the range 5 X 10^{15} to 6 X 10^{16} cm^{-3} has been reported [28, 29]. Device quality absorber with a mobility value of 6 $cm^2/V.s$ has been reported with a carrier concentration in the order 10^{18} cm^{-3} [30]. Electronic properties of both kesterite as well as stannite structures of CZTS family bear remarkable similarity to each other and also to members of CIGS family [31]. CZTS is thus, quality-wise and cost-wise the best substitute for CIGS in solar cells. The valence band is reported to be an antibonding linear combination of Cu (3d) states and S (3p) states and the conduction band is dominated by Sn (5s) and S (3p) states [32]. It has been reported that CZTS with $Cu/[Zn + Sn]$ close to 1.0 and resistivity in the range 10^{-2}-10^4 Ω.cm was employed in developing efficient solar cells [33].

A general observation in many reports is that in spite of favorable properties, the device performance is nowhere comparable with CIGS based devices. It is reported to be due to the lack of understanding of the defect physics of CZTS and lack of knowledge of the various defects that are likely to arise under specific deposition conditions [34]. So along with trials for successful devices, basic studies on the material too have been progressing. In the following section, different works that have been going on in CZTS to identify the band structure, defects etc is discussed.

4.2 Review of works related to defect analysis in CZTS

In a report in 2005 by Raulot et al. [14], the authors have dealt with important defects and defect complexes in CZTS system. Formation energy of V_{Cu} and defect complexes such as $[V_{Cu} + Zn_{Cu}]$ has been calculated and V_{Cu} has low formation energy and is assumed to be the predominant defect in CZTS. A comparison with $CuInSe_2$ would be highly beneficial in this context, where antisite defects such as In on Cu site [In_{Cu}] form at relatively low expense of energy [35]. In CZTS the valency of Cu(I) and Zn(II) in Cu_{Zn} is similar to V_{Cu} and it has every likelihood for occurrence as a strong acceptor defect. Formation of defect complex $[V_{Cu}^{-} + In_{Cu}^{2+}]^0$ has been reported to be beneficial in the case of $CuInSe_2$ absorber. Similarly in CZTS, since there are 3 elements, probability can be assigned to the formation of different defect complexes but energetic considerations favor the formation of $[Vu_{Cu}^{-} + In_{Cu}^{2+}]^0$ owing to lesser disparity in size and chemical nature of the elements.

In a theoretical work by Chen et al. [2], the authors have come up with interesting observations that intrinsic p-type conductivity is due to Cu_{Zn} acceptor defect which is a much deeper acceptor defect than V_{Cu}. In such a system where formation energies of acceptor defects are so low, n type doping is extremely

difficult. Formation of defect complexes like $[Cu_{Zn}^{-} + Zn_{Cu}^{+}]^{0}, [V_{Cu}^{-} + Zn_{Cu}^{+}]^{0}$ etc are important for passivating defects in the bandgap [27]. A work by Romero et al. [36] on the comparative study of properties of Cu-deficient CZTS and CIGS system establishes the close resemblances in the properties. First experimental evidence using microluminescence imaging has been provided in the report, which gives a picture that distinct electronic structure owing to grain boundaries is present in CZTS also.

Hones et al. [37] published a research article on shallow defects in vapour phase grown CZTS crystals. Narrow PL peaks were observed for the first time and a defect recombination model has been proposed involving shallow acceptor states at 10±5 and 30±5 meV as well as a donor state at 5±3 meV below the conduction band. In another report [38], properties of CZTS thin films prepared by sulfurization of metallic precursors coated on glass substrates were analyzed. Asymmetric broad PL emission was recorded whose dependence on excitation power and temperature could not fit in with the explanation of a donor to acceptor pair recombination. The emission was concluded to be due to recombination between electron and a hole bound to an acceptor; ionization energy of acceptor was calculated to be in the range 29-40 meV.

Nagoya et al. [39] in his report calculated the formation energies of vacancies of copper and zinc and antisite defects such as Cu_{Zn}, Zn_{Cu} etc. The most stable defect of all was Cu_{Zn}. In yet another interesting report [40], CZTS thin films grown on 'Si' substrates were analyzed and broad PL peaks at 1.45 eV and 1.31 eV were recorded. The emission at 1.45 eV, which the authors claim to be the first of its kind, exhibited the behavior of a donor to acceptor pair transition and the emission at 1.31 eV was same as that reported by Tanaka et al. Leitao et al. [41] prepared CZTS thin films by sulfurization of metallic thin films prepared on glass substrates and from PL studies information about a

broad emission at 1.24±0.01 eV could be obtained. Dependence of this emission on temperature and excitation power exhibited the nature of transition involving tail states created by potential fluctuations. CZTS is a relatively newcomer in the PV industry and is a system that has not been well studied and analyzed.

Lin et al. [42] have studied CZTS thin films prepared by spin coating Cu_3SnS_4 and ZnS nanoparticles inks followed by subsequent annealing. Broad PL peaks centered at 1.35, 1.30 and 1.28 eV have been recorded which suffer a red shift with increase in Cu/[Zn+Sn] concentration. Two PL bands at 1.27 and 1.35 eV could be recorded in CZTS polycrystals [43] which could be identified as band to impurity recombination and the impurity associated with the transition was assigned as Cu_{Sn}. The authors have proposed that PL band at 1.35 eV arises from the kesterite structure and the other at 1.27 eV from disordered kesterite structure. At low temperature a single broad peak at 1.29 eV could be recorded in CZTS single crystals [44] and could be identified as free to bound transition. The activation energy of 140 meV could be attributed to intrinsic acceptor type Cu_{Zn} defect. Sousa et al. [45] studied CZTS absorber layers by sulfurization in graphite box and in a tubular furnace directly exposed to sulfur vapour. Radiative recombination efficiency was found to be much higher in the latter type of samples. Emission in the range 1-1.5 eV could be recorded for different types of samples.

CZTS thin films were prepared at different annealing temperatures and chosen for study by Kim et al. [46]. Bandgap was estimated from PL measurements as 1.25 eV for films annealed at 200 and 500 ^oC. Intensity of PL peak is higher for sample annealed at 500 ^oC which has been attributed to improvement in crystallinity as evident from X-ray Diffraction studies. CZTS thin films have been deposited using spray pyrolysis and characterized. A broad emission at 1.33 eV

could be recorded for the samples. The authors [47] presume it as a donor acceptor pair recombination. In the article on microphotoluminescence study on CZTS polycrystals, the authors [48] claim the emissions recorded at 1.39 eV and 1.53 eV were band to tail (BT) and band to band (BB) recombination. Unlike ternary chalcopyrites, the BT recombination was visible only at elevated temperatures and high excitation level.

In her review article 'Why are kesterite solar cells not 20% efficient?', Susanne Siebentritt [49] explains the major factors that pull back the efficiency of sulphide kesterite solar cells. The author has mentioned about various 'non-ideal recombination channels' that degrade the performance. Owing to either large density of defects or stannite inclusions in CZTS, obtainable efficiency can be reduced by a large extent. Currently there are numerous methods for deposition of device quality CZTS thin films and in each case the defects may be different depending on the mode of film preparation or the treatment given to the samples.

From the various reports on PL studies, it has been observed that authors have come up with broad defect related emissions in the range 1.2-1.46 eV. In a material where there is no consensus in the case of a basic parameter as bandgap [37] the obtained emission pattern shall also be different. In our work we have recorded (for the first time), broad defect related emissions at 0.797 and 0.805 eV. We have observed the variation of these emissions with different parameters and identified a possible cause for these emissions.

4.3 Observations and discussions

4.3.1 Studies on CZTS thin films- observation of broad defect related emission

CZTS thin films prepared using chemical spray pyrolysis, with Cu:Zn:Sn:S ratio = 2:1:1:12, on sodalime glass substrates maintained at a temperature of 350 ^{o}C

were chosen for studies. Films of this batch shall be referred to as, C, hereafter. Even though PL has been widely acknowledged as a quite useful tool for semiconductor characterization, it is not stand-alone; we require other analysis techniques such as XRD, Raman, EDAX, XPS etc for supportive argument. So prior to PL analysis, structural and compositional studies were also carried out on the samples.

XRD analysis indicates that peaks corresponding to (112), (200), (220), (312) planes of CZTS could be observed in the XRD pattern [JCPDS card no: 26-0575]. These are characteristic of the kesterite structure of CZTS. Preferential orientation of crystallites was along the (112) direction [Figure 4.3].

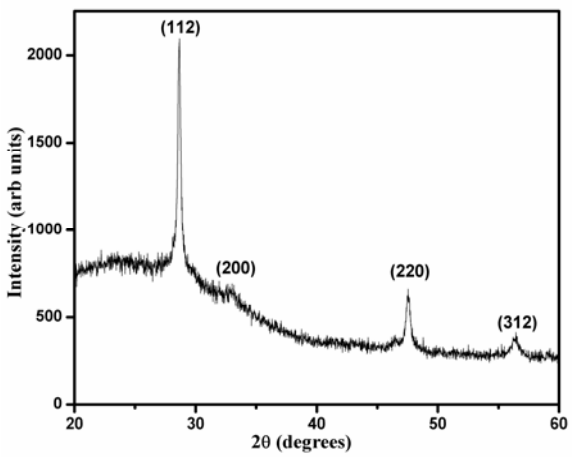

Figure 4.3: XRD pattern of CZTS sample C.

Raman analysis was carried out to confirm the existence of CZTS; this is confirmed by the presence of Raman peaks at 338 cm^{-1}, 288 cm^{-1} and 256 cm^{-1} [Figure 4.4], which are in agreement with the published data for monograins of CZTS [50].

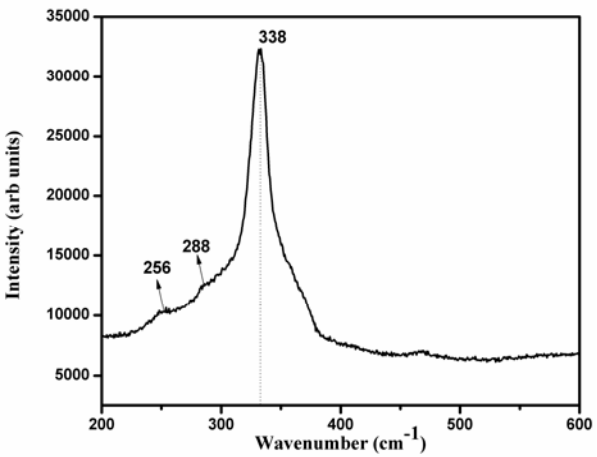

Figure 4.4: Raman spectrum of CZTS sample C.

Composition analysis was done using EDAX measurements [Table 4.1] which indicates that the sample is nearly stoichiometric. For perfect stoichiometry Cu to [Zn+Sn] ratio = 1, Zn to Sn ratio=1 and S to metal ratio=1.

Table 4.1: Results from EDAX measurements on sample C.

Sample	Cu (at.%)	Zn (at.%)	Sn (at.%)	S (at.%)	$\frac{Cu}{(Zn+Sn)}$	$\frac{Zn}{Sn}$	$\frac{S}{metal}$
2:1:1:12	25.2	13.2	12.4	49.2	0.98	1.06	0.97

Figure 4.5 shows the PL spectrum recorded from sample C. The spectrum was recorded at an excitation power of 15 mW and the sample temperature was 15 K. A broad emission at 0.797 eV, much below the bandgap energy of 1.45 eV could be recorded.

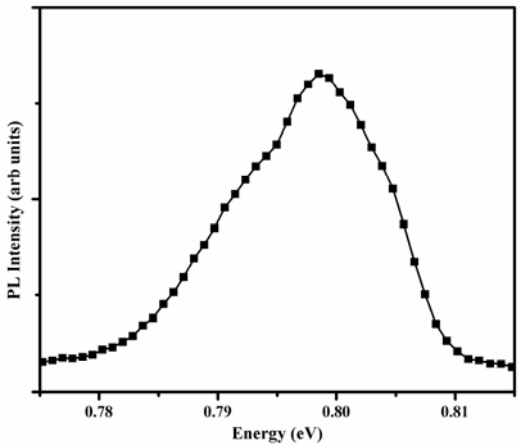

Figure 4.5: PL spectrum recorded at 15 K from CZTS sample C.

To analyze the nature of transition, dependence of integrated PL intensity and PL peak energy with excitation power was studied. Figure 4.6 (a) is the log-log plot of integrated PL intensity vs excitation power and (b) shows the variation of PL peak energy with excitation power. Recalling the relation connecting PL intensity (I) and excitation power (P) i.e., $I \alpha P^{\gamma}$, it is quite obvious that performing a linear fit to the log-log plot of PL intensity with excitation power, 'γ' value can be obtained.

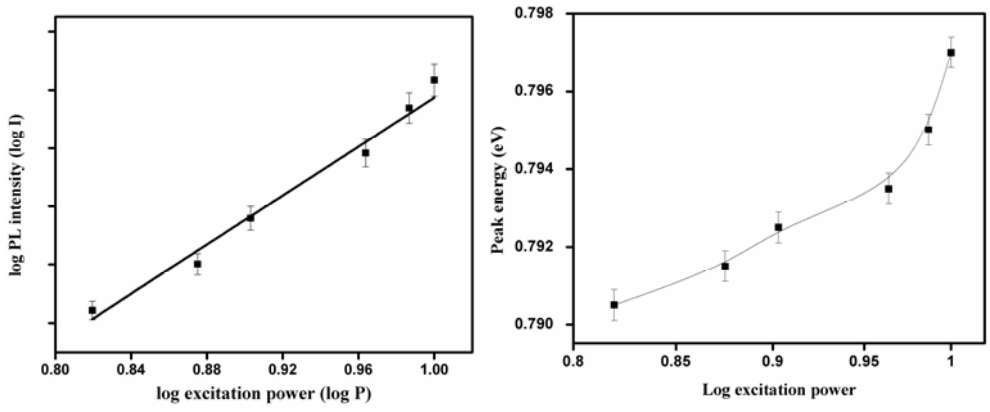

(a) **(b)**

Figure 4.6: (a) Log-log plot of PL intensity with excitation power (b) Variation of PL peak energy with excitation power, for sample C.

On performing linear fit, γ=0.8 was obtained which indicates that the transition is defect assisted [51]. Dependence of PL peak energy with excitation power (shown in Figure 4.6 (b)) indicates a slight shift in the peak energy to the higher energy side with increase in excitation power. Blue shift of peak energy to the higher energy end is a feature of transitions belonging to the donor-acceptor pair (DAP) type.

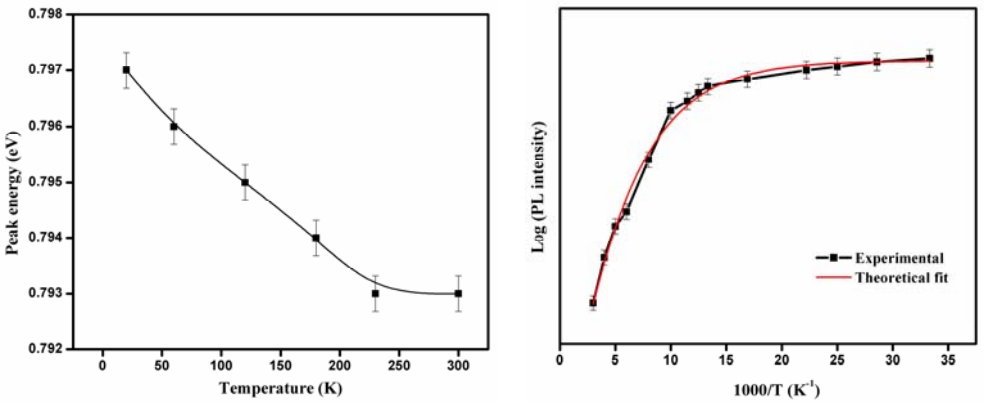

(a) **(b)**

Figure 4.7: (a) Temperature dependence of PL peak energy (b) Arrhenious plot, obtained for sample C.

Temperature dependence of PL peak energy indicates a slight shift in PL peak energy to lower energy side when temperature is increased from 15- 300 K [Figure 4.7 (a)], which is yet another feature of DAP transition. Activation energies of defects involved is calculated by monitoring the temperature dependence of PL emission intensity. Activation energy can be calculated by performing a theoretical curve fit to the Arrhenius plot [log (PL intensity) vs 1000/T] using the relation (which has been mentioned already in Chapter 2),

$$\frac{I(T)}{I(0)} = \frac{1}{\left[1 + Ce^{-\frac{\Delta E}{kT}}\right]}$$

as shown in Figure 4.7 (b). Average value of activation energy obtained from several measurements was 0.12 ± 0.005 eV. First principle calculations predict the occurrence of a prominent acceptor at 0.12 eV above the VBM which has been attributed to Cu_{Zn} defect which is one of the predominant intrinsic defects with very low formation energy [27]. Cu_{Zn} antisite defect is thermodynamically the most stable defect and has negative formation energy for the allowed chemical potential range. This defect accounts for the p-type conductivity in CZTS. Since the films were p-type and the obtained activation energy value coincided with the reported value, we attributed the level at 0.12 eV (from VB edge) to Cu_{Zn} defect. Using relation (neglecting Coulombic interaction and van der Waals interaction),

$$E_{PL} = E_g - (E_D + E_A)$$

we obtain that the emission at 0.797 eV arises from a level at 0.533 eV from CB to an acceptor at 0.12 eV [as the bandgap of sample C is 1.45 eV]. The only way to identify the level at 0.533 eV is to play with stoichiometry but we felt it was better to optimize the essential parameters like substrate temperature and spray rate before going for variation in stoichiometry; so the impact of varying these two parameters on the PL spectra was studied first.

4.3.2 How does the emission respond to variation in substrate temperature?

Substrate temperature is a decisive parameter in the process of film formation. It decides whether film formation is proper, whether secondary phases form, whether there are unreacted precipitates and lot more. All these factors either directly or indirectly affect the optoelectronic properties. PL studies were performed on nearly stoichiometric CZTS thin films prepared for five different substrate temperatures ranging from 300 to 400 ^{o}C in steps of 25 ^{o}C [Figure 4.8]. [Samples have been named C-300, C-325, C-350, C-375 and C-400].

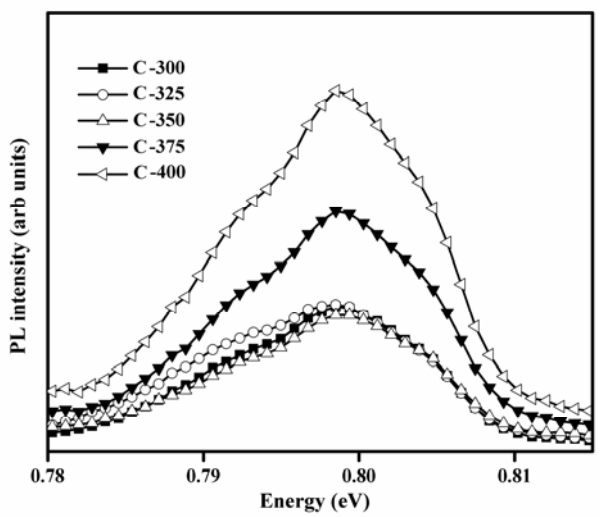

Figure 4.8: PL spectra of CZTS samples C, deposited at different substrate temperatures.

PL intensity is nearly the same for samples C-300, C-325 and C-350 as evident from Figure 4.8. Band to band/ close to bandgap emissions could not be obtained. PL intensity increases progressively for samples prepared at substrate temperatures higher than 350 ^{o}C. Apart from the information obtained from PL, we could observe from XRD studies that crystallinity gets better with progress in substrate temperature from 300 to 350 ^{o}C. For substrate temperatures beyond 350 and up to 400 ^{o}C crystallinity exhibits a reverse trend. I-V measurements performed on the samples indicate that resistivity decreases for an increase in substrate temperature from 300 to 350 ^{o}C; for an increase in substrate temperature beyond 350 ^{o}C, resistivity increases [Table 4.2].

Table 4.2: Crystallite size from XRD and resistivity values obtained for samples prepared at different substrate temperatures.

Samples	Crystallite size from XRD (nm)	Resistivity from I-V measurements (Ω.cm)
C-300	24.89	$8.7X10^{-2}$
C-325	28.41	$2.8X10^{-2}$
C-350	31.27	$1.8X10^{-2}$
C-375	30.94	$3.1X10^{-2}$
C-400	30.12	$5.8X10^{-2}$

For sample C-350, defect related emission was least intense, resistivity was minimum and crystallinity better. Based on the results from PL and supportive characterization techniques, a substrate temperature of 350 ^{o}C can be considered as the optimum.

4.3.3 How does the emission respond to variation in spray rate?

Spray rate is a relevant parameter in deciding the continuity and texture of the films deposited using CSP. The optoelectronic properties of films are largely dependent on factors like roughness, thickness etc which can be determined by spray rate. PL analysis was done on samples prepared at five different spray rates from 2 to 10 ml/min [Figure 4.9; Samples have been named 2, 4, 6, 8 and 10].

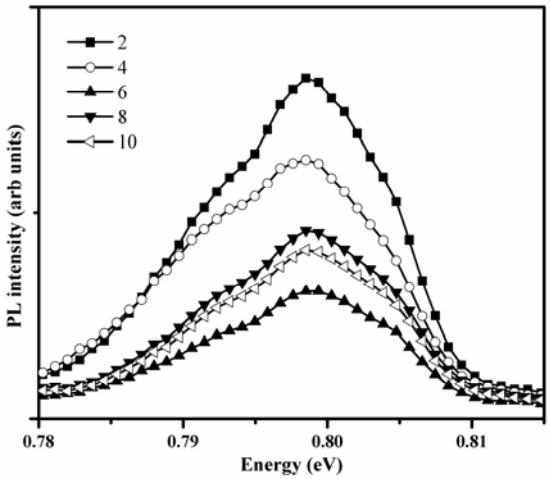

Figure 4.9: PL spectra of CZTS samples C, prepared at different spray rates.

Broad emission peaking at 0.797 eV could be recorded from all the films. PL intensity was observed to be highest for samples prepared at 2 ml/min. Though there was a regular fall in PL intensity with progress in spray rate from 2 to 6 ml/min, beyond 6 ml/min there was a slight increase in the intensity of the emission. PL emission intensity was the least for films prepared at a spray rate of 6 ml/min. Since band edge emission was absent, the choice of best spray rate was done by going for the sample in which defect related emission was least intense. As per our observations 6 ml/min appears to be the optimum spray rate for deposition of CZTS thin films.

4.3.4 How does the emission vary with stoichiometry of the films?

In section 4.3.1 we had identified the acceptor defect at 120 meV as Cu_{Zn} antisite defect. From sections 4.3.2 and 4.3.3, we have seen how using PL, we indirectly identify the substrate temperature and spray rate that yield films with lesser defect density. Therefore films prepared at a substrate temperature of 350 ^{o}C and a spray rate of 6 ml/min was chosen for further analysis. Stoichiometry was altered by varying the concentration of 'Cu' and care was taken to analyze samples with concentration of 'Cu' above and below the concentration required for near stoichiometry. Films prepared for Cu:Zn:Sn:S ratios 1:1:1:12, 1.5:1:1:12 and 2.5:1:1:12 were selected for studies and were named respectively as A, B and D. Structural studies were carried out on these samples to confirm whether the films formed were CZTS. Peaks characteristic to the kesterite structure of CZTS were observed in the XRD pattern [Figure 4.10 (a)] and characteristic Raman peaks [Figure 4.10 (b)] were also obtained. Data obtained for stoichiometric sample C [Cu:Zn:Sn:S= 2:1:1:12] is plotted along with that obtained for films A, B and D for comparison.

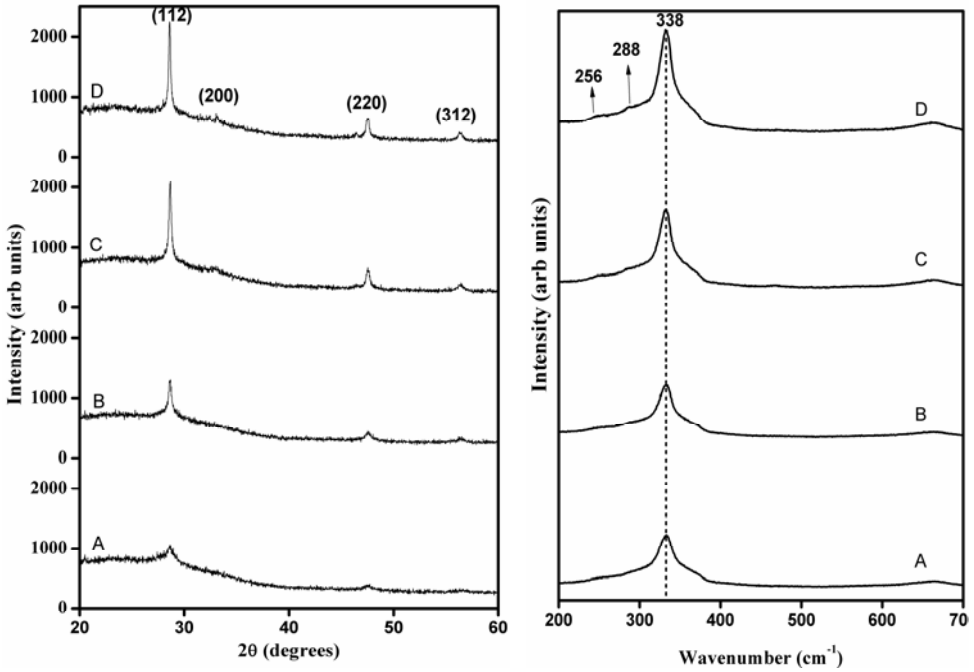

Figure 4.10:(a) X-ray diffraction pattern of samples A, B, C & D (b) Raman spectra of samples A, B, C & D.

Figure 4.11 shows the PL spectrum of samples A, B, and D recorded at 15 K. PL spectrum of stoichiometric sample C is also included in the figure for comparison. PL emission was absent in samples A and B. The absence of emission in samples A and B can be justified because it is Cu poor and therefore formation of the defect Cu_{Zn} is less likely. For sample D, a prominent emission peak occurs at 0.805 eV. Emission at 0.797 eV is also observed as a shoulder to the main peak.

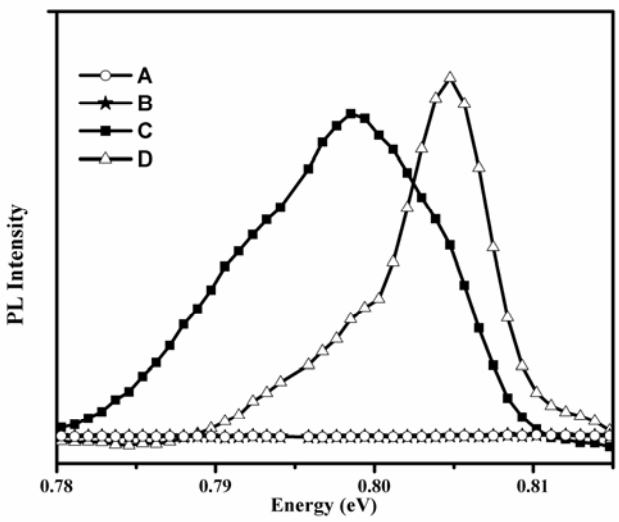

Figure 4.11: PL spectrum of samples A, B, C and D at 15 K.

4.3.1 Analysis of the origin of the emission at 0.797 eV in stoichiometric and Cu-rich CZTS thin films

It is already discussed that the emission at 0.797 eV may be due to a transition from a deep donor level at 0.533 eV to an acceptor at 0.12 eV [Section 4.3.1]. There are reports that generally midgap states are caused by antisite substitutions in tin site viz. Cu_{Sn} etc [1]. A very strong competitor to such defects in spray pyrolysed CZTS thin films is defects related to oxygen. The occurrence of antisite substitution of oxygen on Sn site in spray deposited SnS thin films had been observed by Sajeesh et al. [52]. To determine whether oxygen is the possible cause of formation of a level at 0.533 eV, another set of samples (named E) prepared by subjecting sample C to vacuum annealing under 125^{o}C for one hour were analyzed using PL. It was quite interesting to observe that the emission at 0.797 eV was absent in sample E. The only way to confirm whether the donor is created due to oxygen occupying the lattice sites of tin [i.e., O_{Sn}] is to purposefully increase the tin content in the sample. By doing so the lattice sites expected to be occupied by tin shall be filled and oxygen will be left

with no chance to occupy tin sites and the defect O_{Sn} will not be formed. If the defect associated is O_{Sn}, the emission will disappear with increase in tin content in the sample. We recorded PL from another sample F, prepared by purposefully increasing the Sn content in the stoichiometric sample C from 1 to 1.3 so that Cu:Zn:Sn:S=2:1:1.3:12 and we recorded the PL spectrum. As expected, the emission was absent in sample F. The PL spectrum of samples E and F have been plotted along with the PL spectrum of sample C [Figure 4.12] for comparison.

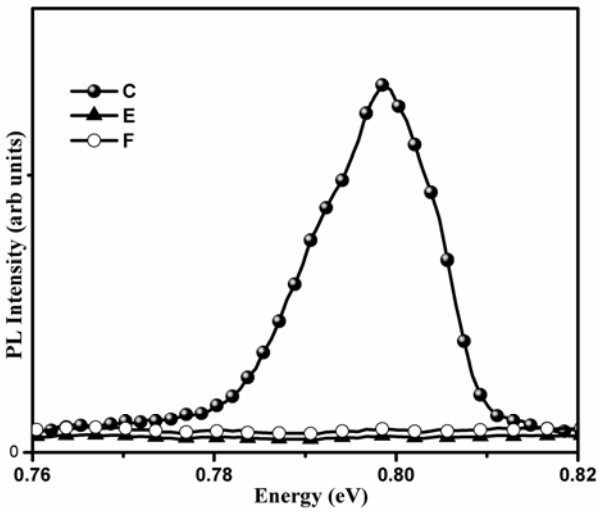

Figure 4.12: PL spectra of samples C, E and F.

X-ray Photoelectron Spectroscopy (XPS) depth profile analysis is the best confirmatory test to prove that increased tin content in the sample restricts oxygen incorporation. Generally from XPS measurements we get information regarding the chemical state and binding energies. Stoichiometric sample C, was also analyzed along with tin rich sample F. Depth profile of atomic concentration of various elements from surface to depth of the samples, was also obtained. In order to get information from the depth, surface layers were etched out by sputtering and measurements from each layer were taken. A graph is then plotted

between atomic concentration and sputter time. Sputter time t=0 min implies the surface of the sample and with progress in sputter time we get information from the depth of the sample.

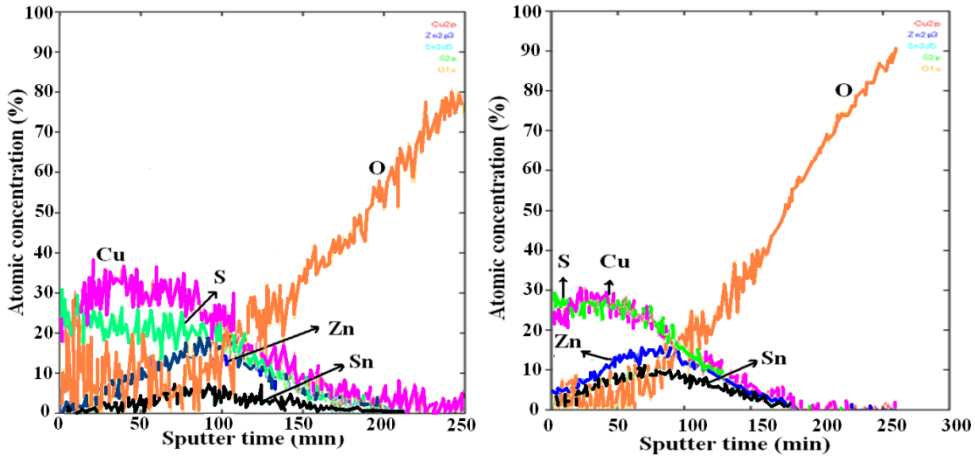

Figure 4.13: Atomic concentration vs sputter time plot of (a) sample C (b) sample F.

Binding energy values indicate the formation of CZTS in both samples C and F. Figure 4.13 (a) is the atomic concentration vs sputter time graph of sample C where we can see that oxygen is present in the sample as a contaminant. Figure 4.13 (b) is a similar plot for sample F which clearly indicates that when 'Sn' content is higher, oxygen incorporation is restricted. This result from XPS supports our assignment that the midgap level is due to O_{Sn} defect. Thus the recorded emission at 0.797eV arises due to recombination between a close to midgap defect due to O_{Sn} and an acceptor created by Cu_{Zn}. The band diagram proposed for stoichiometric sample is shown in Figure 4.14.

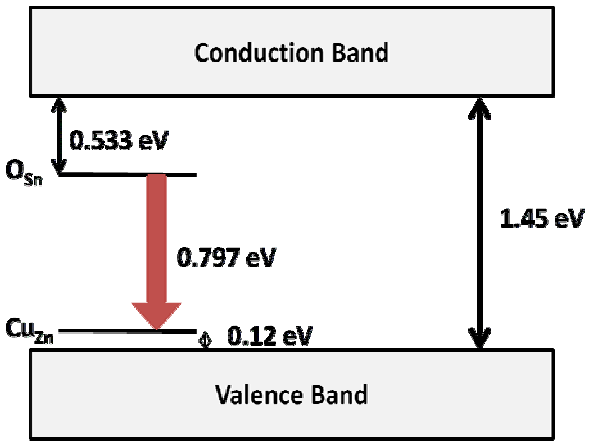

Figure 4.14: Band diagram proposed for stoichiometric CZTS thin film.

4.3.6 Analysis of defects responsible for emission at 0.805 eV in Cu-rich CZTS thin films

In Cu-rich CZTS samples, two emissions could be resolved- one at 0.797 eV and another major peak at 0.805 eV. We had identified the defects responsible for the emission at 0.797 eV as O_{Sn} and Cu_{Zn} (at 0.533 eV and 0.12 eV from CB and VB edges). Bandgap of Cu-rich sample D is 1.35 eV and the thermal activation energy obtained by monitoring the temperature dependence of emission at 0.797 eV is 0.11 ± 0.005 eV; which is the activation energy of Cu_{Zn} defect. Since bandgap is 1.35 eV, we obtain that O_{Sn} and Cu_{Zn} are positioned at 0.443 eV and 0.11 eV for Cu-rich sample D.

The emission at 0.805 eV cannot be due to band to band (BB) recombination since it is much less than the band gap energy, and hence it may be due to either band to impurity (BI), or donor to acceptor pair (DAP) recombination. PL intensity (I) is related to excitation power (P), such that the slope of the log-log plot of PL intensity with excitation power, gives the value of 'γ'. For sample D, we obtained $\gamma = 0.83$; thus it is clear that the transition is defect assisted [51]. Figure 4.15 (a) is the log-log plot of integrated PL intensity vs excitation power and (b) shows the variation of PL peak energy with excitation power.

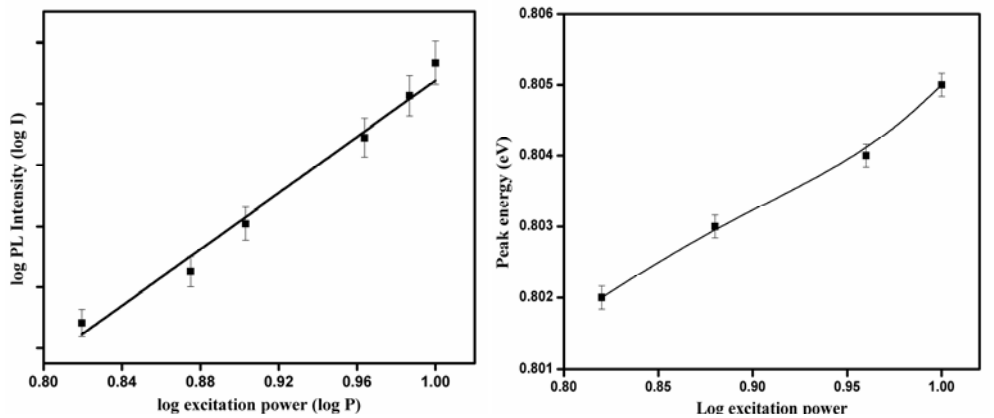

(a) (b)

Figure 4.15: (a) Log-log plot of PL intensity with excitation power for sample D (b) Variation of PL peak energy with excitation power.

Slight blue shift in peak position with increase in excitation power, is a feature of DAP transitions. Temperature dependence of PL peak energy indicates a slight shift in PL peak energy to lower energy side when temperature was increased from 15- 300 K. This is a characteristic feature of transitions belonging to DAP type; thus we conclude that the emission at 0.805 eV is a DAP transition.

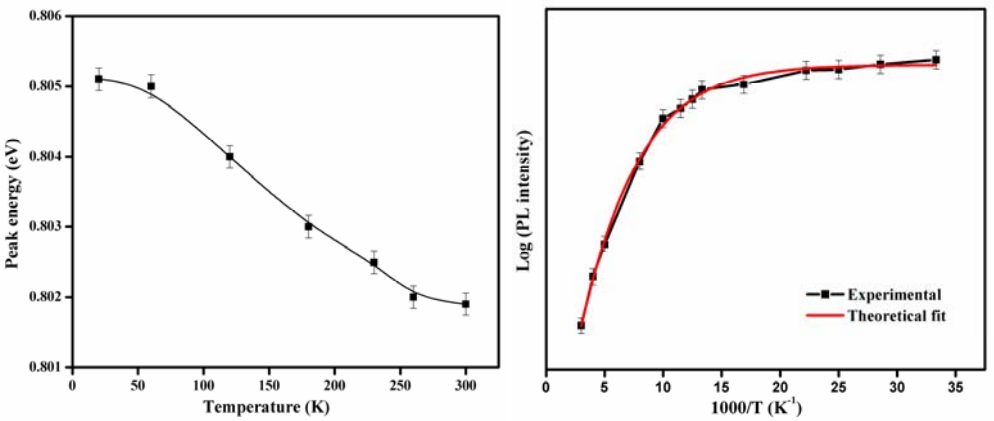

(a) (b)

Figure 4.16: (a) Temperature dependence of PL peak energy of emission at 0.805 eV (b) Arrhenious plot obtained for emission at 0.805 eV.

Activation energies of defects involved were calculated by monitoring the temperature dependence of PL emission intensity. Thermal activation energy of 0.135 eV could be obtained from Arrhenius plot. There are reports that under Cu-rich conditions, Cu_i defect forms easily and under Cu-rich and Sn-poor conditions, Cu_{Sn} defect is extremely likely to occur [1, 27]. This is because the formation energies of these defects have been lowered considerably.

There are reports throwing light on the formation energies of different defects and in one such report by Chen et al. [27], the defect Cu_i has been given a position 0.15 eV below conduction band maximum (CBM). The obtained activation energy is somewhat close to the reported theoretical value and we attribute the obtained activation energy to Cu_i defect. The emission obtained at 0.805 eV occurs in Cu-rich sample D, whose bandgap is 1.35 eV which implies that there may be an acceptor at 0.41 eV, which is a deep level. Cu_{Sn} defect is a predominant defect under Cu-rich and Sn-poor conditions. Midgap states due to Cu_{Sn} defect has been reported to be detrimental and is said to degrade device performance [1]. Grossberg et al. have reported activation energy of 0.289 eV and they have assigned it to Cu_{Sn} defect [43]. Chen et al. in their theoretical work have reported that acceptor defects due to Cu_{Sn}, Zn_{Sn}, V_{Zn} or V_{Sn} could occupy a position of 0.28 eV from valence band edge. Formation energies of Cu_{Sn} and Zn_{Sn} are less under Cu rich conditions, which makes their formation relatively easy compared to the other defects [15]. Theoretical reports indicate that higher ionized states of the acceptor Cu_{Sn} occur even deeper; close to the midgap region [27]. Since the sample chosen was a Cu-rich one, we attribute the level at 0.41 eV to higher ionized states of Cu_{Sn} defect. The experimental proof that we can put forward to substantiate this argument is that, if the acceptor defect is Cu_{Sn}, then defect concentration will increase with increase in 'Cu' concentration and formation of the defect will be restrained if 'Sn'

concentration is increased. If the defects favor radiative recombination, then PL would be the best tool for analysis. PL spectra were recorded from samples C, D and G, with Cu:Zn:Sn:S ratio = 2:1:1:12, 2.5:1:1:12 and 3:1:1:12 respectively [Figure 4.17]. Samples with higher concentration of Cu were eliminated from study because there was a tendency for secondary phase formation when concentration of Cu was increased beyond 3.

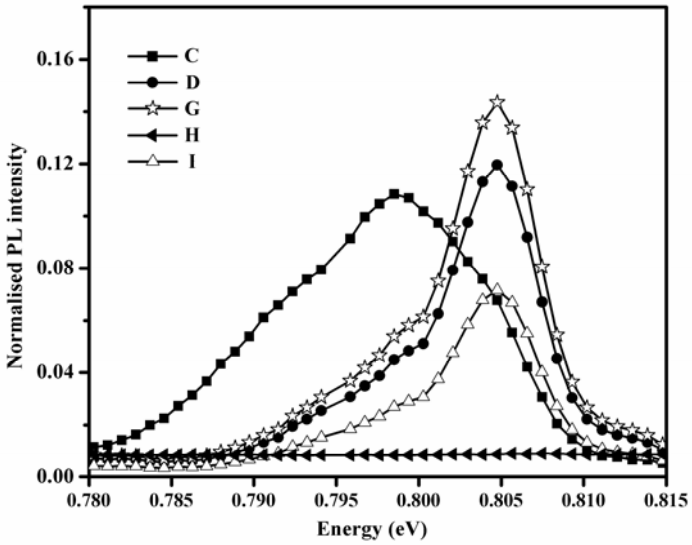

Figure 4.17: PL spectra of CZTS thin films C, D, G, H and I.

It is clear from the figure that with increase in 'Cu' concentration, the emission intensity increases. Clearly, the emission depends on 'Cu' concentration. If the defect is Cu_{Sn}, then the emission is expected to vary when concentration of tin is varied. To confirm this we analyzed, samples H, where Cu:Zn:Sn:S= 2.5:1:1.3:12. No emission could be obtained from the sample and this can be attributed to the fact that when 'Sn' concentration is increased, incorporation of 'Cu' in 'Sn' lattice sites is restricted to a large extent. This is in clear support to our assignment that the acceptor defect involved is Cu_{Sn}. We have identified sample C as stoichiometric with Cu:Zn:Sn:S=2:1:1:12; when tin

concentration is purposefully lowered in this case from 1 to 0.7, the condition is as good as Cu-rich condition. The emission at 0.805 eV is present in this sample named as I. All these observations are concurrent with our proposal that the emission at 0.805 eV arises from a donor due to Cu_i defect to an acceptor created by ionized states of Cu_{Sn} antisite defect. Based on our observations, a band diagram has been proposed for Cu-rich CZTS thin film as shown in Figure 4.18.

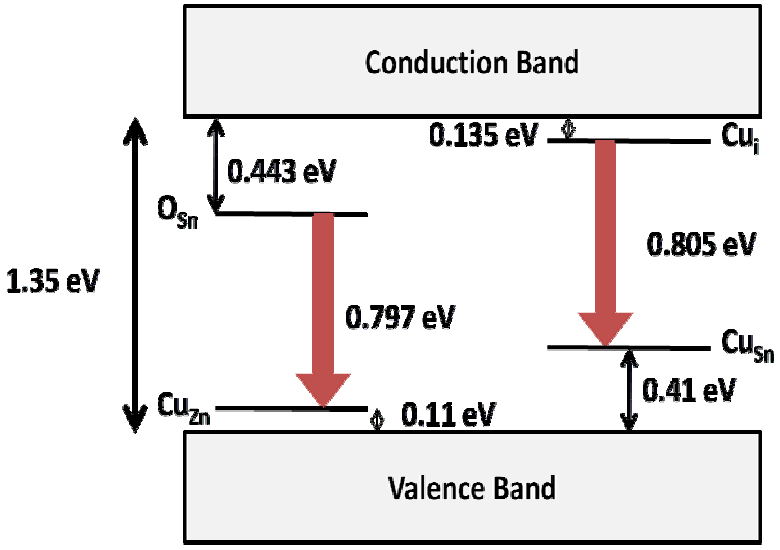

Figure 4.18: Band diagram proposed for Cu-rich CZTS thin film.

4.4 Conclusions

Mid-gap defects specific to spray pyrolysed CZTS thin films could be identified using PL. An emission at 0.797 eV could be recorded in stoichiometric CZTS thin films. This emission could be identified as a donor-acceptor pair transition involving O_{Sn} donor and Cu_{Zn} acceptor. Two emissions at 0.797 eV and 0.805 eV could be recorded in Cu-rich CZTS films. The former involves O_{Sn} and Cu_{Zn} defect. The latter has been identified as another donor-acceptor transition involving Cu_i donor and ionized Cu_{Sn} as acceptor. Defects identified

have been tabulated in Table 4.3. From PL, we could also indirectly identify deposition parameters yielding films which are relatively defect-free.

Table 4.3: Defects identified in CZTS thin film.

Sample	No: of samples tested	Impurity	Type	Activation energy (meV)
Stoichiometric (2:1:1:12)	10	Cu_{Zn}	Acceptor	120±5
		O_{Sn}	Donor	533±5
Cu-rich (2.5:1:1:12)	6	Cu_{Zn}	Acceptor	110±5
		O_{Sn}	Donor	443±5
(3:1:1:12)	6	Cu_i	Donor	135±5
(2:1:0.7:12)	4	Ionized Cu_{Sn}	Acceptor	410±5

References

[1]. **M. J. Romero, H. Du, G. Teeter, Y. Yan, M. M. Al-Jassim.** 2011, Physical Review B, Vol. 84, p. 165324 .

[2]. **S. Chen, X. G. Gong, A. Walsh, S. H. Wei.** 2010, Applied Physics Letters, Vol. 96, p. 021902 .

[3]. **K. Moriya, K. Tanaka, H. Uchiki.** 2007, Japanese Journal of Applied Physics, Vol. 46, p. 5780.

[4]. **J. S. Seol, S. Y. Lee, J. C. Lee, H. D. Nam, K. H. Kim.** 2003, Solar Energy, Vol. 75, p. 155.

[5]. **K. Ito, T. Nakazawa.** 1988, Japanese Journal of Applied Physics, Vol. 27, p. 2094.

[6]. **J. J. Scragg, P. J. Dale, L. M. Peter, G. Zoppi, I. Forbes.** 2008, Physica Status Solidi B, Vol. 245, p. 1772.

[7]. **A. Weber, H. Krauth, S. Perlt, B. Schubert, I. Kötschau, S. Schorr, H. Schock.** 2009, Thin Solid Films, Vol. 517, p. 2524.

[8]. **T. Todorov, M. Kita, J. Carda, P. Escribano.** 2009, Thin Solid Films, Vol. 517, p. 2541.

[9]. **S. Chen, X. G. Gong, A. Walsh, S. H. Wei.** 2009, Applied Physics Letters, Vol. 94, p. 041903 .

[10]. **B. Shin, O. Gunawan, Y. Zhu, N. A. Bojarczuk, S. J. Chey, S. Guha.** 2013, Progress in Photovoltaics: Research and Applications, Vol. 21, p. 72.

[11]. **B. G. Mendis, M. C. J. Goodman, J. D. Major, A. A. Taylor, K. Durose.** 2012, Journal of Applied Physics, Vol. 112, p. 124508 .

[12]. **S. B. Zhang, S. H. Wei, A. Zunger, H. K. Yoshida.** 2010, Physical Review B, Vol. 81, p. 245204 .

[13]. **S. H. Wei, S. B. Zhang, A. Zunger.** 1998, Applied Physics Letters, Vol. 72, p. 3199.

[14]. **J. M. Raulot, C. Domain, J. F. Guillemoles.** 2005, Journal of Physics and Chemistry of Solids, Vol. 66, p. 2019.

[15]. **A. Nagoya, R. Asahi, R. Wahl, G. Kresse.** 2010, Physical Review B, Vol. 81, p. 113202 .

[16]. **R. A. Wibowo, W. S. Kim, E. S. Lee, B. Munir, K. H. Kim.** 2007, Journal of Physics and Chemistry of Solids, Vol. 68, p. 1908.

[17]. **K. Oishi, G. Saito, K. Ebina, M. Nagahashi, K. Jimbo, W. S.Maw, H. Katagiri, M. Yamazaki, H. Araki, A. Takeuchi.** 2008, Thin Solid Films, Vol. 517, p. 1449.

[18]. **M. Grossberg, J. Krustok, K. Timmo, M. Altosaar.** 2009, Thin Solid Films, Vol. 517, p. 2489.

[19]. **S. R. Hall, J. T. Szymanski, J. M. Stewart.** 1978, Canadian Mineralogist, Vol. 16, p. S.131.

[20]. **K. Ito, T. Nakazawa.** 1988, Japanese Journal of Applied Physics 1-Regular Papers, Short Notes & Review Papers, Vol. 27, p. 2094.

[21]. **H. Katagiri, K. Jimbo, S. Yamada, T. Kamimura, W.S. Maw, T. Fukano, T. Ito, T.Motohiro.** 2008, Applied Physics Express, Vol. 1, p. 041201.

[22]. **J. J. Scragg, D. M. Berg, P. J. Dale.** 2010, Journal of Electroanalytical Chemistry, Vol. 646, p. 52.

[23]. **N. Nakayama, K. Ito.** 1996, Applied Surface Science, Vol. 92, p. 171.

[24]. **Y. B. Kishore Kumar, G. S. Babu, P. U. Bhaskar, V. S. Raja.** 2009, Solar Energy Materials and Solar Cells, Vol. 93, p. 1230.

[25]. **R. A. Wibowo, W. S. Kim, E. S. Lee, B. Munir, K. H. Kim.** 2007, Journal of Physics and Chemistry of Solids, Vol. 68, p. 1908.

[26]. **T. Todorov, M. Kita, J. Carda, P. Escribano.** 2009, Thin Solid Films, Vol. 517, p. 2541.

[27]. **S. Chen, J. H. Yang, X. G. Gong, A. Walsh, S. H. Wei.** 2010, Physical Review B, Vol. 81, p. 245204.

[28]. **H. Katagiri.** 2005, Thin Solid Films, Vol. 426, p. 480.

[29]. **J. J. Scragg, P. J. Dale, L. M. Peter.** 2008, Electrochemistry Communications, Vol. 10, p. 639.

[30]. **T. Tanaka, T. Nagatomo, D. Kawasaki, M. Nishio, Q. Guo, A. Wakahara, A. Yoshida, H. Ogawa.** 2005, Journal of Physics and Chemistry of Solids, Vol. 66, p. 1978.

[31]. **S. Botti, D. Kammerlandar, M. A. L. Marques.** 2011, Applied Physics Letters, Vol. 98, p. 241915.

[32]. **M. Cao, Y. Shen.** 2011, Journal of Crystal Growth, Vol. 318, p. 1117.

[33]. **H. Katagiri, N. Ihigaki, T. Ishida, K. Saito.** 2001, Japanese Journal of Applied Physics, Vol. 40, p. 500.

[34]. **H. Katagiri, K. Jimbo, W. S. Maw, K. Oishi, M. Yamazaki, H. Araki, A. Takeuchi.** 2009, Thin Solid Films, Vol. 517, p. 2455.

[35]. **C. Persson, Y. J. Zhao, S. Lany, A. Zunger.** 2005, Physical Review B, Vol. 72, p. 035211.

[36]. **M. J. Romero, H. Du, G. Teeter, Y. Yan, M. M. Al-Jassim.** 2011, Physical Review B, Vol. 84, p. 165324.

[37]. **K. Hones, E. Zscherpel, J. Scragg, S. Siebentritt.** 2009, Physica B, Vol. 404, p. 4949.

[38]. **J. P. Leitao, N. M. Santos, P. A. Fernandes, P. M. P. Salome, A. F. da Cunha, J. C. Gonzalez, G. M. Ribeiro, F. M. Matinaga.** 2011, Physics Review B, Vol. 84, p. 024120.

[39]. **A. Nagoya, R. Asahi, R. Wahl, G. Kresse.** 2010, Physical Review B, Vol. 81, p. 113202.

[40]. **K. Oishi, G. Saito, K. Ebina, M. Nagahashi, K. Jimbo, W. S. M. Oishi, G. Saito, K. Ebina, M. Nagahashi, K. Jimbo, W. S. Maw, H. Katagiri, M. Yamazaki, H. Araki, A. Takeuchi.** 2008, Thin Solid Films, Vol. 517, p. 1449.

[41]. **J. P. Leitão, N. M. Santos, P. A. Fernandes, P. M. P. Salomé, A. F. da Cunha, J. C. González, F. M. Matinaga.** 2011, Thin Solid Films, Vol. 519, p. 7390.

[42]. **X. Lin, J. Kavalakkatt, K. Kornhuber, S. Levcenko, Martha Ch. L. Steiner, A. Ennaoui.** 2013, Thin Solid Films, Vol. 535, p. 10.

[43]. **M. Grossberg, J. Krustok, J. Raudoja, T. Raadik.** 2012, Applied Physics Letters, Vol. 101, p. 102102.

[44]. **S. Levcenko, V. E. Tezlevan, E. Arushanov, S. Schorr,T. Unold.** 2012, Physical Review B, Vol. 86, p. 045206.

[45]. **M. G. Sousa, A. F. da Cunha, P. M. P. Salomé, P. A. Fernandes, J. P. Teixeira, J. P. Leitão.** 2013, Thin Solid Films, Vol. 535, p. 27.

[46]. **H. D. Kim, D. Kim, C. Park.** 2012, Molecular Crystals and Liquid Crystals, Vol. 564, p. 155.

[47]. **M. A. Majeed Khan, S. Kumar, M. Alhoshan, A.S.Al Dwayyan.** 2013, Optics and Laser Technology, Vol. 49, p. 196.

[48]. **M. Grossberg, P. Salu, J. Raudoja, J. Krustok.** 2013, Journal of Photonics of Energy, Vol. 3, p. 030599 .

[49]. **S. Siebentritt.** 2013, Thin Solid Films, Vol. 535, p. 1.

[50]. **X. Fontane, L. Calvo-Barrio, V. Izquierdo-Roca, E. Saucedo, A. P. Rodriguez, J. R. Morante, D. M. Berg, P. J. Dale, S. Siebentritt.** 2011, Applied Physics Letters, Vol. 98, p. 181905.

[51]. **T. Schmidt, K. Lischka, W. Zulehner.** 1992, Physical Review B, Vol. 45, p. 8989.

[52]. **T. H. Sajeesh, K. B. Jinesh, M. Rao, C. S. Kartha, K. P. Vijayakumar.** 2012, Phys. Status Solidi A, Vol. 209, p. 1274.

[53]. **S. Lany, A. Zunger.** 2008, Vol. 100, p. 016401.

[54]. **H. Katagiri, K. Jimbo, S. Yamada, T. Kamimura, W. S. Maw, T. Fukano, T. Ito, T. Motohiro.** 2008, Applied Physics Express , Vol. 1, p. 41201.

.....ൠ.....

Chapter 5

ANALYSIS OF DEFECTS IN ZINC SULPHIDE THIN FILMS

5.1 Introduction

Zinc Sulphide (ZnS) is an important II-VI compound semiconductor which has received tremendous attention over the past century. Reports on this material date back to 1950s and various properties of this material have been well documented. Ample literature is available on the energy band structure [1], crystal structure and optical properties [2] extinction coefficient [2], refractive index [3] etc of ZnS. Even though vacuum deposition [4] is the most widely preferred technique, alternate deposition techniques like spray pyrolysis, liquid phase epitaxy, chemical bath deposition etc [5] have also been reported on ZnS. There are also several reports on developing phosphors based on ZnS for purposes like lighting, detecting, displaying and so on [6]. ZnS can also be used as buffer layer in solar cell applications [7].

Luminescence mechanism in ZnS is reported in several review articles [8, 9]. The origin of blue and green emission in ZnS is still under much argument [10]. Optical and electrical properties of ZnS are governed by various point defects [11]. If we go for fabricating electronic devices, for instance a solar cell using ZnS as buffer layer, either there has to be some sort of modeling about the possible defects or a thorough defect level analysis by techniques as photoluminescence (PL),

thermally stimulated current measurements (TSC) etc. The defects likely to appear depend on the preparation conditions as well as doping. In this chapter we have attempted a defect level analysis of ZnS thin films using PL and have tried to propose whether ZnS is a suitable candidate for buffer layer in thin film solar cells.

5.2 Review on PL studies in ZnS

The phenomenon of photoluminescence quenching by applying a weak alternating electric field has been discussed by Vereshchagin et al. [12]. The authors propose that quenching is brought about by processes happening in local regions of the crystal. Quenching involves transition of valence electrons to luminescent centres and such electrons derive this energy from the electric field. Quenching characteristics obtained theoretically matches quite very well with experimental data.

Studies on spray deposited ZnS:Mn films were reported by Falcony et al. [13] who mentions about the observation of two emissions- one at 490 nm which is associated with a self activated centre and one at 590 nm associated with 'Mn^{2+}' ions in ZnS lattice. Corresponding to the emission at 590 nm, activation energy of 0.71 ±0.05 eV could be calculated. Denzler et al. [14] reported luminescence studies of ZnS nanocrystals fabricated for electroluminescent applications, light converting electrodes etc. Transitions in the ultraviolet region (416.1, 423.9, 430.1 and 437.8 nm) have been identified as arising from vacancy and interstitial sites of zinc and sulphur. 'Mn' impurity assisted visible emission at 590.1 nm was also observed. Photoluminescence in ZnS:Mn thin films has been reported by Lu et al. [15]. In addition to the yellow-orange emissions, there is blue and red emission which is apparently due to chloride impurities. Red emission has been associated with 'Mn-Cl' defect pair and in intentionally 'Cl' doped films, self activated blue emission has also been observed.

Dinsmore et al. [16] reported on the light emitting and structural properties of ZnS:Mn nanoparticles annealed in vacuum at temperatures up to 525 ^{o}C. It was observed that particle size has no significant effect on the emission wavelength. Optical studies on nanocrystalline ZnS thin films (both undoped and doped with 'Mn') were carried out by Maity et al. [17]. The authors have mentioned about a strong luminescence band at 2.07 eV. Variation of optical properties with annealing temperature has been analyzed. They have also come up with an observation that the emission in the 600-606 nm region diminished in intensity with increase in 'Mn' concentration.

The effects of 'Ag', 'Ag+Cl' and 'Ag+In' co-doping on p-type conductivity of ZnS:N grown on GaAs substrates was studied by Kishimoto et al. [18]. It was observed that in films ZnS:(N, Ag, In) an emission at 436 nm was dominant whereas in ZnS:(N, Ag) and ZnS:(N, Ag, Cl) films an emission appeared at 420 nm. The emission at 420 nm has been described as a transition from CB to 'Ag' acceptor level. The authors have highlighted the appearance of blue emission and p-type conductivity simultaneously in ZnS: (N, Ag, In) co-doped sample. PL studies on 'In' doped ZnS thin films were reported (19] and emission in the range 430-480 nm was observed and attributed to the incorporation of indium. This band has been attributed to donor acceptor pair recombination and another emission at 425 nm in undoped ZnS has been attributed to a localized centre.

In a report on high quality ZnS thin films grown on GaAs substrate by Thiandoume et al. [20], low linewidths were observed from diffraction data and the presence of free excitonic emission with linewidths as low as 4.7 meV is taken as an indication of high crystalline quality. Kumbhojkar et al. [21] have commented in their report on various PL transitions and the effects of size quantization and surface conditions on the electronic structure of ZnS. Strong band gap luminescence was observed for mercaptoethanol capped ZnS quantum dots.

The effect of 'Er' doping in ZnS thin films results in creation of luminescent centers as well as shallow donors, deep acceptors, sulphur vacancies, zinc vacancies etc and its effect on the electroluminescence properties of ZnS:Er based device has been monitored by Zhidong et al. [22]. The effect of incorporation of isovalent element 'Te' in ZnS thin films on the optoelectronic properties was studied by Chan et al. [23]. The work involves first principle calculation on the possible defects resulting due to 'Te' incorporation in ZnS thin films. Experimental evidences from XPS studies also suggest that highly luminescent centers in $ZnS_{1-x}Te_x$ are probably due to incorporation of 'Te' in antisite positions. Kryshtab et al. [24] synthesized blue and green light emitting structures by doping with 'Al', 'Cu', 'Ga' and 'Cl'. The effect of doping, presence of impurity and type of substrate on the structural and luminescence properties is also studied. An interesting observation is that when a phase transition occurs from sphalerite to wurtzite lattice, the blue emission band position shifts to shorter wavelength range by 10 nm.

Zhu et al. [25] observed visible room temperature photoluminescence from ZnS nanoparticle thin films embedded in SiO_2 matrices without the need for any dopant. The mechanism of PL and its blue shift with sample annealing has been attributed to sulphur vacancies and formation of $ZnS(0_2^-)$ in the surface layers of the nanoparticles adjacent to SiO_2. Occurrence of blue and green emission peaks in ZnS powder sintered at various temperatures was reported by Lee et al. [26]. Sphalerite and wurtzite phases coexist in the ZnS powder and various emission peaks were assigned to zinc vacancy and sulfur vacancy defects formed in sphalerite and wurtzite structures.

Hu et al. [27] have synthesized ZnS micrometer sized diskettes and nano sized ribbons for possible foreseen interesting and novel electronic and optoelectronic applications. The highlight of these nanostructures is their strong

luminescence when compared to the source material. Through PL measurements Ishizumi et al. [28] have tried to establish that sequential ion implantation is an effective technique for creation of luminescent nanocrystals of ZnS. Thin films containing ZnS nanoparticles and ZnS nanoparticles embedded in SiO_2 matrix were prepared by sol-gel method by Bhattacharjee et al. [29]. They observed a size-dependent blue emission in ZnS nanoparticles and UV as well as red emission from ZnS-SiO_2 nanoparticles. Degradation of luminescence quality with aging was much reduced in the case of ZnS nanoparticles embedded in SiO_2 matrix.

Ye et al. [10] have studied the optical properties of sulfur rich ZnS nanobelts and they have attributed the blue emission to surface sulfur species rather than the earlier proposed self activated mechanism. Properties of nanocrystalline particles of ZnS coated on nano porous silicon were analyzed by Murugan et al. [30]. Measurement at room temperature indicates luminescence peaks covering the blue to red region of electromagnetic spectrum. Optical properties of surface sulfur rich ZnS nanobelts have been investigated [31] by means of PL and PLE spectroscopy. Anomalous shift was observed in the PL peak energy and FWHM of green band. This has been attributed to thermal population in localized states due to unsaturated orbitals of dangling bonds in surface states of sulfur.

Liu et al. [32] synthesized ZnS microspheres using solvothermal route and PL studies were carried out. A strong emission band at 520 nm and a weak blue band at 457 nm were observed of which the blue band has been described as similar to the emission at 438 nm observed in ZnS nanocrystals and the authors have mentioned that they are not sure about the cause of green emission. Jayanthi et al. [33] have reported on the study of ZnS:Cu nanoparticles prepared by CBD technique. Green emission in ZnS has been attributed to ‘Cu’ impurities

and blue/purple emission to intrinsic defects. ZnS tetrapods were synthesized and studied by Deng et al. [34]. A strong emission in the green (495.2 nm) was observed and the authors comment that along with 'S' vacancy morphology of the nanotetrapods is also responsible for this emission.

Works on using EXAFS studies to analyze ZnS: (Cu, Cl) nanocrystals and to correlate the results especially with PL were done by Corrado et al. [35]. The optical emission has been assigned to recombination of trapped electron and hole within the bandgap. The effect of ultraviolet irradiation on the luminescence properties of ZnS nanoparticles both undoped and doped with 'Ag' was analyzed by Qu et al. [36]. Lifetime shortening due to introduction of 'Ag^{+}' ions occurs which has been verified from the temporal variation of PL under UV irradiation.

Hernandez-Fenollosa et al. [37] studied the variation in properties of spray deposited ZnS films prepared for various Zn:S ratios and precursors. Defect related emission was observed in the samples and a conclusion was arrived that the samples for which the PL intensity was least is the best. In another work [38], PL and I-V studies were performed on ZnS grown on 'Si' nanoporous pillar array (Si-NPA). The authors have observed five emission peaks of which they have attributed the emission at 648 and 705 nm as arising from Si-NPA. UV band and two blue bands have been attributed to unsaturated sp^3 orbitals of sulfur atoms, defect states related to vacancy of sulfur and other surface states. Sadekar et al. [39] have characterized ZnS thin films deposited using solution growth technique on glass substrates at a temperature of 90 ^{o}C. PL studies reveal a strong midgap emission at 2.02 eV which has been attributed to native defects due to interstitial zinc atoms in the films.

ZnS nanocrystals embedded in PVA matrix were synthesized and their properties were studied by Jyoti et al. [40]. Two emissions- one at 315 nm and

the other at 425 nm were observed of which emission at 315 nm has been attributed to bandgap transitions while the latter has been assigned to sulfur vacancy. Point defects in ZnS films grown under different conditions were studied and band diagram illustrating the position of various defect related energy levels was proposed by Kurbatov et al. [41]. Liu et al. [42] studied ZnS nanoparticles synthesized from a single-source precursor in a continuous spray pyrolysis reactor. PL spectrum showed two emission bands- one at 390 nm and the other at 440 nm. The former was attributed to be due to ZnO impurities which were removed by HF treatment. The latter was attributed to emission from ZnS whose quantum yield increased to 15 % on HF treatment.

Tiwary et al. [43] have synthesized wurtzite phase of ZnS nanocrystals by annealing its cubic form in the temperature range 200-600 ^{o}C. A strong stable green emission at 518 nm was observed from these samples which the authors presume to be arising from donors due to sulfur vacancies and acceptors due to zinc vacancies. Won et al. [44] in their report have come up with an economic method for synthesis of ZnS:Mn^{2+} particles. PL emission at 472 nm was dominant in 'Cl^{-}' doped samples which on co-doping with 'Mn^{2+}' yielded an emission at 587 $\pm$ 1 nm. ZnS particles prepared with large amount of NaCl flux display smoother surfaces, good dispersity and high luminescence efficiency.

In another report [45], ZnO-ZnS: [Ag, Ga] thin films were deposited using MOCVD technique. Blue and green emissions were observed in these films. Blue emission has been related to 'Ag' incorporation and green has been attributed to presence of oxygen. Influence of argon pressure on the structural, morphological and optical properties of ZnS films deposited using PLD technique has been studied by Chalana et al. [46]. Focusing specially on the PL properties, it could be observed that PL intensity was high for films prepared under argon-free ambience compared to those prepared under argon ambience

and this has been attributed to the presence of structural disorders and defects. PL spectra recorded at an excitation of 325 nm showed an intense yellow emission.

The properties of ZnS films grown on porous 'Si' substrates of different porosity were analyzed by Wang et al. [47]. As porosity is varied the emission also changes and the authors have come up with an interesting possibility of combining the blue and green emission from ZnS with the red emission of the porous silicon substrates to produce white light which would be a cheap route for synthesis of white LED. In yet another report [48], ZnS nanocrystals prepared by treatment under H_2S atmosphere were analyzed- blue, green and orange emissions were observed which were attributed to surface states, electron transfer from sulfur vacancies to interstitial sulfur states and recombination between interstitial zinc and zinc vacancy sites. Chen et al. [49] have reported on the cause of green luminescence (at 525 nm) in ZnS nanostructures. The emission depended largely on the size of the nanostructures as well as the Zn:S ratio.

In a report on the experimental and theoretical investigations on the role of a capping agent in ZnS nanoparticles and its key role in PL activity, Santana et al. [50] have remarked that PL arises due to distinct distortions in the lattice. PL studies on ZnS QDs prepared by co-precipitation, UVP and UVP+PSH treatments have been presented in their report by Sahai et al. [51]. Reason for improved brightness in samples prepared by UVP+PSH treatment has been attributed to efficient donor-acceptor recombinations. PL peak at 420 nm is attributed to self activated luminescent centre arising due to association of 'Zn^{2+}' vacancy and coactivator 'Al^{3+}' as donor. PL peak at 456 nm is reported to be recombination between 'Al^{3+}' donor and 'Ag^{+}' acceptor. Time resolved PL measurements were employed [52] to find out the sample with least radiative

decay time which is best for nano-based display systems. ZnS nanowire bundles with excellent superhydrophobic properties were synthesized and studied. The nanowires exhibit excellent yellow emission and can be put to use in optical, optoelectronic as well as self cleaning surface micro/nanodevices.

Synthesis of ZnS nanocombs has been dealt with by Lan et al. [53]. Nanocombs were formed via a two step process on the sides of nanobelts. PL emission of the nanobelts indicates a strong emission at 530 nm with a shoulder at 625 nm. The reason for emission at 530 nm is still under debate. The band at 625 nm may arise due to structural defects like point defects, microtwins or dopants. The emission at 530 nm has been constrained in nanocombs. New emission at 570 nm has been observed which has been attributed to some self activated centres. Another emission band at 635 nm observed in nanocombs is due to the introduction of impurity 'Sn'.

Effect of oxygen in the energy band structure of ZnS has been studied by Morozova et al. [54]. Self activated oxygen containing complexes are formed which are responsible for the emission in the visible region of the spectra and the bound excitonic emission (I_1). Wang et al. [55] describe the temperature dependence of excitonic and defect related emissions in nanobelts/wires of ZnS from 10-250 K in their report. Presence of free exciton and associated LO phonon replicas indicate the superior quality of nanobelts whereas polycentric defect complexes present in nanowires indicate abundance of defects. The properties of 'Cr' doped ZnS nanoparticles have been studied by Zeng et al. [56] and the authors have observed from the absorption spectra that in addition to the intrinsic absorption there are two characteristic bands of 'Cr^{3+}' in the visible. Band-edge emission exhibits a blue-shift with increase in concentration of 'Cr^{3+}'. Emission peaks related to surface states and zinc vacancies have been observed in the 400-500 nm range.

In their report, Tiwari et al. [57] have synthesized sodium hexametaphosphate (SHMP) capped ZnS nanoparticles and size dependent PL properties of 'Cu' doped SHMP capped ZnS particles have been studied. The observation of excitonic emission is a proof for the excellent optical quality. A sharp emission peak at 510 nm was observed and the authors presume it to be due to complex interaction between host lattice and dopant ion and also due to the modification of luminescent centres by the capping agent and chalcogenide source.

The central theme in most of the reports on PL studies in ZnS is on creation of luminescent centres by doping with suitable elements and identification of various defects present. In most of the reported works, the focus is on tailoring ZnS for phosphor applications. ZnS which is a wide bandgap material with bandgap ~3.5 eV and can be used as buffer layer in thin films solar cells. As the bandgap of ZnS is high, there is a scope for improvement in open circuit voltage. Also if there are defects within the bandgap which assist sub-bandgap absorption, a major portion of the solar spectrum can be utilized effectively. In this work we have tried to identify various defects in ZnS using PL and also to find the optimum deposition parameters using PL. Resistance of pristine ZnS thin films is quite high, but for application as buffer layer, resistance should be low. 'Cu' doping has been done to bring down the resistivity of ZnS thin films and we have done PL studies on 'Cu' doped ZnS thin films also. We have tried to propose an explanation for reduction in resistivity of ZnS thin films on 'Cu' doping.

5.3 Observations and discussions

In CSP technique, there are numerous parameters which drastically affect the optoelectronic properties of deposited films. PL studies were carried out on films prepared by varying different deposition parameters.

5.3.1 Studies on films prepared using different precursors of zinc

Films deposited using zinc acetate, zinc chloride and zinc nitrate as precursors for zinc, were selected for the current study. These films were deposited at a substrate temperature of 460 ^{o}C and spray rate of 6 ml/min. Films were named respectively as A-460, C-460 and N-460 respectively. Figure 5.1 shows the PL spectra recorded from samples A-460, C-460 and N-460.

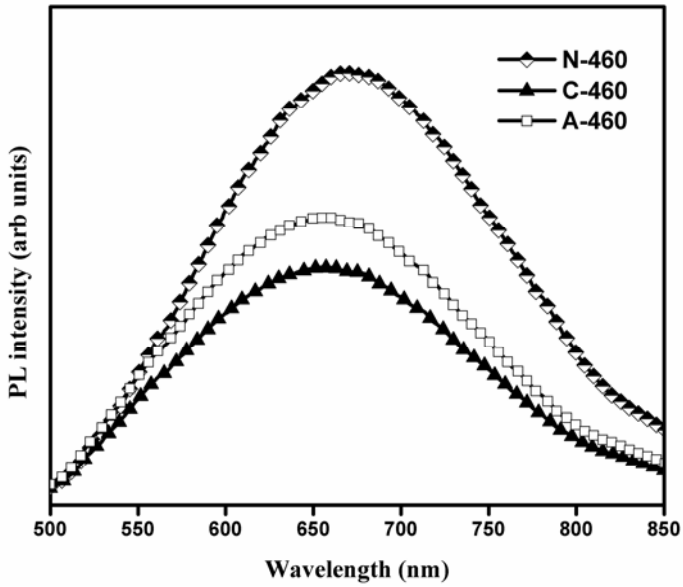

Figure 5.1: PL spectra of ZnS thin films prepared using different precursors for zinc.

A broad emission centered at 1.88 eV with FWHM of ~0.54 eV could be recorded in all the three samples. Peak energy of the emission is much less than the bandgap energy of 3.5 eV and therefore it has to be associated with defects. Introducing dopants like 'Mn' in ZnS is done generally to make it suitable for phosphor application and red emission has been reported in such films [15, 17]. But seldom has a red emission at 1.88 eV been reported in pristine ZnS thin films.

Detection of band to band emission or free excitonic emission from samples is treated as an indication of high sample quality. But for these three samples, we did not observe any emission belonging to these two categories. Instead a stray defect related emission was observed at 1.88 eV. The intensity of this peak varied with samples prepared using different precursors for zinc. It is observed that the emission intensity is minimum for sample prepared with zinc chloride as precursor showing that defects may be less in this sample.

Results from XRD measurements complement the results from PL [Figure 5.2].

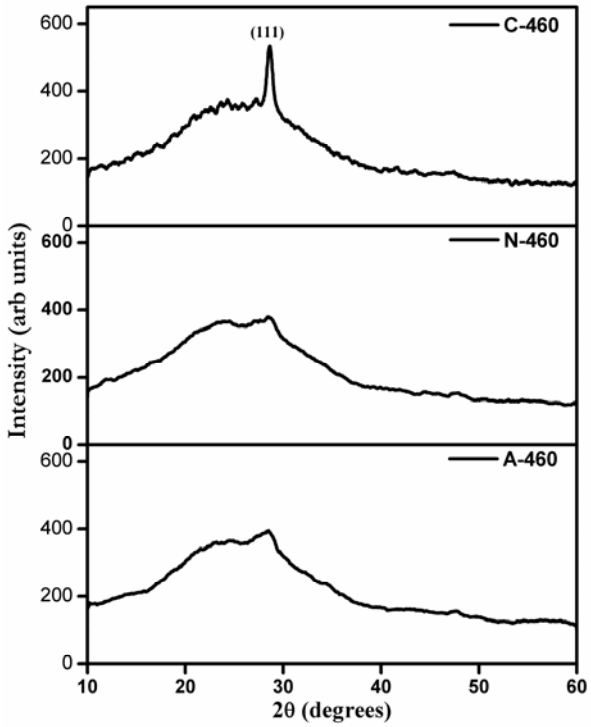

Figure 5.2: XRD pattern of ZnS thin films prepared using different precursors for zinc.

XRD patterns of N-460 and A-460 indicate the amorphous nature of these films. For films C-460, well-defined diffraction peak along (111) direction corresponding to the 'cubic structure' is present [JCPDS card no. 05-0566].

Based on the results from PL and XRD, we conclude that zinc chloride is the better choice for precursor of zinc compared to zinc acetate and zinc nitrate.

5.3.2 Studies on ZnS thin films prepared at different substrate temperatures

ZnS thin films prepared at different substrate temperatures- 400, 420, 440, 460 and 480 ^{o}C, with zinc chloride and thiourea as precursors, were selected for study. Figure 5.3 shows the PL spectra obtained from ZnS thin films prepared at different substrate temperatures.

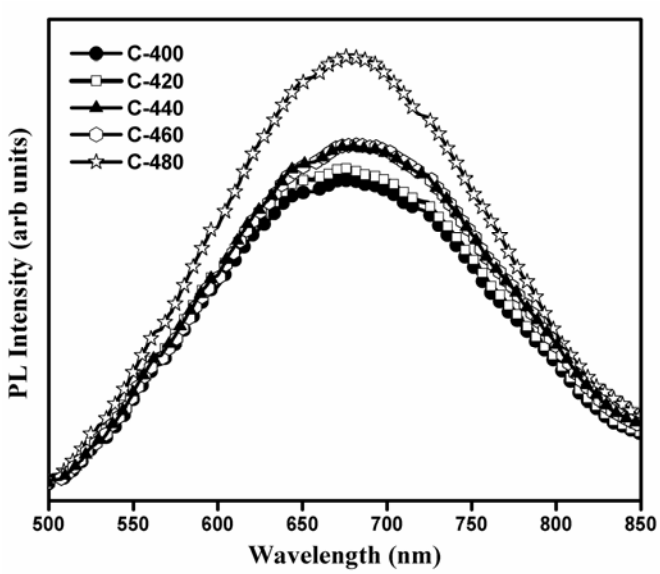

Figure 5.3: PL spectra of ZnS thin films prepared at different substrate temperatures.

Broad emission at 1.88 eV, could be observed in films prepared at different substrate temperatures all the films. Up to substrate temperatures of 460 ^{o}C, PL emission intensity was almost the same, beyond which emission intensity showed a clear enhancement. Figure 5.4 shows the XRD pattern obtained for ZnS films deposited at different temperatures.

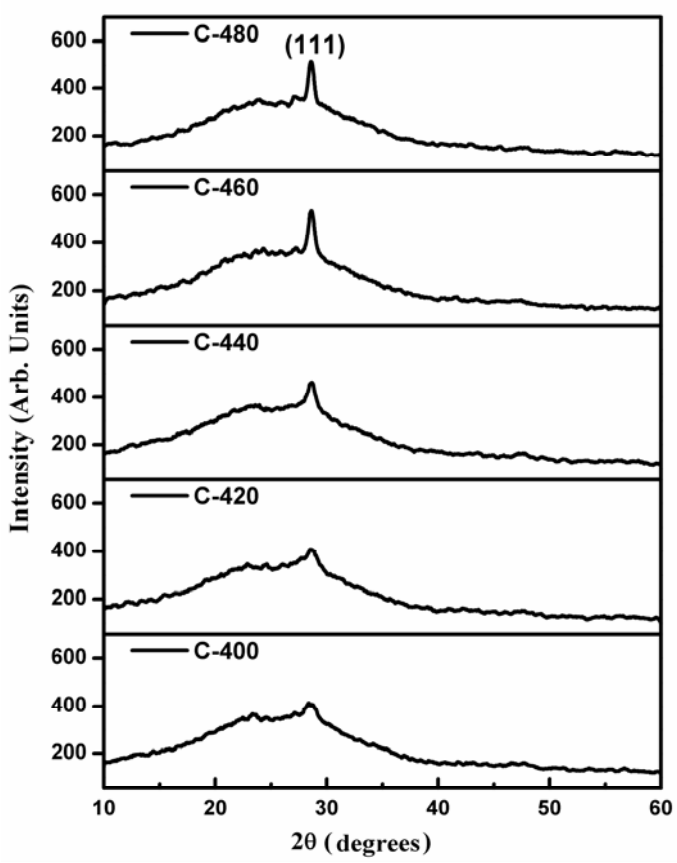

Figure 5.4: XRD pattern of ZnS thin films prepared at different substrate temperatures.

For sample prepared at 460 ^{o}C, defect-related PL emission intensity is low and crystallinity is found to be better. Thus based on results from PL and XRD, we conclude that 460 ^{o}C is the optimum substrate temperature.

5.3.3 Studies on ZnS thin films prepared for different Zn:S ratios

ZnS films prepared for Zn:S ratios 1:2, 1:4 and 1:6 were selected for study. PL studies were carried out on these samples and the PL spectra are shown in Figure 5.5.

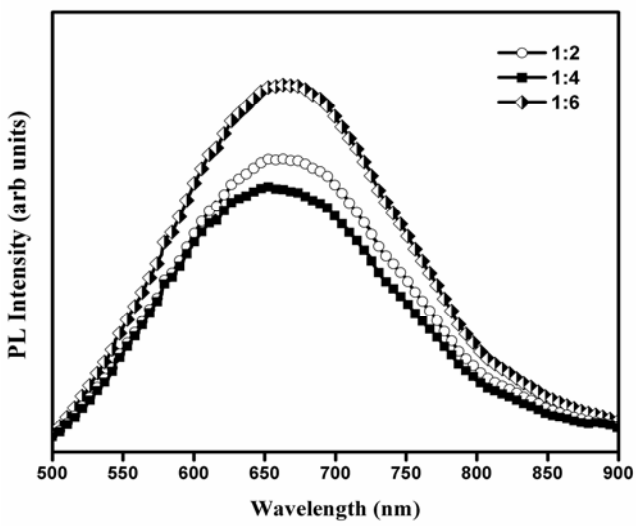

Figure 5.5: PL spectra of samples prepared with different Zn:S ratios.

Defect related emission intensity is minimum for ZnS thin films with Zn:S ratio 1:4. FWHM of the emission, which is an indicator of defect concentration, is also least [~ 0.54 eV] for these samples. So results from PL indicate that Zn:S ratio 1:4 is better.

5.3.4 Identifying the origin of the emission at 1.88 eV

The emission at 1.88 eV is present in ZnS films prepared at different substrate temperatures, using different precursors and for different Zn:S ratios. Temperature dependent PL measurements and excitation power dependent PL measurements were done to identify the defects responsible for the emission. ZnS thin films prepared at a substrate temperature of 460 ^{o}C, using zinc chloride and thiourea for Zn:S ratio 1:4, i.e., films C-460, were chosen for measurements.

5.3.4.1 Excitation power dependence of the emission at 1.88 eV

Recalling the relation connecting PL intensity (I) and excitation power (P) i.e., $I \alpha P^{\gamma}$, it is quite obvious that performing a linear fit to the log-log plot of PL intensity with excitation power, 'γ' value can be obtained. Figure 5.6 shows the log-log plot of variation in PL intensity with excitation power.

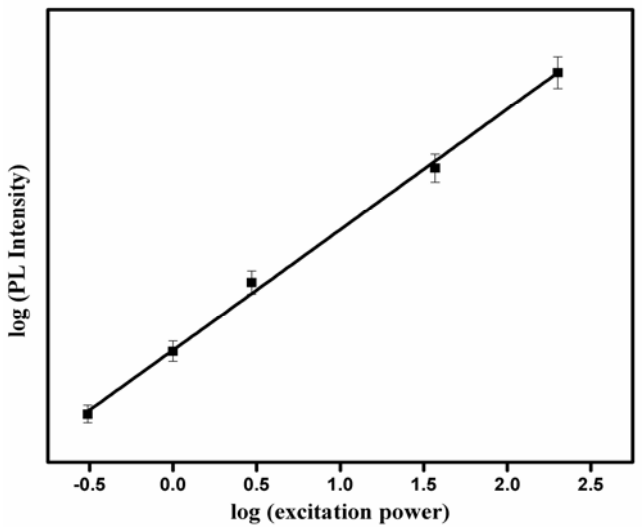

Figure 5.6: Log-log plot of variation in PL intensity with excitation power.

Value of γ is 0.998, which indicates that the transition is defect-assisted. Figure 5.7 shows the variation of PL peak energy with excitation power. Blue shift in peak energy with increase in excitation power is a feature of donor-to-acceptor pair (DAP) transition.

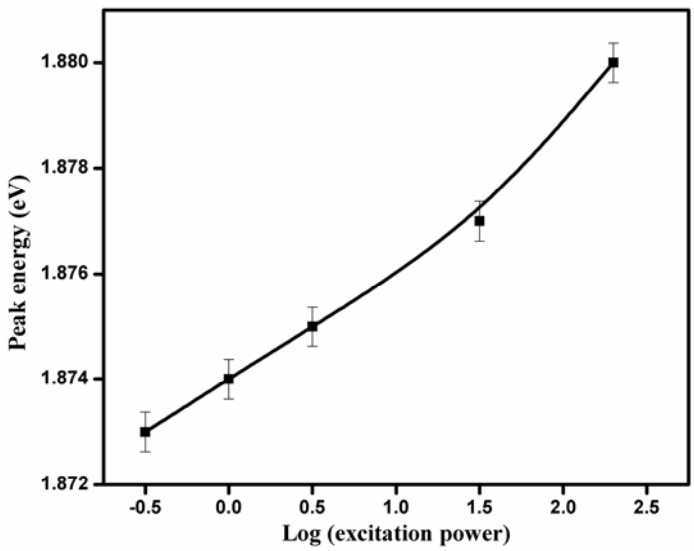

Figure 5.7: Variation of PL peak energy with excitation power.

5.3.4.2 Temperature dependence of the emission at 1.88 eV

PL spectra were recorded by varying the sample temperature from 15 to 300 K. Variation in intensity of the emission at 1.88 eV with temperature was observed. Activation energy can be calculated by performing a theoretical curve fit to the Arrhenius plot [log (PL intensity) vs 1000/T] using the relation (which has been mentioned already in Chapter 2),

$$\frac{I(T)}{I(0)} = \frac{1}{\left[1 + Ce^{-\frac{\Delta E}{kT}}\right]}$$

as shown in Figure 5.8.

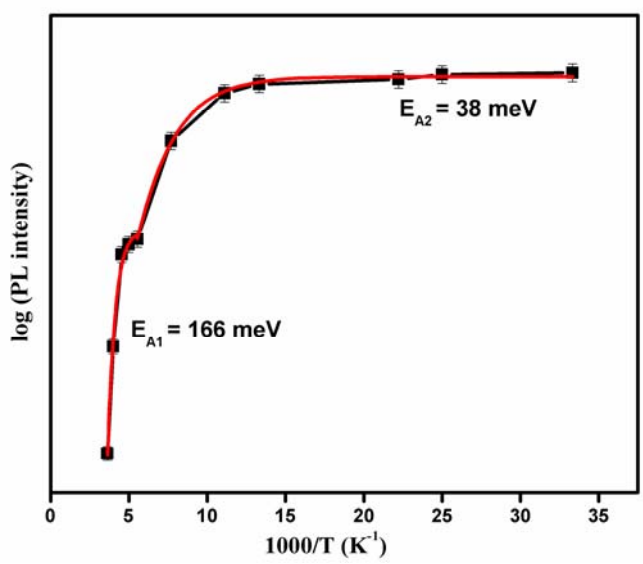

Figure 5.8: Arrhenious plot. Red line indicates theoretical fit to the experimental data.

On performing theoretical fit to the Arrhenious plot, we could calculate two activation energies- 38 meV and 166 meV. The activation energy of 166 meV is close to the delocalization energy of electrons from strong localized state in

unsaturated orbitals of surface sulfur species [167 meV] reported by Gibbons and Spear [58].

In spray pyrolyzed ZnS thin films, defects related to oxygen are quite likely. Thus the activation energy at 38 meV may probably be due to such defects. To prove this, we recorded the PL spectrum from C-460 film subjected to vacuum annealing (named C-460 v). Figure 5.9 shows the PL spectrum obtained from C-460 v film; PL spectrum obtained from C-460 has been plotted along with for comparison. PL spectrum of C-460 v shifts to the low energy side and the FWHM also decreases significantly from ~ 0.54 eV to ~ 0.38 eV indicating a decrease in defect concentration. This may be due to removal of oxygen related defects on vacuum annealing.

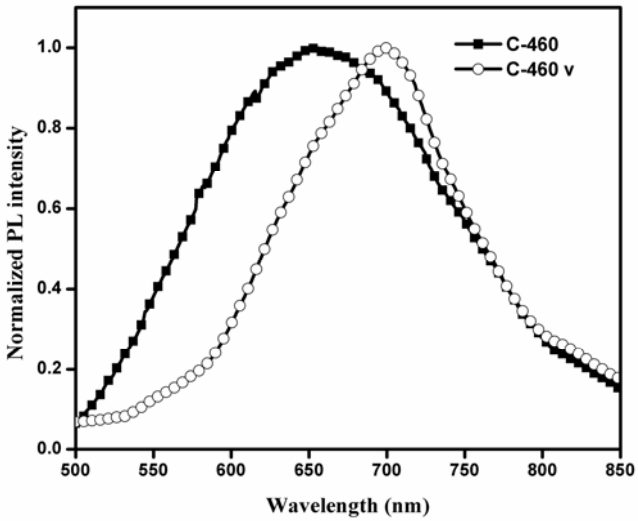

Figure 5.9: PL spectra of C-460 and C-460 v thin films.

Temperature dependent PL measurements were done on C-460 v and from the Arrhenious plot [Figure 5.10], activation energy was calculated.

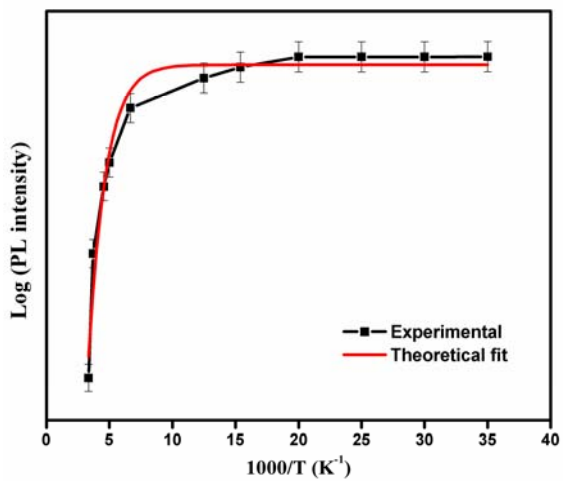

Figure 5.10: Arrhenious plot obtained for C-460 v thin film.

Only a single activation energy [i.e. 169 meV] was obtained from the Arrhenious plot. It is not surprising that the activation energy of 38 meV was not obtained for C-460 v thin films; this may be due to removal of oxygen related surface defects on vacuum annealing.

XPS depth profile measurements were done on both C-460 and C-460 v thin films to analyze the effect of vacuum annealing. Figure 5.11 (a) & (b) are the atomic concentration vs sputter time plots of C-460 and C-460 v thin films.

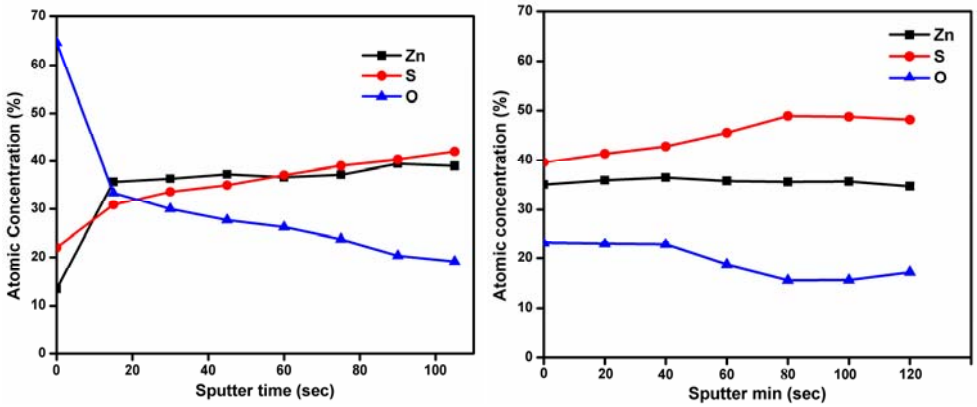

(a) **(b)**

Figure 5.11: Atomic concentration vs sputter time plot of (a) C-460 and (b) C-460 v thin films

It is evident from Figure 5.11(a) that oxygen is present as a surface contaminant in C-460 thin films whereas in C-460 v [Figure 5.11(b)] the atomic concentration of oxygen has been considerably reduced. Also on vacuum annealing, the activation energy at 38 meV is absent. Thus surface defects due to oxygen are the reason for a level at 38 meV.

Thus, two donors at 38 meV and 166 meV have been identified. To find the acceptor involved, we make use of the relation (neglecting Coulomb interaction and van der Waals interaction)

$$E_{PL} = E_g - (E_D + E_A)$$

The acceptor has to be broad so that the FWHM of the emission at 1.88 eV can be accounted for. The acceptor is at ~ 1.6 eV which based on references can be assigned to ionized vacancies of sulphur [59]. Based on our observations, we have proposed a band diagram [Figure 5.12] indicating the position of various defects within the band gap.

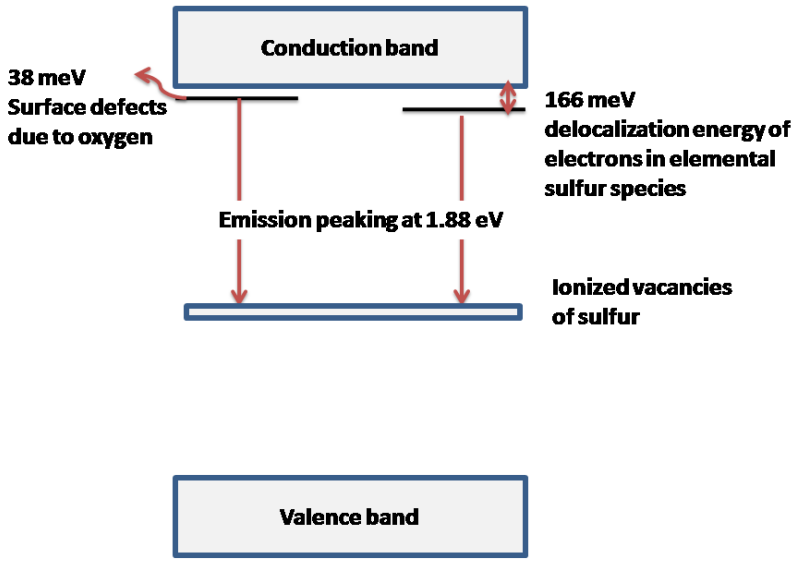

Figure 5.12:Band diagram proposed for pristine ZnS thin films with bandgap of 3.5 eV.

Materials with suitable bandgap with midgap defects can be used as buffer layer in solar cells, as it can contribute to carrier generation process by absorbing sub- bandgap photons. There are reports on using defects within the bandgap for enhancing absorption of sub-bandgap photons [60]. Thus, our ZnS thin films can also be good candidates for buffer layer in solar cells. Doping is generally done to bring down resistivity but it can also be used to create luminescent centres in ZnS. Green emission is reported in 'Cu' doped ZnS thin films and the activation energy associated with acceptor defects of 'Cu' is reported to be at 1.2 eV from valence band edge [61]. For ZnS films with a bandgap of ~ 3.5 eV, if a deep acceptor at 1.2 eV is created, it is more probable that the defect will be rather dormant with respect to electrical properties and active in absorption processes. So to enhance absorption 'Cu' doping was done in ZnS thin films. Fortunately, on 'Cu' doping resistivity of ZnS thin films also reduced considerably from 1.7 X 10^5 Ω.cm (for pristine ZnS) to 17 Ω.cm for maximum percentage of 'Cu' doping. Such a drastic change in conductivity cannot be due to a deep acceptor. It has to be associated with some 'shallow donor level' which is introduced on doping ZnS thin films with 'Cu'. Since 'Cu' is reported to form an acceptor level at 1.2 eV, the reason for occurrence of this 'shallow donor level' has to be identified. 'Cu' doped ZnS thin films (C:2.5 Cu, C:5 Cu, C:7.5 Cu, C:10 Cu and C:15 Cu) were selected for studies and Figure 5.13 shows the PL spectrum of 'Cu' doped ZnS thin films.

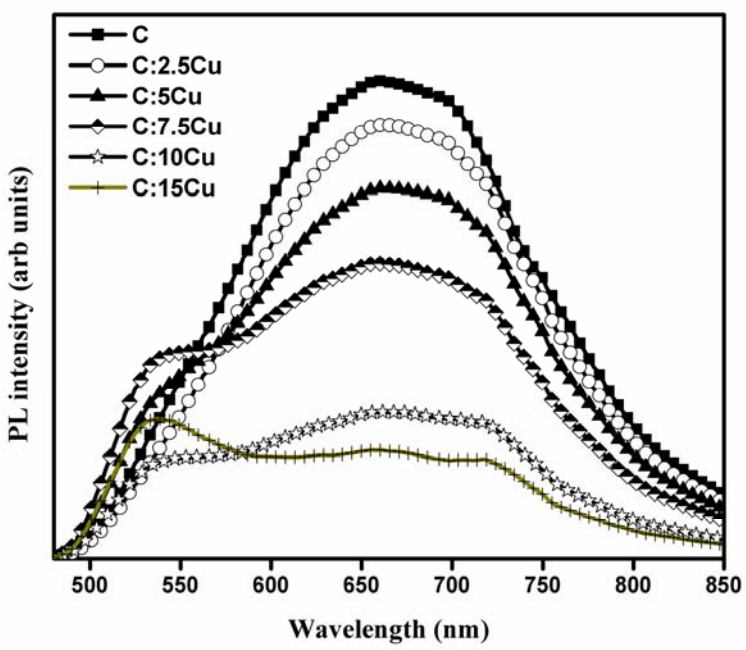

Figure 5.13: PL spectrum of 'Cu'doped ZnS thin films.

It is quite evident from the PL spectra that on doping ZnS thin films with 'Cu', a new emission centered at ~540 nm (2.28 eV) appears and with increase in percentage of doping the emission intensity increases. This green emission is consistent with the green emission reported in 'Cu' doped ZnS thin films [61]. Activation energy of the green emission was calculated for 'Cu' doped ZnS thin films. The calculated activation energies are tabulated in Table 6.1.

Table 6.1: Activation energies obtained for 'Cu' doped ZnS thin films.

Sample	Activation energy (meV)
C:2.5 Cu	35
C:5 Cu	30
C:7.5 Cu	20
C:10 Cu	10
C:15 Cu	8

We see that, with progress in doping, the level is shifting closer to the conduction band which explains the reduction in resistivity. 'Cu' doping is accomplished by adding small quantities of copper chloride; so the shallow level might be equally associated with a defect due to 'Cl_S'. While 'Cu' plays the role of activator, 'Cl' plays the role of co-activator. We have also come across reports that stable incorporation of 'Cu' necessitates 'Cl' incorporation [24]. In yet another report we found that 'Cu' was getting incorporated in place of a complex acceptor due to vacancy of zinc [62]. Hence probably the favorable explanation that we can put forward is that the emission at 2.28 eV may be due to a transition from 'Cl_S' donor levels to acceptor levels created by 'Cu'. We propose that the intensity of green emission is primarily governed by concentration of acceptor species 'Cu' and conductivity is governed by 'Cl_S' donor concentration. Based on our observations we have proposed a band diagram for 'Cu' doped ZnS thin film C:2.5 Cu [Figure 5.14].

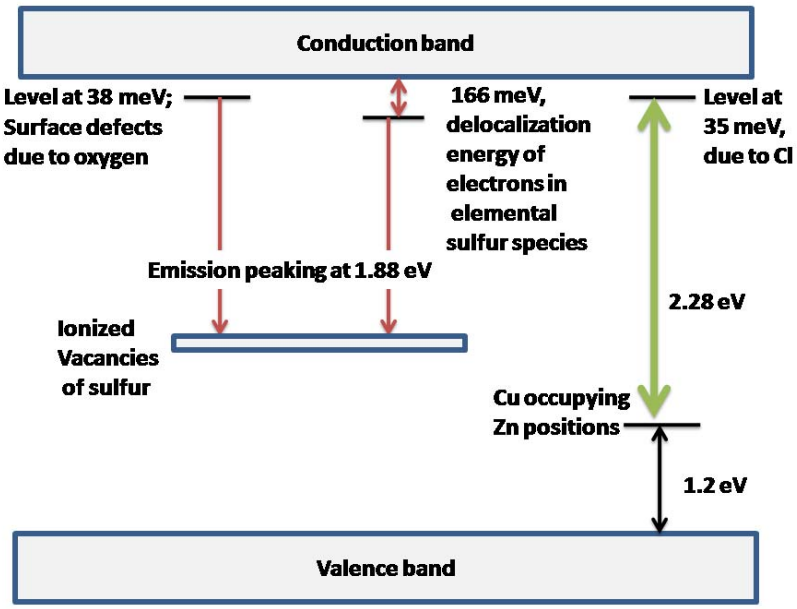

Figure 5.14: Band diagram proposed for 'Cu' doped ZnS thin film C:2.5 Cu with bandgap ~ 3.5 eV.

5.4 Conclusions

Defect analysis of pristine as well as 'Cu' doped ZnS thin films was done using PL. A broad red emission at 1.88 eV was present in both pristine and 'Cu' doped samples. Defects responsible for this emission were identified. In 'Cu' doped ZnS thin films, in addition to the emission at 1.88 eV, a green emission at 2.28 eV could be recorded and defects responsible for this emission also were identified. Band diagram, indicating the position of various defects, was proposed for pristine and 'Cu' doped ZnS thin films

An explanation for reduction in resistivity of 'Cu' doped ZnS thin films could be given using PL. Using PL measurements, we could non-destructively identify that 'Cu' doped ZnS is a better option compared to pristine ZnS for buffer layer application.

References

[1]. **Edited by O. Madelung.** *Semiconductors other than Group IV Elements and III–V Compounds.* s.l. : Springer, 1992. p. 26.

[2]. **E. D. Palik.** *Handbook of Optical Constants of Solids.* s.l. : FL:Academic, 1985. p. 597.

[3]. **J. R. De Vore.** 1951, Journal of Optical Society of America, Vol. 41, p. 416.

[4]. **L. J. Ericksson, W. T. Peria.** 1970 , Thin Solid Films, Vol. 5, p. 303.

[5]. **Y. B. Nicolau, M. Dupuy, M. Brunel.** 1990, Journal of Electrochemical Society , Vol. 137 , p. 2915.

[6]. **M. V. Nazarov.** 2002, Materials Science and Engineering B, Vols. 91–92, p. 349 .

[7]. **D. Hariskos.** 2005, Thin Solid Films, Vol. 480/481, p. 99.

[8]. **S. Musikant.** *Optical Materials: An Introduction to Selection and Application.* s.l. : Marcel Dekker, 1985.

[9]. **S. Shionoya, T. Koda, K. Era.** 1964, Journal of Physical Society of Japan, Vol. 19, p. 1157.

[10]. **C. Ye, X. Fang, M. Wang, L. Zhang.** 2006, Journal of Applied Physics, Vol. 99, p. 063504.

[11]. **R. Pareja, R. M. de la Crus, P. Moser.** 1992, Journal of Physics: Condensed Matter , Vol. 4 , p. 7153.

[12]. **I. K. Vereshchagin, Ye. A. Serov, I. V. Homjak.** 1977, Journal of Luminescence, Vol. 15, p. 315.

[13]. **C. Falcony, M. Garcia, A. Ortiz, J. C. Alonso.** 1992, Journal of Applied Physics , Vol. 72, p. 1525.

[14]. **D. Denzler, M. Olschewski, K. Sattler.** 1998, Journal of Applied Physics, Vol. 84, p. 2841.

[15]. **X. Lu, C. Chen, S. Husurianto, M. D. Koretskya.** 1999, Journal of Applied Physics, Vol. 85, p. 4154.

[16]. **A. D. Dinsmore, D. S. Hsu, S. B. Qadri, J. O. Cross, T. A. Kennedy, H. F. Gray, B. R. Ratna.** 2000, Journal of Applied Physics, Vol. 88, p. 4985.

[17]. **R. Maity, K. K. Chattopadhyay.** 2004, Nanotechnology , Vol. 15, p. 812.

[18]. **S. Kishimoto, T. Hasegawa, H. Kinto, O. Matsumoto, S. Iida.** 2000, Journal of Crystal Growth , Vol. 214/215, p. 556.

[19]. **J. Zhou, H. Goto, N. Sawaki, I. Akasaki.** 1986, Journal of Luminescence, Vol. 35, p. 255.

[20]. **C. Thiandoume, O. Ka, A. Lusson, O. Gorochov.** 1999, Journal of Crystal Growth , Vol. 197, p. 805.

[21]. **N. Khumbojkar, V. V. Nikesh, A. Kshirsagar, S. Mahamuni.** 2000, Journal of Applied Physics, Vol. 88, p. 6260.

[22]. **L. Zhidong, A. N. Georgobiani, X. Zheng, X. Chunxiang, T. Feng, Y. Lei, X. Xurong.** 1998, Chinese Science Bulletin, Vol. 43, p. 518.

[23]. **S. K. Chan, H. J. Liu, C. T. Chan, Z. Q. Zhang, W. K. Ge, I. K. Sou.** 2005, Physical Review B, Vol. 71, pp. 195421.

[24]. **T. Kryshtab, V.S. Khomchenko, J.A. Andraca-Adame, V.E. Rodionov, V.B. Khachatryan, Yu.A. Tzyrkunov.** 2006, Superlattices and Microstructures , Vol. 40 , p. 651.

[25]. **Y. Zhu, C. L. Yuan, P. P. Ong.** 2002, Journal of Applied Physics, Vol. 92, p. 6828.

[26]. **J. C. Lee, D. H. Park.** 2003, Materials Letters , Vol. 57, p. 2872.

[27]. **J. Hu, Y. Bando, J. Zhan, D. Golberg.** 2005, Advanced Functional Materials, Vol. 15, p. 757.

[28]. **A. Ishizumi, C.W. White, Y. Kanemitsu.** 2005, Physica E , Vol. 26, p. 24.

[29]. **B. Bhattacharjee, C. H. Lu.** 2006, Thin Solid Films , Vol. 514 , p. 132.

[30]. **A. V. Murugan, O. Y. Heng, V. Ravi, A. K. Viswanath, V. Saaminathan.** 2006 , Journal of Material Science, Vol. 41, p. 1459.

[31]. **C. Ye, X. Fang, M. Wang, L. Zhang.** 2006, Journal of Applied Physics, Vol. 99, p. 063504.

[32]. **X. Liu, J. Cui, L. Zhang, W. Yu, F. Guo, Y. Qian.** 2006, Materials Letters, Vol. 60, p. 2465.

[33]. **K. Jayanthi, S. Chawla, H. Chander, D. Haranath.** 2007, Crystal Research Technology, Vol. 42, p. 976.

[34]. **Z. Deng, J. Qi, Y. Zhang, Q. Liao, Y. Huang.** 2007, Nanotechnology , Vol. 18 , p. 475603.

[35]. **C. Corrado, Y. Jiang, F. Oba, M. Kozina, F. Bridges, J. Z. Zhang.** 2009, Journal of Physical Chemistry A , Vol. 113, p. 3830.

[36]. **H. Qu, L. Cao, G. Su, W. Liu, Y. Sun.** 2009, Journal of Applied Physics, Vol. 106, p. 093506.

[37]. **M. A. Hernández-Fenollosa, M. C. López, V. Donderis, M. González, B. Marí, J. R. Ramos-Barrado.** 2008, Thin Solid Films , Vol. 516 , p. 1622.

[38]. **H. J. Xu, H. S. Jia, Z. T. Yao, X. J. Li.** 2008, Journal of Material Research, Vol. 23, p. 121.

[39]. **H. K. Sadekar, N. G. Deshpande, Y. G. Gudage, A. Ghosh, S. D. Chavhan, S. R. Gosavi, R. Sharma.** 2008, Journal of Alloys and Compounds, Vol. 453 , p. 519.

[40]. **J. P. Borah, J. Barman, K. C. Sarma.** 2008, Chalcogenide Letters, Vol. 5, p. 201.

[41]. **D. Kurbatov, V. Kosyak, A. Opanasyuk, V. Melnik.** 2009, Physica B, Vol. 404, p. 5002.

[42]. **S. Liu, H. Zhang, M. T. Swihart.** 2009, Nanotechnology , Vol. 20, p. 235603.

[43]. **C. S. Tiwary, P. Kumbhakar, A. K. Mitra, K. Chattopadhyay.** 2009, Journal of Luminescence, Vol. 129, p. 1366.

[44]. **C. W. Won, H. H. Nersisyan, H. I. Won, D. Y. Jeon, J. Y. Han.** 2010, Journal ofLuminescence, Vol. 130, p. 1026.

[45]. **V. I. Kushnirenko, V. S. Khomchenko, T. V. Zashivailo, L. V. Zavyalova.** 2012, Physica Status Solidi C, Vol. DOI 10.1002/pssc.201100618, p. 1.

[46]. **S. R. Chalana, R. Vinodkumar, I. Navas, V. Ganesan, V. P. Mahadevan Pillai.** 2012, Journal of Luminescence, Vol. 132, p. 944.

[47]. **W. C. Fenga, H. Bo, Y. Hou-hui, L. Wei-bing.** 2011, Optics & Laser Technology, Vol. 43, p. 1453.

[48]. **X. Wang, J. Shi, Z. Feng, M. Lia, C. Li.** 2011, Physical Chemistry Chemical Physics, Vol. 13, p. 4715.

[49]. **H. Chen, Y. Hu, X. Zeng.** 2011, Journal of Material Science, Vol. 46, p. 2715.

[50]. **Y. V. B. de Santana, C. W. Raubach, M. M. Ferrer, F. La Porta, J. R. Sambrano.** 2011, Journal of Applied Physics, Vol. 110, p. 123507.

[51]. **S. Sahai, M. Husain, V. Shanker, N. Singh, D. Haranath.** 2011, Journal of Colloid and Interface Science , Vol. 357 , p. 379.

[52]. **W. Jia, B. Jia, X. Wu, F. Qu.** 2012, Crystal Engineering Communications, Vol. DOI: 10.1039/c2ce25144b.

[53]. **C. Lan, J. Gong, Y. Jiang, Y. Song, S. Yang.** 2012 , Crystal Engineering Communications, Vol. 14, p. 708.

[54]. **N. K. Morozova, I. A. Karetnikov, K. V. Golub, N. D. Danilevich, V. M. Lisitsyn, V. I. Oleshko.** 2005, Semiconductors, Vol. 39, p. 485.

[55]. **H. Y. Wang, C. R. Wang, J. Xu, X. Liu, X. F. Xu, H. Z. Xing, L. J. Zhao, X. S. Chen.** 2012, Journal of Physics D: Applied Physics, Vol. 45 , p. 095301.

[56]. **X. Zeng, J. Zhang, F. Huang.** 2012, Journal of Applied Physics, Vol. 111, p. 123525.

[57]. **A. Tiwari, S.A.Khan, R.S.Kher.** 2012, Journal of Luminescence, Vol. 132, p. 1564.

[58]. **D. J. Gibbons, W. E. Spear.** 1966, Journal of Physics and Chemistry of Solids, Vol. 27, p. 1917 .

[59]. **D. Kurbatov, V. Kosyak, A. Opanasyuk, V. Melnik.** 2009, Physica B, Vol. 404, p. 5002.

[60]. **Y. S. Lee.** *Defect engineering of Cu_2O thin-films for photovoltaic applications.* s.l. : Massachusetts Institute of Technology, 2013. Ph.D thesis..

[61]. **S. Shionoya.** Photoluminescence. [book auth.] Edited by D.R.Vij. *Luminescence of Solids.* s.l. : Plenum Press, 1998.

[62]. **P.V.Ben, P.T.Tue.** 2008, VNU Journal of Science, Mathematics - Physics. Vol. 24, p. 181.

.....ꕥ.....

Chapter 6

EVALUATION OF In_2S_3/MEH-PPV HETEROJUNCTION USING PHOTOLUMINESCENCE TECHNIQUE

6.1 Introduction

Photoluminescence (PL) is a highly reliable probe which can be used for analysis at any stage of sample processing [1]. The operating principle is quite simple and PL is treated with increased respect in the PV industry because a wide range of solar cell parameters can be obtained using luminescence imaging. In a market survey conducted by PHOTON in 2011 it is clear that the number of companies marketing luminescence imaging systems and cameras is on the rise. The figures in the survey reaffirm the bullish trend in the market for companies dealing with the sales of cameras, complete systems for luminescence imaging etc. The number of companies dealing with sale of such featured products also has tripled in a span of one year [2]. The prospects of PL was reported only a couple of years back [3, 4]; from then on PL has escalated itself from a supporting role to the lead role mainly owing to the undeniable advantage offered by the non-contact nature of this technique.

6.2 Review on role of PL in PV industry

This section is a quick glance on how PL has been and is being employed by different research groups for characterization of either materials for PV or finished devices themselves.

A report by Smestad and Ries in 1992 [5], explains vividly how luminescence is related to the output device characteristics of a device. Generally in solar cells and other devices, luminescence is considered as a loss but under open circuit condition when no carriers are extracted from the device, the only pathway for the carriers is mainly through radiative recombination and luminescence can be taken as a measure of the ability of a material to produce useful work. The report also says that measuring luminescence is helpful in assessing the absorber quality and for betterment of device fabrication technique. Another report by Smestad in the same year deals with photovoltaic effect in photoluminescent porous silicon. Tarasov et al. [6] have used room temperature scanning photoluminescence studies to analyze solar grade multicrystalline silicon wafers. In regions of the wafer where band to band emission is intense, minority carrier lifetime is relatively high whereas in certain regions of the wafer where there is strong defect PL band, minority carrier lifetime is degraded.

In 1998, Halliday et al. [7] have used PL to study CdTe/CdS solar cells fabricated under different conditions. PL emissions have been analyzed and variation in cell characteristics has been correlated to the observed emission. Ostapenko et al. [8] have come up with similar observations where they have utilized low temperature PL with which identification of annealing induced oxygen defects has been done. A report by Bridge et al. [9] says that partial type conversion of CdTe from n to p type results in enhancement of properties of n-CdTe/n-CdS solar cell structures and the centres responsible for type conversion could be detected using PL. CdS/CdTe solar cells have been a subject of study again by Hernandez-Fenellosa et al. [10] where they have reported differences in cell performance on treatment with oxygen. The treatment has triggered some differences in the PL spectra also and correlation could be observed between evolution of certain PL bands and the device performance. Ghimpu et al. [11] have

used PL to identify the extent of contamination in CdTe/CdS heterojunction prepared by closed space sublimation technique using a source with residual Cu impurities. In 2005, Van Gheluwe et al. [12] have used PL successfully to study the difference in performance of CdS/CdTe cells given chloride treatments under air ambient and under vacuum. The performance of CdS/CdTe solar cells has been evaluated using PL. Mendoza-Perez et al. [13] observed in their study that best performing cells had a particular proportion of sulphur vacancies which controlled the minority carrier recombination at the CdS/CdTe interface and this was evident in the PL spectra as an intense band corresponding to sulphur vacancies.

Yang et al. [14] have reported a correlation between photoluminescence and solar cell parameters for InGaP solar cells. Minority carrier lifetime can be estimated from PL and generally lifetime is affected by dislocations. Different process-induced defects can be distinguished from the difference in PL intensities. An interesting report in 2001 by Medvedkin et al. [15] points out that in polycrystalline ZnO/CdS/$CuInGaSe_2$ solar cell, the device efficiency was reduced considerably on exposure to moisture and heat. This happens for the unincapsulated device and the PL intensity was also lowered for such devices. Disappearance of edge photoluminescence band and preservation of defect bands indicate degraded device quality and the authors have projected the requirement for encapsulation using the supplementary results from PL. Basewicz et al. [16] have used PL to probe the absorber layer properties in ZnO/CdS/$CuInGaSe_2$ solar cell. PL emission efficiency has been treated with utmost importance in connection with performance of cells since it is a measure of the relative contributions of radiative and non-radiative transitions. Degradation in PL intensity has been related to poor performance of device.

Tarasov et al. [17] have come up with interesting observations in passivated multicrystalline Si wafers for solar cell applications. Passivation by

hydrogenation improves the lifetime by orders and this is reflected in the PL spectrum also. The upgradation in lifetime has been expressed as a ratio of intensities of PL emission after and prior to hydrogenation. Another report on a-Si:H/c-Si-heterojunction cells by Tardon et al. [18] narrates the effect of surface treatment on the photoluminescence yield. The PL yield also depends on the type of n and p layers as well as on undoped amorphous silicon passivation layers. A correlation between PL and the device performance can be arrived at because the latter is also a function of the aforementioned parameters. Merdzhanova et al. [19] have studied the different mechanisms that tend to limit open circuit voltage in microcrystalline silicon solar cells. The effect of various parameters on the PL energy and V_{oc} provide an insight that both are related to the separation between quasi-Fermi levels.

In a report in 2005, Trupke et al. [20] have put forward PL as a robust tool in the characterization of photovoltaics. The only difficulty is in the conversion of PL intensity into carrier concentration. They have come up with a simple calibration technique for conversion of the same. Abbott et al. [21] have reported that the performance of a solar cell is affected by edge recombination and to overcome this, isolation trench techniques have been employed. They have used PL to assess such isolation techniques which are helpful in improving the device as well as bulk properties. An important observation by Bardos et al. [22] in 2006 is that when minority carrier trapping occurs, photoconductance measurements are drastically affected whereas photoluminescence measurements are not significantly affected. Minority carrier lifetimes calculated using PL and also the implied current-voltage graphs obtained using PL is reliable. Another report by Abbott et al. [23] projects PL as a highly efficient characterization tool for lab scale monitoring as well as industrial level processing. Different aspects are to be taken care of in the case of highly efficient solar cell fabrication such as

wafer handling, furnace contamination, process-induced defects and design of cell. Concerns regarding any of the aforementioned aspects can be addressed to by employing quasi steady state PL measurements. Jurgens et al. [24] have mentioned in their report that splitting of quasi Fermi levels gives a measure of the attainable voltage out of a cell and also it decides the intensity of PL signal. So monitoring the variation in PL intensity over the entire cell can give an idea of the fluctuations in quasi Fermi level splitting under open circuit and short circuit conditions. In a work by Trupke et al. [25], luminescence imaging has been used for obtaining spatially resolved series resistance of silicon solar cells. Quantitative evaluation of series resistance and its variation over the entire sample has been done.

PL imaging has been used for detection of linear shunts in silicon solar cells along with electroluminescence (EL) imaging by Breitenstein et al. [26]. Effect of proton irradiation on the properties of $CuInGaSe_2$ solar cells have been investigated by Yoshida et al. [27]. Rudigier et al. [28] have successfully accomplished the analysis of absorber layer in $CuInS_2$ based solar cells using PL spectroscopy in combination with Raman spectroscopy. PL measurements on each individual layers exhibit changes on irradiation and PL properties have been correlated with the electrical properties of the cell. Gundel et al. [29] employed micro-PL and micro-Raman spectroscopy measurements to estimate carrier recombination lifetime and doping density with submicron resolution in multicrystalline silicon samples. Saturation currents in GaAs solar cell have been evaluated by Delamarre et al. [30] and the values obtained using PL exhibit quite good correlation with that obtained from electrical measurements.

In this present work, we have tried to extend the theory developed mainly for determining the performance parameters of traditional silicon based solar cells using PL to predict the open-circuit voltage that can be obtained in

In_2S_3/MEH-PPV solar cell. Then by employing PL we have tried to study the performance parameters under open circuit conditions.

6.3 Theoretical Background

From generalized Planck's law, the rate of spontaneous emission (which determines the intensity of PL signal) bears an exponential dependence on $\Delta\eta$, the quasi Fermi level separation [31]. Intensity of PL signal can be expressed as

$$I = ABn_i^2 \exp\frac{\Delta n}{kT} \quad \text{----------(1)}$$

where A is a scaling factor, B the radiative recombination coefficient and n_i the carrier concentration. $\Delta\eta = eV$, where V is the open-circuit voltage which can be expressed as

$$V = \frac{kT}{e}\ln(I_{PL}) + C \quad \text{----------(2)}$$

In equation (2) calibration constant C incorporates A,B and n_i has to be determined separately. In the case of In_2S_3/MEH-PPV bilayer heterojunction, it is quite difficult to determine the carrier concentration experimentally as both layers constituting the heterojunction are highly resistive. Thus the calibration constant was found by iterating different values and the value of C which yielded voltage values close to experimental value was chosen. Interfacial defects do play an important role in deciding the carrier concentration, recombination mechanisms etc and hence the value of calibration constant for sure varies for different parts of the same device. Here we have chosen an average value for C. Thus by measuring PL intensities at different points on the device, the local voltages can be determined [23]. A solar cell can be visualized as a two dimensional network of building blocks comprising current generator, diode,

shunt and series resistances. Regions where the shunt resistance is low reduce the voltage locally and thus manifest themselves as low luminescence intensity regions [32]. Hence mapping the PL intensity would give a qualitative picture of the variation of shunt resistance over the sample. This method is non-destructive and is highly useful in obtaining an idea of the good and bad areas of the device fabricated. PL measurements were done in open circuit condition because at open circuit, all sorts of recombination (i.e. luminescence, trap assisted recombination etc) dominate, as not a single carrier is extracted.

6.4 Experimental details

Heterojunctions were prepared by spin coating a solution of MEH-PPV in chlorobenzene (5 mg/ml), on top of the In_2S_3 film deposited using spray pyrolysis on ITO substrates. Variations have been brought about in the In_2S_3 layer deposited. Four devices, namely 1, 2, 3 and 4 were fabricated, each device being different with respect to the In_2S_3 layer going in to cell fabrication. In the case of devices 1, 2 and 3 the In_2S_3 layer has not been subjected to annealing unlike device 4 in which the In_2S_3 layer (with In:S ratio=2.5:3) was annealed for one hour. The In:S ratio in the In_2S_3 layer used in devices 1, 2 and 3 were respectively 1.2:8, 2:3 and 2.5:3. For electrical contact at the top, silver electrodes of 12 mm^2 area were vacuum evaporated (at a pressure of 6×10^{-6} Torr) using a shadow mask on top of the polymer layer. For PL measurements, the heterojunction with structure ITO/In_2S_3/MEH-PPV/Ag electrode [33] was illuminated by light focused with the help of lens, from a halogen lamp. Under open circuit condition, the illumination intensity was varied from 5-50mW/cm^2 and the PL spectra were recorded using Ocean Optics USB2000 spectrophotometer interfaced to the computer via custom made software OOIBase32 [34]. An infrared filter, along with a water jacket, was used to ensure that there was no heating of the device during measurement. The

challenge was in isolating the detector from the excitation beam. For PL mapping studies, the sample was fixed on a translation stage provided with XYZ movements using a stepper motor control. PL emission spectra were recorded for low illumination intensity [from 5-50 mW/cm^2]. A schematic of the experimental set up used for PL measurements is shown in Figure 6.1.

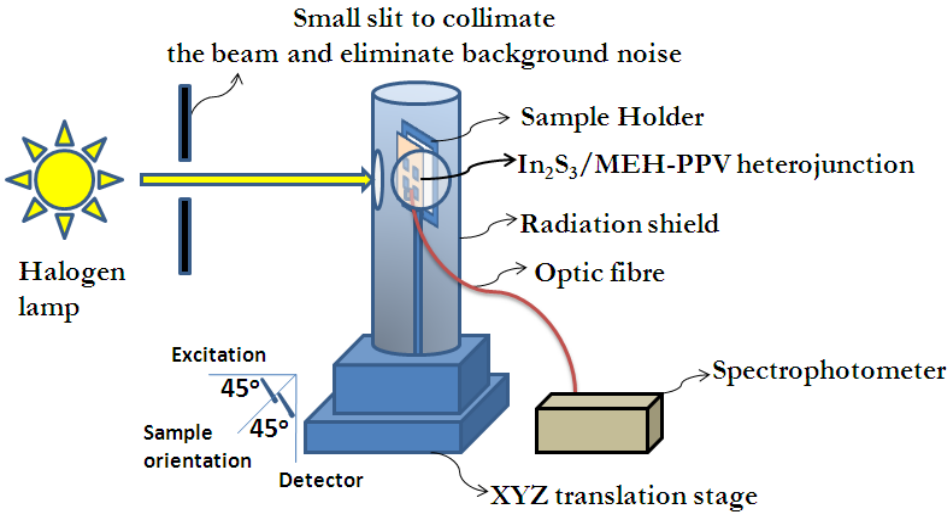

Figure 6.1: Experimental set up for performing PL measurements.

Data obtained from different points of the same sample was plotted as a color map. The color palette chosen was BGYOR with intensity increasing from blue to red. J-V measurements were done on the same set of samples [for different illumination intensities in the range, 5-50 mW/cm^2] using Keithley 236 Source Measure Unit [SMU] interfaced to computer via custom made ICS software. Shunt resistance from the J-V curves were obtained by taking inverse slope at short circuit condition V_{oc}=0 [35]. Our next aim was to predict voltages using PL and then confirm the results using J-V measurements. For that, we did PL measurements on ITO/In_2S_3/MEH-PPV bilayer [without electrode]. The open-circuit voltage was predicted and shunt resistance map was plotted using

absolute PL intensity. Ag electrodes of area 12 mm^2 were later on given over the bilayer of area approximately 1.5 × 2.5 cm^2. J-V measurements were performed to get the actual values of open circuit voltages and shunt resistances from the same set of points where the PL measurements were carried out.

6.5 Results and discussions

In the heterojunctions fabricated, the In_2S_3 layer is quite thin facilitating just the formation of junction and thus its contribution to PL is quite negligible as compared to that of MEH-PPV which is strongly luminescent. The PL spectrum of MEH-PPV is shown in Figure 6.2.

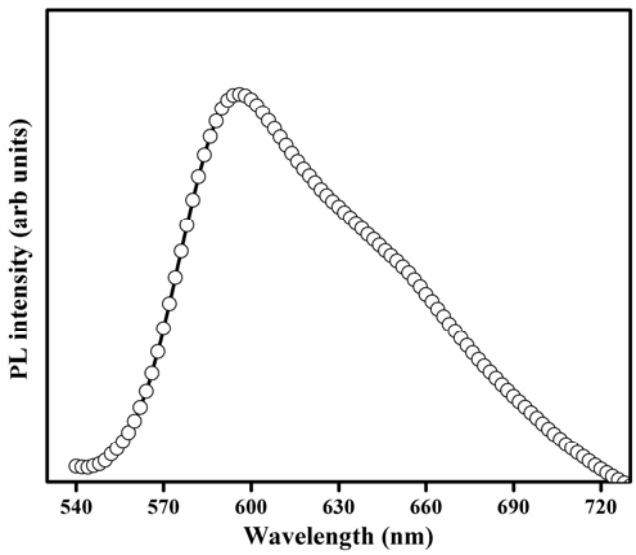

Figure 6.2: PL spectrum of MEH-PPV.

The peak at ~580 nm corresponds to pure electronic transition from LUMO to HOMO level of MEH-PPV. Variation in intensity of PL emission from the heterojunction (the sole contributor to luminescence being MEH-PPV) when incident intensity is varied from 5-50 mW/cm^2 was studied. From the measured PL intensity values, implied voltage was calculated using relation (2).

V_{oc} values for the same variation in incident light intensity were obtained from J-V measurements. Transport mechanisms and conductivity of organic layers are modelled quite differently unlike inorganic semiconductors. But for calculating open circuit voltage, the model used for calculating open-circuit voltage in a conventional inorganic semiconductor-based solar cell, is used. Correlation between the calculated V_{oc} and experimental V_{oc} values is presented in Table 6.1.

Table 6.1: Implied voltage and experimental V_{OC} values obtained for device 1.

Incident Light Intensity (mW/cm^2)	Implied voltage (mV)	Experimental Voltage (mV)
5	496.5	496.8
10	515.5	500.5
15	521.8	506.6
20	528.9	513.1
25	534.9	527.5
30	538.7	532.0
35	541.9	546.8
40	543.9	550.4
45	548.3	567.3
50	553.1	579.8

There is only a slight discrepancy between voltage values predicted using PL and that obtained experimentally. V_{oc} in trap free solar cells is related to the generation rate of carriers which in turn is a function of incident intensity. This implies that V_{oc} varies logarithmically with incident light intensity and for trap free solar cells, the slope of V_{oc} vs. *ln* (*incident intensity*) plot should be kT/q [36]. The slope of experimental V_{oc} vs. *ln* (*incident intensity*) is much higher than the thermal voltage kT/q which implies that there are defects and traps which open up recombination pathways other than radiative recombination [37].

PL intensity was recorded from different points of the same device and V_{oc} was calculated from PL. Calculated V_{oc} and experimental V_{oc} values (calculated and measured at six different points of a device) for three devices has been tabulated [Table 6.2].

Table 6.2: Implied voltage and V_{OC} values for devices 2, 3 and 4.

Device 2			Device 3			Device 4		
V_{oc} (mV)	**Implied voltage (mV)**	**% deviation**	**V_{oc}(mV)**	**Implied voltage (mV)**	**% deviation**	**V_{oc} (mV)**	**Implied voltage (mV)**	**% deviation**
584.4	564.7	3	693.4	679	2	545	576.3	5.7
587.9	567.3	3.5	692.7	678.7	2	--	--	--
600.9	570	5	694.1	680	2	546.7	578	5.8
576.1	561.2	2.5	685.8	676.6	1.3	541.5	566.2	4.6
579.8	563	2.9	688.6	677.8	1.6	545.5	569.2	4.3
577.9	562.4	2.7	691.4	678.2	1.9	544.5	568	4.3

The percentage deviation of implied voltage values from V_{oc} values has also been included in Table 6.2. For all the devices the deviation is below 5 % of V_{oc} at all points from where measurement has been taken. This indicates that the implied voltage calculated from PL does not differ much from V_{oc}. *Device* 3 appears to be the best among the lot as the deviation of implied voltage from V_{oc} is the least. The variation in implied voltage as well as V_{oc} values from point to point is also least. The data obtained for device 3 is plotted as a 'color map' where X and Y axes of the color map indicate different points along the breadth and length of the sample from where the PL intensity was recorded. V_{oc} values obtained from J-V measurements are also depicted in the implied voltage map [Figure 6.3].

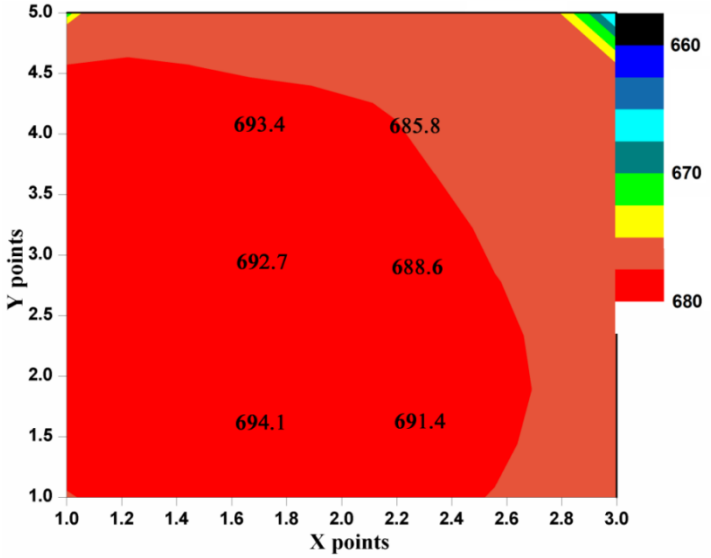

Figure 6.3: Variation in open-circuit voltage values calculated from PL, at different points of the sample plotted as a color map. V_{OC} values experimentally have been depicted in the color map.

In order to confirm the authenticity of the above observations, PL measurements were done on an unfinished device. Parameters were predicted first and electrical measurements were done later on to confirm the predictions. PL predicts voltage in the range 550-590 mV at different points of the bilayer. To verify the observations from PL, 'Ag' electrodes were given on top of the bilayer for J-V measurements. The top view of the bilayer after electrodes are given is shown in Figure 6.4. This structure is named device 5.

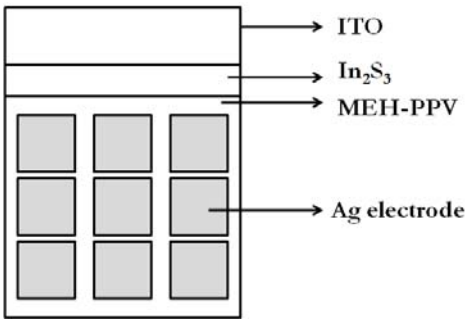

Figure 6.4: Top view of the bilayer after electrodes are given.

Open-circuit voltages obtained from PL, in the region lying between the centre and left hand side of the bilayer, was higher which suggest that V_{oc} values also obtained in this region will in general be higher compared to the other regions of the device. The voltage obtained from PL and experimental V_{oc} values of device 5 have been tabulated [Table 6.3]. The V_{oc} values obtained from J-V measurements were quite close to the voltages calculated from PL. V_{oc} values obtained from the left half of device 5 were higher as predicted using PL.

Table 6.3: Voltage from PL and V_{oc} values of device 5.

V_{oc} (mV)	Voltage from PL (mV)	% deviation
593	577.1	2.7
626.1	582.6	6.9
600.2	578	3.7
591.9	576.8	2.6
612.7	585.4	4.5
557	573.5	3
590.9	576	2.5
592.7	576.9	2.7
575.4	574.9	1

Another important parameter that governs the performance of a solar cell is the shunt resistance. For an ideal solar cell, shunt resistance is infinite. In this heterojunction, since both MEH-PPV and In_2S_3 layers are highly resistive, shunt resistance is high. However, due to insufficient interface thickness and non uniform interface, there are regions in the device where shunt resistance is low. Regions of low shunt resistance are easy paths for recombination and generally they tend to reduce the luminescence intensity and open circuit voltage. So regions of low shunt resistance will be regions where PL intensity is also low. Thus mapping the PL intensity from different points of the device will for sure be a map of the shunt resistance. The measured PL intensity was mapped for all samples and it could be observed that the images were rightly an indicator of the

manner in which shunt resistance varied from point to point over the samples. Low shunt resistance regions are regions of low PL intensity and hence yield lower voltages; the map obtained was also perfectly in accordance with the voltage color map. Figure 6.5 is the color map indicating the variation of PL intensity (or in fact the shunt resistance) at different points for Device 3.

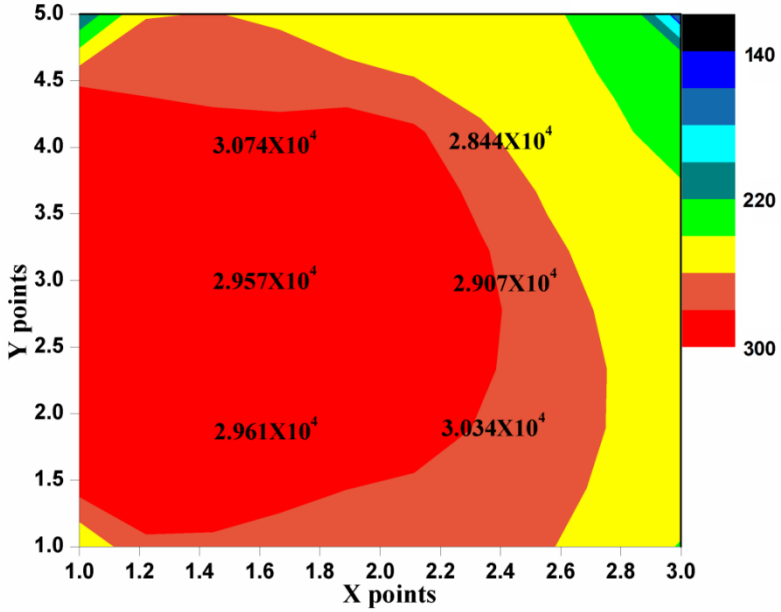

Figure 6.5: Variation in luminescence intensity over different points of the sample. Shunt resistance values obtained experimentally have also been mentioned on the color map.

The experimentally obtained shunt resistance values have been mentioned in the map [Figure 6.5] for reference. Variation in shunt resistance from point to point on this device is quite low. This map is quite similar to the voltage color map of Device 3 [see Figure 6.3]. This asserts the point that high shunt resistance values imply lesser leakage current and higher open circuit voltages.

Apart from calculating V_{oc} and mapping V_{oc} as well as shunt resistance using PL, we have also proved that PL measurements do not affect the life of the heterojunctions under study. Device 3 was under observation for 30 days and PL

measurements were done repeatedly. Apart from the normal degradation of parameters due to ageing, there was no damage to the heterojunction due to PL measurements. The variation in V_{oc} as well as voltage calculated from PL with progress in days is shown in Figure 6.6.

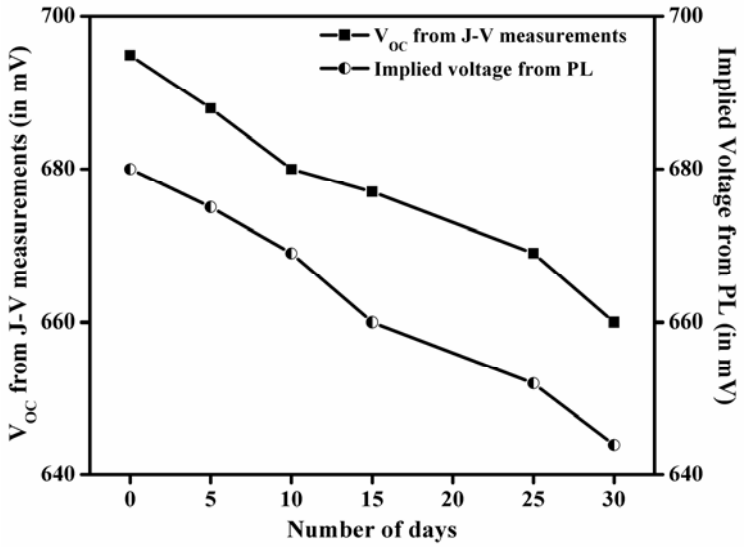

Figure 6.6: Variation in experimental V_{oc} as well as V_{oc} calculated from PL with progress in days.

6.6 Conclusion

We have observed that the experimental values of voltage and the variation of shunt resistance were as predicted from PL. Thus PL can be used well beyond doubt to calculate the attainable voltages. It can also be used to point out the good regions of In_2S_3/ MEH-PPV heterojunction so that we can leave aside the 'poor performance zones'. The study has been carried out on cells prepared under different conditions. From the present study, we could identify that device 3 has comparatively better parameters. Thus the preparation parameters, which are employed for depositing the best cell, can also be indirectly identified. We have also demonstrated that PL measurements do not damage the devices under study.

References

[1]. **T. H. Gfroerer.** *Photoluminescence in the Analysis of Surfaces and Interfaces- Encyclopaedia of Analytical Chemistry.* Chichester : R.A.Meyers (Ed.), John Wiley & Sons Ltd, 2000.

[2]. **S. K. Chunduri.** 2011, Photon International, p. 156.

[3]. **T. Fuyuki, H. Kondo, T. Yamazaki, Y. Takahashi, Y. Uraoka.** 2005, Applied Physics Letters, Vol. 86, p. 262108.

[4]. **T. Trupke, R. A. Bardos, M. C. Schubert, W. Warta.** 2006, Applied Physics letters, Vol. 89, p. 044107.

[5]. **G. Smestad, H. Ries.** 1992, Solar Energy Materials and Solar Cells, p. 51.

[6]. **I. Tarasov, S. Ostapenko, V. Feifer, S. McHugo, S. V. Koveshnikov, J. Weber, C. Haessler, E. -U. Reisner.** 1999, Physica B, Vols. 273-274, p. 549.

[7]. **D. P. Halliday, J. M. Eggleston, K. Durose.** 1998, Journal of Crystal Growth, Vol. 186, p. 543.

[8]. **S. Ostapenko, I. Tarasov, J. P. Kalejs, C. Haessler, E. -U. Reisner.** 2000, Semiconductor Science and Technology, Vol. 15, p. 840.

[9]. **C. J. Bridge, P. Dawson, P. D. Buckle, M. E. Ozsan.** 2000, Semiconductor Science and Technolgy, Vol. 15, p. 975.

[10]. **M. A. Hernandez-Fenollosa, D. P. Halliday, K. Durose, M. D. Campo, J. Beier.** 2003, Thin Solid Films, Vols. 431-432, p. 176.

[11]. **L. Ghimpu, V. V. Ursaki, T. Potlog, I. M. Tiginyanu.** 2005, Semiconductor Science and Technology, Vol. 20, p. 1127.

[12]. **J. V. Gheluwe, J. Velsluys, D. Poelman, P. Clauws.** 2005, Thin Solid Films, Vols. 480-481, p. 264.

[13]. **R. Mendoza-Perez, J. Aguilar-Hernandez, J. Sastre-Hernandez, N. Ximello-Quiebras, G. Contreras-Puente, G. Santana-Rodriguez, O. Vigil-Galan, E. Morena-Garcia, A. Morales-Acevedo.** 2006, Solar Energy, Vol. 80, p. 682.

[14]. **M. J. Yang, M. Yamaguchi, T. Takamoto, E. Ikeda, H. Kurita, M. Ohmori.** 1997, Solar Energy materials and Solar Cells, Vol. 45, p. 331.

[15]. **G. A. Medvedkin, E. I. Terukov, K. Sato, Yu. Hasegava, K. Hirose.** 2001, Semiconductors, Vol. 2001, p. 1329.

[16]. **R. Bacewicz, P. Wuk, R. Trykozko.** 2003, Opto-Electronics Review, Vol. 11(4), p. 277.

[17]. **I. Tarasov, S. Ostapenko, K. Nakayashiki, A. Rohatgi.** 2004, Applied Physics Letters, Vol. 85, p. 4346.

[18]. **S. Tardon, M. Bosch, R. Bruggemann, T. Unold, G. H. Bauer.** 2004, Journal of Non-Crystalline Solids, Vols. 338-340, p. 444.

[19]. **T. Merdzhanova, R. Carius, S. Klein, F. Finder, D. Dimova-Malinovska.** 2004, Thin Solid Films, Vols. 451-452, p. 285.

[20]. **T. Trupke, R. A. Bardos, M. D. Abbott.** 2005, Applied Physics Letters, Vol. 87, p. 184102.

[21]. **M. D. Abbott, J. E. Cotter, T. Trupke, R. A. Bardos.** 2006, Applied Physics Letters, Vol. 85, p. 114105.

[22]. **R. A. Bardos, T. Trupke, M. C. Schubert, T. Roth.** 2006, Applied Physics Letters, Vol. 88, p. 053504.

[23]. **M. D. Abbott, J. E. Cotter, F. W. Chen, T. Trupke, R. A. Bardos, K. C. Fisher.** 2006, Journal of Applied Physics, Vol. 100, p. 114514.

[24]. **T. Jurgens, L. Gutay, G. H. Bauer.** 2006, Thin Solid Films, Vols. 511-512, p. 678.

[25]. **T. Trupke, E. Pink, R. A. Bardos, M. D. Abbott.** 2007, Applied Physics Letters, Vol. 90, p. 093506.

[26]. **O. Breitenstein, J. Bauer, T. Trupke, R. A. Bardos.** 2008, Progress in Photovoltaics:Research and Applications, Vol. 16, p. 325.

[27]. **K. Yoshida, M. Tajima, S. Kawakita, K. Sakurai, S. Niki, K. Hirose.** 2008, Japanese Journal of Applied Physics, Vol. 47, p. 857.

[28]. **E. Rudigier, T. Enzenhofer, R. Scheer.** 2005, Thin Solid Films, Vols. 480-481, p. 327.

[29]. **P. Gundel, M. C. Schubert, F. D. Heinz, R. Woehl, J. Benick, J. A. Giesecke, D. Suwito, W. Warta.** 2011, Nanoscale Research Letters, Vol. 6:197, p. 1.

[30]. **A. Delamarre, L. Lombez, J. F. Guillemoles.** 2012, Applied Physics Letters, Vol. 100, p. 131108.

[31]. **T. Trupke, R. A. Bardos, M. D. Abbott, J. E. Cotter.** 2005, Applied Physics Letters, Vol. 87, p. 093503.

[32]. **M. D. Abbott, J. E. Cotter, F. W. Chen, T. Trupke, R. A. Bardos, K. C. Fisher.** 2006, Journal of Applied Physics, Vol. 100, p. 114514.

[33]. **M. R. Rajesh Menon, M. V. Maheshkumar, K. Sreekumar, C. Sudha Kartha, K. P. Vijayakumar.** 2010, Solar Energy Materials and Solar Cells, Vol. 94, p. 2212.

[34]. **R. Jayakrishnan, T. T. John, C. Sudha Kartha, K. P. Vijayakumar, T. Abe, Y. Kashiwaba.** 2005, Semiconductor Science Technology, Vol. 20, p. 1162.

[35]. **F. Khan, S. N. Singh, M. Husain.** 2010, Semiconductor Science Technology, Vol. 25, p. 0150.

[36]. **M. Kuik, H. T. Nicolai, M. Lenes, Gert-Jan A. H. Wetzelaer, M. Lu, P. W. M. Blom.** 2011, Applied Physics Letters, Vol. 98, p. 093301.

[37]. **M. M. Mandoc, F. B. Kooistra, J. C. Hummelen, B. de Boer, P. W. M. Blom.** 2007, Applied Physics Letters, Vol. 91, p. 263505.

[38]. **T. Q. Nguyen, I. B. Martini, J. Liu, B. J. Schwartz.** 2000, Journal of Physical Chemistry B, Vol. 104, p. 237.

.....ൠ.....

Chapter 7

SUMMARY AND FUTURE OUTLOOK

A quick look at the history of events in a span of hundred years in the semiconductor microelectronics industry indicates a rather rapid hike in the demand for semiconductors. It is but commendable to see the improvement in performance of the devices fabricated using semiconductors compared to their entry-level performance. Persistent research and better understanding of the properties of these materials are the key factors which has made this possible. A better insight in to material properties is generally achieved by different material characterization techniques. If we specifically analyze the photovoltaics (PV) industry alone, we can see that it is still revolving around Si, GaAs etc due to some technological and other considerations. This might be due to the lack of understanding about the electronic structure and defects present in alternate materials.

In this doctoral thesis, attempt has been made to analyze three compound semiconductors and a solar cell using the non-destructive optical technique Photoluminescence (PL). Spray pyrolysed thin films of zinc oxide (ZnO), copper zinc tin sulphide (CZTS) and zinc sulphide (ZnS) which are prospective candidates for transparent conducting oxide layer, absorber layer and buffer layer in thin film solar cells and In_2S_3/MEH-PPV heterojunction solar cell were analyzed. Our aim was to prove that PL is a technique suitable for analyzing the important layers comprising a basic thin film solar cell and a completely fabricated solar cell also. Various aspects of PL spectroscopy have been used to accomplish this aim.

As far as a TCO is concerned the important property required is low resistivity. To develop low resistive ZnO thin films for TCO applications, different

deposition conditions and doping was tried. PL measurements were done on all these films and PL spectra recorded consisted of two emissions- the near band edge emission (NBE) and deep level emission (DLE). We could work out a connection between ratio of integrated intensities of DLE to NBE (i.e. I_{DLE}/I_{NBE}) and resistivity of ZnO thin films. An empirical relation could be proposed connecting the order of resistivity (Y) and order of I_{DLE}/I_{NBE} (X) as $Y = 10^{-1}X$. So the major finding in works on ZnO is that, just by finding out the values of I_{DLE}/I_{NBE} from PL spectra it is possible to evaluate the order of resistivity of ZnO thin films. From PL studies, we could also understand that 'in-situ' doping is more effective than 'ex-situ' doping.

Our next work was on proposed absorber layer candidate- CZTS. A sub-bandgap emission at 0.797 eV was identified in stoichiometric CZTS thin films. From excitation power dependence of PL emission, we concluded the transition to be donor- to- acceptor (DAP) type. An acceptor at 0.12 eV could be identified as 'Cu_{Zn}' defect and the deep donor defect at 0.533 eV could be identified as 'O_{Sn}' (with the help of supporting evidences from XPS measurements). The emission at 0.797 eV was proposed to be a transition between 'O_{Sn}' donor and 'Cu_{Zn}' acceptor. In 'Cu' rich CZTS films another emission at 0.805 eV was recorded and it was identified as a DAP transition. The defects responsible for this emission could be identified as a donor created by 'Cu_i' and ionized acceptors of 'Cu_{Sn}'. A band diagram was proposed for stoichiometric as well as 'Cu' rich CZTS thin films indicating the different defects within the bandgap. Indirect identification of deposition parameters which yield relatively defect-free films could be identified using PL.

Defect analysis was done on ZnS thin films and the attempt was to identify using PL, whether ZnS is good for buffer layer applications in solar cells. A broad emission at 1.88 eV could be recorded which could be identified as arising

from transitions between two donor levels and a broad acceptor level. The two donor levels proposed are- level due to surface defects of oxygen (at 38 meV) and energy level corresponding to delocalization energy of electrons in elemental sulfur species (at 166 meV). The broad acceptor at ~ 1.6 eV was attributed to ionized vacancies of sulphur. 'Cu' doped ZnS thin films were analyzed using PL and a green emission at 2.28 eV could be identified. On further analysis we suspect that the emission arises from a donor due to 'Cl_S' to acceptor created by 'Cu'. Reduction in resistivity of ZnS thin films on 'Cu' doping could be understood using PL. Based on the observation that there are sub-bandgap levels which facilitate absorption of more wavelengths and that films are low resistive, 'Cu' doped ZnS thin films could be identified as suitable candidates for buffer layer applications.

In the last part of our work we have tried to use PL to study a completed solar cell- In_2S_3/MEH-PPV heterojunction. We could extend the theory that is generally used to find the open-circuit voltage for silicon solar cells to this type of heterojunction with reasonable degree of success. Open-circuit voltage of In_2S_3/MEH-PPV heterojunctions, calculated from PL differed from values obtained from J-V measurements by a maximum of only ~ 5 %. We could also demonstrate that apart from normal ageing, PL measurements do not damage the devices under study.

Future prospects

In the case of spray deposited materials or solar cells, major defects are due to grain boundaries. We have monitored only the bulk PL from materials. A modification of the existing system can be done to extract PL from sub-micron features like grains or defects present by using a Near-field Scanning Optical Microscopy (NSOM) tip which enables near-field imaging. This is quite similar to Atomic Force Microscopy (AFM). The NSOM tip can either be a pulled or

stretched optical fibre or an AFM cantilever tip with a small hole in the middle. Such a measurement will give clear idea about the grain boundaries and defects present. Also by changing the excitation wavelength in such an experimental set up, penetration depth can be controlled. Scanning can be done by using a micro-translation arrangement that can be integrated using LABVIEW. In the present system, measurement of carrier lifetime is not possible. Photothermal Beam Deflection (PTD) spectroscopy is another optical technique which can be used to find carrier lifetime, surface recombination velocity etc. So a combination of the complementary techniques PL and PTD, can be used to evaluate the optical and electronic properties of semiconductors and in fact we have initiated works in this direction.

We proved that PL can be used to estimate the order of resistivity of ZnO thin films and we could propose a quantitative relation connecting PL and order of resistivity of ZnO thin films (1). But an area yet to be explored is whether PL can be used to estimate resistivity of other materials too. In fact in In_2S_3, Rajesh et al have reported that on 'In' diffusion, there is an evident change in the PL spectrum and resistivity (2). For different materials, the manner in which PL can be correlated to resistivity will be different. If it is possible to standardize such a relation connecting PL and resistivity for different materials then it will be a remarkable achievement that a non-contact and non-destructive technique can be used for analyzing the electrical properties.

We have calculated the open-circuit voltage of In_2S_3/MEH-PPV heterojunction using PL. Predicting other performance parameters like short-circuit current density, efficiency etc using PL has not been done. Also purely semiconductor based heterojunctions like CZTS/In_2S_3 or $CuInS_2$/In_2S_3 heterojunctions have not been analyzed using PL.

References

[1]. **N. Poornima, T.V.Vimalkumar, V.G.Rajeshmon, C.Sudha Kartha, K.P.Vijayakumar.** 2013, International Journal of Photoenergy, Vol. 2013, p. 1.

[2]. **V.G.Rajeshmon, N. Poornima, C. Sudha Kartha, K.P.Vijayakumar.** 2013, Journal of Alloys and Compounds, Vol. 553 , p. 239.

.....ഇ൹.....